

**Modulation of the
apical efflux transporter
P-glycoprotein by Vitamin E TPGS:
Structure-activity relationships
and mechanism of inhibition**

Dissertation
zur Erlangung des Grades
des Doktors der Naturwissenschaften
der Naturwissenschaftlich-Technischen Fakultät III
Chemie, Pharmazie, Bio- und Werkstoffwissenschaften
der Universität des Saarlandes

von
Eva-Maria Collnot
Saarbrücken
2007

Tag des Kolloquiums: 27.04.07

Dekan: Prof. Dr. Uli Müller

Berichterstatter: Prof. Dr. Claus-Michael Lehr
Prof. Dr. Volkhard Helms
Prof. Dr. Michael F. Wempe

Short summary	1
Kurzzusammenfassung	2
1 General introduction	3
1.1 <i>Drug absorption across epithelial barriers and the role of active transport systems</i>	3
1.2 <i>Efflux transporters</i>	5
1.2.1 ABC transporters	5
1.2.2 P-glycoprotein	6
1.3 <i>Surfactants</i>	13
1.3.1 Definition and pharmaceutical application	13
1.3.2 Surfactants as oral absorption enhancers	14
1.3.3 D-Alpha-tocopheryl poly(ethylene glycol 1000) succinate	16
1.4 <i>Aim of the work</i>	18
2 Structure-activity relationship of the interaction of vitamin E TPGS with P-glycoprotein	21
2.1 <i>Introduction</i>	22
2.2 <i>Materials and methods</i>	25
2.2.1 Materials	25
2.2.2 Synthesis of TPGS	25
2.2.3 Cell culture	25
2.2.4 Preparation of TPGS stock solutions	26
2.2.5 Transport assay	26
2.2.6 Sample analysis	27
2.2.7 Data processing and statistical analysis	28
2.2.8 Cytotoxicity	28
2.2.9 Determination of the critical micelle concentration (CMC)	29
2.2.10 Computational modelling	29
2.2.11 Data fitting and statistical analysis	29
2.3 <i>Results</i>	30
2.3.1 Transport assay	30
2.3.2 Cytotoxicity	43
2.3.3 Determination of physicochemical properties	46
2.4 <i>Discussion</i>	51
2.4.1 Analogues with modified PEG chains	51
2.4.2 Influence of experimental conditions	54
2.4.3 Analogues with modified hydrophobic moieties	57
2.4.4 SAR and mechanism of P-gp inhibition by TPGS	58
2.4.5 <i>In vivo</i> impact of TPGS	59
2.5 <i>Conclusion</i>	61

3	Mechanism of Vitamin E TPGS interaction with P-glycoprotein	63
3.1	<i>Introduction</i>	64
3.2	<i>Materials and methods.....</i>	65
3.2.1	Materials.....	65
3.2.2	Cell culture	65
3.2.3	ESR spectroscopy	65
3.2.4	ATPase assay	67
3.2.5	Immunocytochemical staining	68
3.2.6	UIC2 shift assay	69
3.2.7	Statistical analysis	70
3.3	<i>Results.....</i>	71
3.3.1	ESR.....	71
3.3.2	ATPase assay	74
3.3.3	UIC2 shift assay	78
3.4	<i>Discussion.....</i>	81
3.4.1	Influence on membrane environment	81
3.4.2	Influence on P-gp ATPase.....	84
3.4.3	Influence on P-gp conformation.....	88
3.5	<i>Outlook.....</i>	89
3.6	<i>Conclusion</i>	91
4	Summary	93
5	Zusammenfassung.....	97
6	Appendix: ESR spectroscopy	101
6.1	<i>Theoretical background.....</i>	101
6.2	<i>Spectral anisotropy</i>	104
6.3	<i>Spin probes and the order parameter S.....</i>	107
7	References	109
8	Abbreviations	122
9	Curriculum vitae	123
10	List of publications.....	124
11	Danksagung.....	126

Short summary

The non-ionic surfactant D-alpha-tocopheryl poly(ethylene glycol 1000) succinate (TPGS 1000) has been previously shown to increase oral bioavailability of P-glycoprotein (P-gp) substrates by modulating activity of the efflux pump. In the present thesis structure activity relationship of the interaction and possible mechanism of inhibition of the efflux transporter were investigated to optimize the TPGS structure. P-gp inhibitory activity of TPGS could be increased by modifying the length of the PEG chain with optimal inhibition being achieved at a PEG molecular weight of ~1500 Da. The inhibitory effect of TPGS on P-gp could be also increased by modifications to the hydrophobic part of the molecule, such as the exchange of the alpha-tocopherol moiety for cholesterol. The inhibitory activity of the TPGS analogues does not correlate with their physicochemical properties such as molecular weight, molecule volume, or lipophilicity. In agreement with these findings, an unspecific alteration of the P-gp membrane environment could be ruled out in electron spin resonance experiments. TPGS was shown not to be a P-gp substrate itself nor does it interact with one of the transport active drug binding sites of P-gp to competitively block drug efflux. Rather, the inhibitory effect of the TPGS analogues correlates with their inhibition of substrate induced ATPase activity, indicating that the depletion of the energy source of the efflux pump is an integral part in the inhibitory mechanism of TPGS.

Kurzzusammenfassung

Für das nicht ionische Tensid D-Alpha-tocopheryl poly(ethylene glycol 1000) succinat (TPGS 1000) wurde kürzlich gezeigt, dass es die orale Bioverfügbarkeit von Substraten des Effluxtransporters P-Glykoprotein (P-gp) durch Hemmung der Effluxpumpe steigert. In der vorliegenden Arbeit wurden die Strukturwirkungsbeziehungen der Wechselwirkung zwischen TPGS und P-gp und der Mechanismus, der der Hemmung zu Grunde liegt, untersucht, um die TPGS Struktur zu optimieren. Die P-gp Hemmung durch TPGS konnte durch Variation der PEG Kettenlänge erhöht werden, wobei der optimale Hemmeffekt bei einem PEG Molekulargewicht von ungefähr 1500 Da beobachtet wurde. Des Weiteren steigerten auch Modifikationen des hydrophoben Molekülteils, wie der Austausch des Alpha-Tocopherol-Restes durch Cholesterol, das Hemmpotenzial von TPGS. Die inhibitorische Wirkung der TPGS Derivate korreliert nicht mit ihren physikochemischen Eigenschaften wie Molekulargewicht, Molekülvolumen oder Lipophilie. In Übereinstimmung mit diesen Ergebnissen konnte eine unspezifische Änderung der Membrenumgebung von P-gp in Elektronenspinresonanz-Untersuchungen ausgeschlossen werden. Für TPGS konnte gezeigt werden, dass es selbst kein Substrat von P-gp ist und nicht mit einer der transportaktiven Bindungsstellen von P-gp, im Sinne einer kompetitiven Hemmung interagiert. Vielmehr korreliert der inhibitorische Effekt mit der Hemmung der Substrat-induzierten ATPase Aktivität, was darauf hinweist, dass diese Depletion der Energiequelle der Effluxpumpe ein essentieller Bestandteil des Hemmmechanismus von TPGS ist.

1 General introduction

1.1 *Drug absorption across epithelial barriers and the role of active transport systems*

On the way from the application site to the biological target a drug is subject to four major steps of pharmacokinetics: absorption, distribution, metabolism and excretion (the so called ADME process). The interplay of these four processes will determine the extent to and time after which a drug will appear at its site of action, thereby influencing the pharmacological effect. The drug's fate in the ADME process is interwoven with its ability to cross epithelia, a major biological barrier to drug distribution.

Absorption of a molecule across an epithelial barrier is the sum of competing processes that influence the net absorption to varying extents: Depending on its physicochemical properties, mainly size and hydrophilicity, a molecule may transverse an epithelial barrier by two routes: one) through the cells (transcellular transport; Figure 1-1 A) or two) in between the cells (paracellular transport; Figure 1-1 B) via pores formed by the tight junctions. The radius of the tight junctional pores in human intestine has been estimated to be between 0.5 and 5 nm, limiting the size and weight of paracellularly transported molecules to < 300 Da [1]. Furthermore very hydrophilic compounds will be transported paracellularly, as they distribute poorly into the lipophilic membranes, a prerequisite for transcellular diffusion. Transcellular diffusion is also limited to a certain extent. According to Lipinski's rule of five, only compounds with a logP < 5, molecular weight of up to approximately 500 Da and up to 5 H-bond donors and 10 H-bond acceptors are likely to be absorbed to a high extent [2]. Both transports, transcellular and paracellular diffusion, are passive processes and follow a concentration gradient between apical and basolateral side of the epithelial barrier.

Transporter proteins, exhibiting low to high specificity, are integrated in the cell membrane and may modify transcellular transport, enabling otherwise poorly permeable drugs to cross the cell layer.

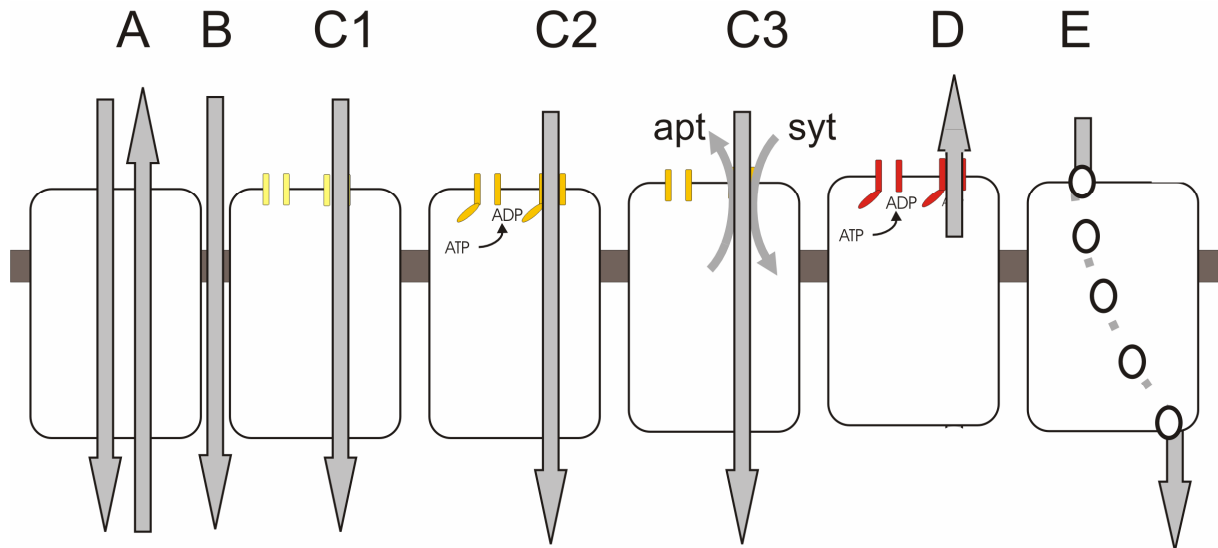


Figure 1-1 Transport routes across epithelia: A: transcellular passive diffusion, B: paracellular passive diffusion, C1: carrier mediated transcellular transport, C2: primary active transport, C3 secondary active transport (either symport (syt) or antiport (apt)), D: active efflux, E: (receptor-mediated) endocytosis.

A substrate may be transported along a concentration gradient, without the need for a primary or secondary energy source (facilitated transport, Figure 1-1 C1). Active carriers on the other hand either actively pump their substrates across the membrane by ATP hydrolysis (Figure 1-1 C2) or utilize the concentration gradient of another compound simultaneously translocated either in the same direction (symport) or in the opposite direction (antiport; Figure 1-1 C3). Depending on the direction of transport, one may distinguish two groups of active transporters: influx transporters, which pump their substrates into the cells and efflux transporters which confer transport in the opposite direction (Figure 1-1 D).

Although diverse transport systems can be found ubiquitously in the body, the respective tissue distribution for specific transporters may differ. By their expression in epithelia, transporters may influence all steps of the ADME process [3]. While influx transporters generally positively influence absorption and bioavailability of substrates, efflux transporters often have negative effects on substrate pharmacokinetics, as they limit permeability of epithelia and support substrate excretion and metabolism [4]. Thereby they can pose a significant challenge to the development of new pharmaceutical entities and formulations.

1.2 Efflux transporters

1.2.1 ABC transporters

With few exceptions, such as the solute carrier LRP (lung resistance related protein), most known efflux systems in the human body belong to the so called ATP binding cassette (ABC) superfamily of transporters. ABC transporters are found in most organisms, from bacteria to humans [5]. Thus far, 48 human ABC transporters belonging to seven subfamilies (ABCA-ABCG) have been described. They include not only efflux pumps such as P-glycoprotein (P-gp), the multidrug resistance associated proteins (MRP1-7), and the half transporter breast cancer resistance protein (BCRP), but also non-transporters, such as the chloride channel CFTR, or SUR1/2, a modulator of ATP sensitive potassium channels [6]. ABC transporters are characterised by a highly conserved nucleotide binding fold with a characteristic Walker A and Walker B and a signature or C motif, whereas the organisation, number and localisation of their transmembrane domains may differ (Figure 1-2) [6].

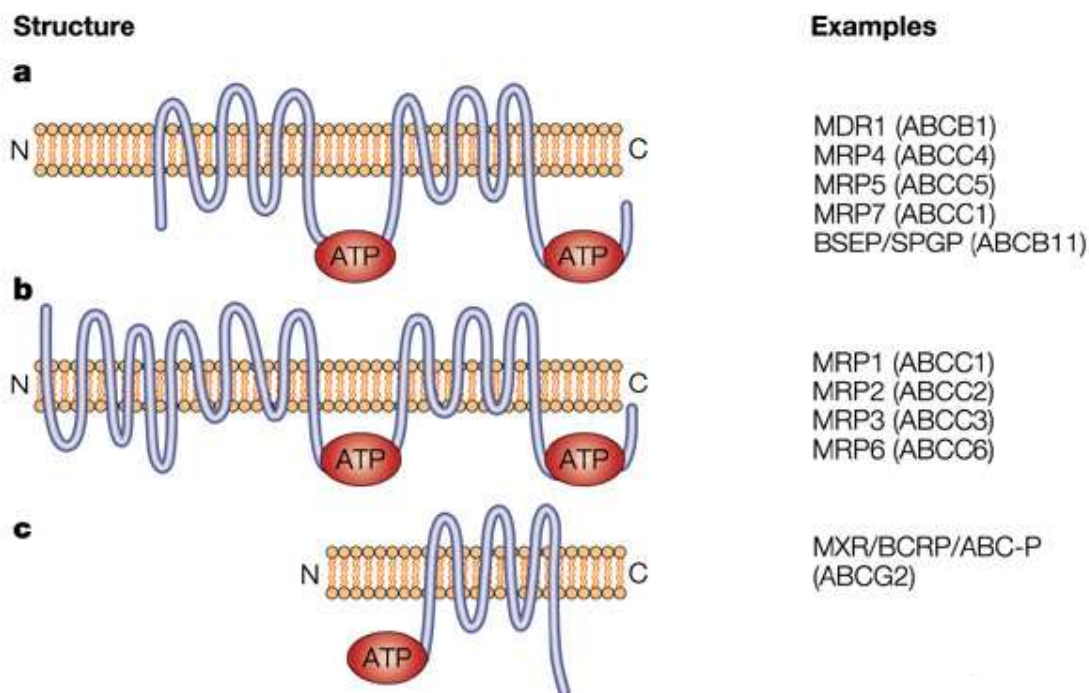


Figure 1-2 Membrane topology of ABC transporters known to confer drug resistance; adopted from [6].

ABC efflux pumps use energy released from ATP hydrolysis to actively pump substrates, if necessary against a concentration gradient, out of cells [7]. They have been identified as the primary cause for the so called multidrug resistance phenomenon in cancer cells: overexpression of MRP1, BCRP and P-gp was shown

to protect cancerous tissues from the intracellular accumulation of a broad variety of structurally unrelated chemotherapeutics, thus weakening their therapeutic impact [5, 8-10]. In addition, ABC transporters have important physiological functions, as they protect the body in general and sensitive tissues like the brain in particular from entrance of potential toxins and help to eliminate metabolites [3]. Substrate spectra of different ABC efflux systems overlap. For example, P-gp and MRP1 have similar transport specificity. Whereas P-gp only transports neutral and cationic compounds, MRP1 in addition translocates anionic compounds, frequently metabolite conjugates with glutathione [11]. The convoluted substrate-transporter interactions complicate the identification of transport and multidrug resistance pathways and the interpretation of pharmacokinetic data.

1.2.2 P-glycoprotein

P-gp was the first ABC transporter to be discovered and is probably the most extensively studied human efflux pump. The special interest in P-gp is based on its prominent role both in drug pharmacokinetics and cancer chemotherapy. P-gp was discovered in the 1970s when studies with Chinese hamster ovary (CHO) cells revealed a 170 kDa carbohydrate containing protein, which was unique to drug resistant mutants, and conferred cross-resistance to a variety of structurally unrelated anticancer agents such as actinomycin D, methotrexate, daunorubicin and colchicine [12]. The protein was named P(ermeability)-glycoprotein because it was thought to reduce the permeability of cancer cells towards drugs [12]. However, this theory was soon refuted, as it was revealed that P-gp unidirectionally pumps drugs out of cells, thus reducing the intracellular concentration of the anticancer agents [13]. (Over)expression of P-gp has since then been shown in a variety of primary and treated tumors and today P-gp is considered the mainstay among ATP-dependent efflux transporters that confer multidrug resistance in tumor cells [14, 15].

The gene responsible for P-gp expression, named MDR1 [16], is located on chromosome 7q21 and is transcribed into a 4.5 kilobase mRNA. The corresponding glycoprotein consists of 1280 aminoacids, which are arranged as 2 homologous halves joined by a linker region. Each half consists of a transmembrane domain (TMD) with 6 membrane-spanning α -helices (transmembrane segments, TM) and a hydrophilic region with a nucleotide binding domain (NBD) (Figure 1-3).

The two halves, which are not completely symmetrical [17], build together a cup-like structure with a 5 nm central pore [18, 19]. It was shown that the deletion of the central core of the linker region results in normal expression of the protein at the cell surface, but no functional transport or drug-stimulated ATPase activity [20]. Replacement of the depletion with a peptide with a predicted flexible secondary structure restored the function, indicating that interaction of both halves is critical for the functioning of the molecule. P-gp is glycosylated at three sites in the first extracellular loop [21]. The glycosylation appears to be essential for trafficking of the efflux pump to the cell surface, but does not influence the transport function [21].

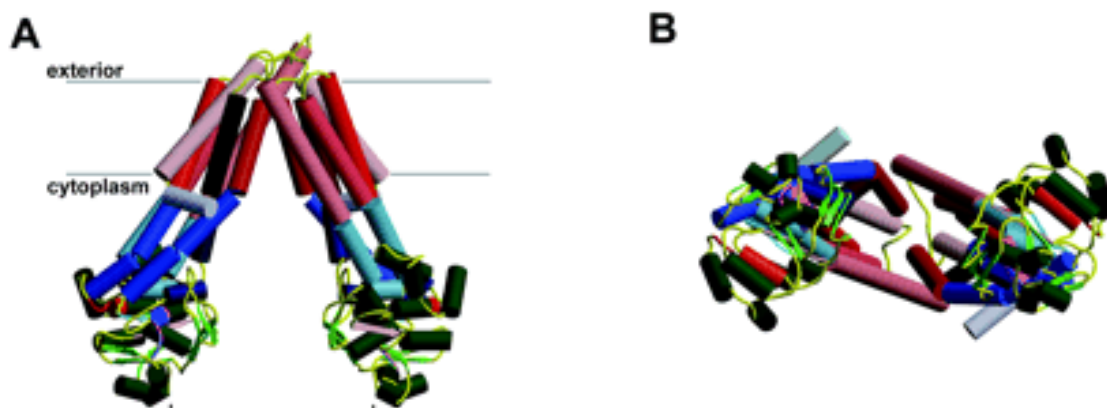


Figure 1-3: Structure of P-gp as obtained by homology modelling (in ribbon representation). A: Side view; B: intracellular view. TM helices are colored from *light rose* to *dark red* from TM1 to TM6 and TM7 to TM12. Intracellular domain (ICD) helices are coloured from *light* to *dark blue* from ICD1 to ICD3 and ICD4 to ICD6. NBD helices and strands are coloured in *dark* and *light green*, respectively. The Walker A, signature region, and Walker B of each NBD are coloured in *magenta*, *orange*, and *pink*, respectively; adopted from [22].

P-gp is an ATPase, requiring energy derived from ATP hydrolysis to actively pump a substrate out of the cell back into the extracellular fluid. According to the “hydrophobic vacuum cleaner” hypothesis (Figure 1-4), the P-gp ligand binding site(s) are located in the inner membrane leaflet of the lipid bilayer [23, 24]. In a multi-step process [25], the substrate first partitions into the outer leaflet of the membrane bilayer before flip-flopping from the outer membrane interface to the inner interface. The subsequent substrate binding in the cytoplasmic leaflet of the lipid bilayer leverages the two-dimensional, lateral diffusibility of partitioned compounds within the lipid membrane; a more efficient process than interactions that would randomly occur after three-dimensional diffusion from the aqueous environment. The P-gp pump then undergoes a conformational change in response to substrate binding and ATP hydrolysis.

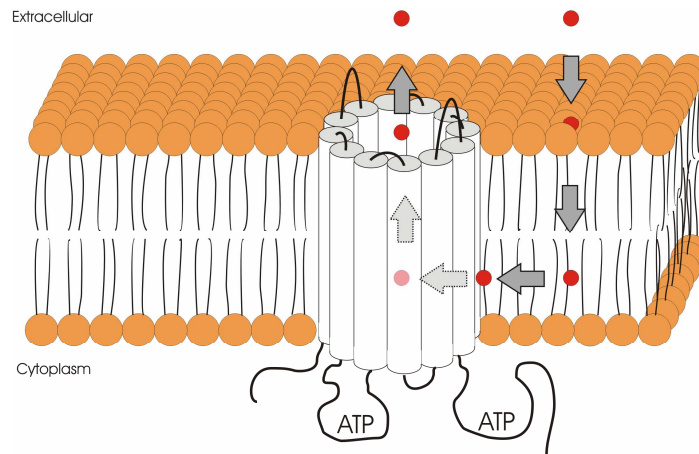


Figure 1-4 Idealized representation of P-gp within the lipid membrane bilayer and the hydrophobic vacuum cleaner model of P-gp substrate transport.

Different mechanisms for the next step have been proposed. The most popular suggest a transfer of the bound ligand to the core of the ring or 'flipping' it back to the exoplasmic leaflet. Consequently, affinity of the drug binding site strongly decreases and the substrate is released. The exact catalytic cycle of the conformational change in P-gp and other ABC transporters has been extensively studied and so far is best described by the so called 'ATP switch model' [26]: Binding of a substrate to the high affinity drug binding site results in increased affinity of the two nuclear binding domains for ATP and two molecules of ATP bind cooperatively to generate a closed NBD dimer. The subsequent conformational changes in the transmembrane domains extracellularly expose the drug-binding site and reduce its affinity, releasing the bound drug. ATP is hydrolyzed to form a transition-state intermediate and the sequential release of a phosphate ion and ADP restores the transporter to its basal configuration.

P-gp transports a wide range of structurally diverse substrates. Examples (Table 1-1) include cancer drugs such as paclitaxel, doxorubicin or vinblastine, the calcium channel blocker verapamil, antibiotics (e.g. erythromycin, actinomycin D) and different HIV protease inhibitors (e.g. indinavir, saquinavir).

Substrate (Pharmacological class)	Substrate/Inhibitor (Pharmacological class)	Inhibitor (Pharmacological class)
Topotecan (Topoisomerase I inhibitor)	Verapamil (Calcium channel blocker)	Ketoconazole (Fungicide)
Etoposide, Teniposide (Topoisomerase II inhibitors)	Nicardipine, Nifedipine, Nitrendipine (Dihydropyridine)	Sodium orthovanadate (ATP hydrolysis inhibitor)
Actinomycin D (Antitumor antibiotic)	Cyclosporine A (Cs A) (Immunosuppressant)	Clarithromycin (Antibiotic)
Paclitaxel, Docetaxel (Taxanes)	Progesterone (Steroid hormone)	Reserpine (Antihypertensive)
Colchicine (Spindle inhibitor)	Chloroquine (Malaria medication)	GF120918 (Specific P-gp inhibitor)
Digoxin (Cardiac glycoside)	Daunorubicin, doxorubicin (Anthracyclines)	PSC833 (Specific P-gp inhibitor)
Puromycin (Antibiotic)	Ritonavir, saquinavir, indinavir (HIV protease inhibitors)	Tween 80, Cremophor EL, Pluronic P85 (Surfactants)
Rhodamine 123, Calcein AM, Hoechst 33342 (Fluorescent dyes)	Erythromycin (Antibiotic)	Cis-(Z)-flupentixol (Antipsychotic)
Dexamethasone, hydrocortisone (Glucocorticoids)	Vinblastine, vincristine, (Vinca alkaloids)	Silymarin, Flavone, Biochanin A (Flavonoids)
Morphine (Opioid)	Talinolol (Beta-adrenergic antagonist)	Sodium taurodeoxycholate, sodium deoxycholate (Bile salts)
L-Dopa (Antiparkinson-prodrug)	Amiodarone (Antiarrhythmic agent)	Dimethyl-beta-cyclodextrin (Excipient, solubilization enhancer)

Table 1-1 Examples of P-gp substrates, modulators and inhibitors, assembled from [5, 27, 28].

The only common P-gp substrate feature seems to be that they are all hydrophobic with a molecular mass between 300 and 2000 Da [29], while anionic compounds are not transported by P-gp. This broad substrate specificity is incompatible with a traditional enzyme-substrate interaction theory and instead may be explained by the existence of more than one transport-active drug binding site.

At least four binding sites, which can influence each other allosterically, are currently being discussed in literature. The first two sites initially discovered are the Hoechst 33342-selective 'H-site' of P-gp that binds colchicine and the RHO selective 'R-site', which binds anthracyclines such as doxorubicin and daunorubicin [30]. Later, a third P-gp drug-binding site, selective for prazosin and progesterone, was discovered [31]. Some groups have also suggested a fourth site specific for dihydropyridines, such as nifedipine [32, 33].

The exact localisation of the binding sites in the molecule is still unclear. Data so far only indicates that both the R- and the H-site are located near the cytoplasmic leaflet of the lipid membrane bilayer, with the R-site located slightly more shallowly or closer to the interfacial phospholipids head group region [34, 35]. Photoaffinity labelling, cross linking and homology modelling studies place the substrate binding domains at the interface between TMD1 and TMD2 [36, 37], with TMs 4,5,6 in TMD1 and TMs 9,10,11 and 12 in TMD2 contributing residues [37, 38]. Several substrates are known to bind to more than one binding site of P-gp, indicating a clear overlap of the binding regions and the formation of a bigger drug binding pocket [39]. Such a common drug binding pocket, could use residues from different TMs for binding the different substrates (induced fit); the number and type of residues involved deciding affinity for a particular substrate [40].

The expression and distribution of P-gp within tissues influences the ADME of substrate molecules [41]. P-gp is found in the lung, gut, liver, kidney, brain, testis, and placenta [42-48] (Figure 1-5). Furthermore P-gp is also expressed in peripheral blood mononuclear cells, such as macrophages and lymphocytes [49, 50]. Leading to an asymmetric transport of substrate compound across the cell layer, the efflux pump is expressed only on one membrane domain of a differentiated and functionally polarized cell type. Thereby these cells act as biochemical barriers and prevent access of possibly toxic xenobiotics to underlying tissues and systemic circulation or facilitating removal of substrate metabolites [51, 52].

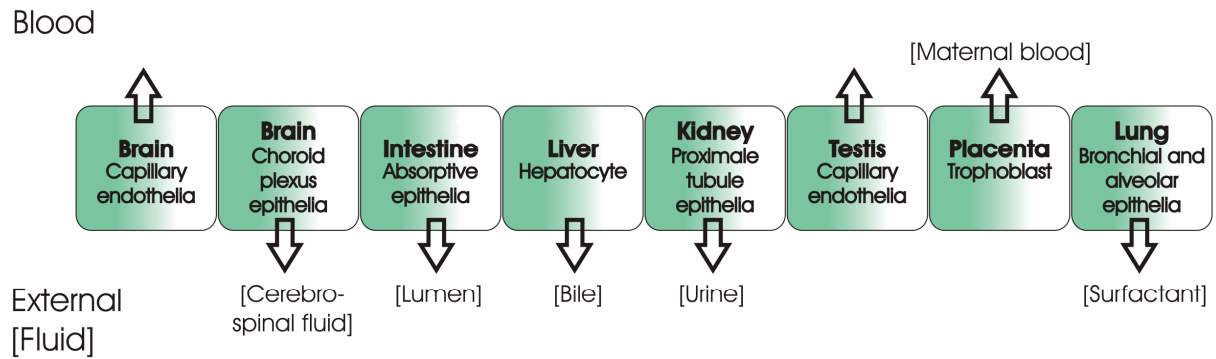


Figure 1-5 Tissue distribution of P-glycoprotein and the net flux accomplished by its asymmetric location on the cells; adapted from [53].

The extent to which P-gp influences pharmacokinetics (PK) and thus the pharmacodynamics (PD) of a substrate depends on the route of application, the therapeutic target and the physicochemical properties of the compound. In the case of oral absorption, many compounds that are P-gp substrates are virtually unaffected by P-gp as they either bypass the efflux pump via rapid passive diffusion or they are applied in such high dose that they saturate P-gp [54-56]. However, the importance of P-gp efflux to oral drug absorption increases with drugs known to have low aqueous solubility, slow passive diffusion (BCS classes II-IV) and/ or marked first-pass metabolism, or if only low doses of the P-gp substrate are applied [57, 58]. Furthermore, compounds that are targeted to the central nervous system are often quantitatively influenced by P-gp efflux because the exposing free concentrations in plasma are typically not high enough to saturate the efflux pump at the blood-brain barrier [59]. A selective inhibition of P-gp was shown to improve oral bioavailability of otherwise poorly absorbed P-gp substrates such as docetaxel, paclitaxel, topotecan, or cyclosporine A [58, 60-62] and increased effectiveness of cancer chemotherapy in multidrug resistant tumors in a number of clinical studies [63-65].

The first P-gp inhibitors to be discovered such as verapamil, quinidine, or cyclosporine A, are merely modulators of P-gp activity as they are substrates of the efflux pump themselves and show a dose-dependent competitive inhibition of substrate binding. High doses of these first generation inhibitors are required to effectively inhibit P-gp, with strong toxic side effects due to the inherent primary pharmacological effect of the drugs. Second generation inhibitors, which are either non-racemic enantiomers (e.g. dexverapamil) or are structurally derived from the first

generation substances (e.g. the cyclosporine A analogue PSC833 or the pipercolinate derivative VX710), lack the pharmacological properties of their predecessors and can be employed in much lower doses. However, these substances are not very specific for P-gp, as they also modulate activity of other transporters [66] and/or metabolizing enzymes such as CYP450 3A4 with overlapping substrate specificities [67]. To avoid the resulting convolutions in drug pharmacokinetics and drug-drug and drug-food interactions, a third generation of very potent and selective P-gp inhibitors was generated, e.g. tariquidar XR9576, laniquidar R101933 and GF120918 [38]. The potency of these third generation inhibitors is about 10 times higher than the potency of first or second generation inhibitors.

Besides these xenobiotics small molecular inhibitors, endogenous substances such as bile salts (e.g. sodium taurochenodeoxycholate, sodium deoxycholate) and phospholipids have also been shown to modulate P-gp activity. Furthermore, naturally occurring flavonoids (e.g. flavone, biochanin A, silymarin) were found to improve absorption of P-gp substrates *in vitro* and *in vivo* [68-71]. Of special interest for pharmaceutical technology is the ability of certain non-ionic surfactants such as Tween 80, different Spans, several Pluronic block copolymers, Cremophor EL, and vitamin E TPGS (TPGS 1000) to inhibit P-gp mediated efflux (see 1.3.2) [72-77].

1.3 Surfactants

1.3.1 Definition and pharmaceutical application

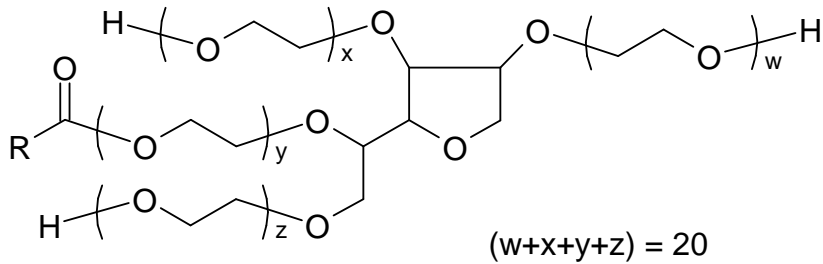
Surfactants (surface active agents) are tensides, i.e. by aligning themselves at the interface, they reduce the interfacial tension at liquid-liquid or air-liquid interfaces. In bulk solutions, surfactants may assemble into aggregates called micelles. The concentration at which surfactants begin to form micelles is known as the critical micelle concentration (CMC).

Surfactants are amphiphilic and may be classified according to structure: i) anionic, ii) cationic, iii) ampholytic, and iv) non-ionic surfactants. Anionic surfactants (e.g. sodium dodecyl sulphate (SDS), traditional soaps or fatty acid salts) are widely used in products for personal hygiene, detergents and washing agents. Because of their high irritating potential and toxicity towards biological membranes, anionic surfactants only play a minor role in overall pharmaceutical formulations. Cationic surfactants (e.g. Cetyl trimethylammonium bromide (CTAB), polyethoxylated tallow amine (POEA), benzalkonium chloride) possess great antimicrobiological properties and are therefore incorporated as preservatives in aqueous and semi-solid formulations.

Non-ionic surfactants play the biggest role in galenics. They are more hydrophobic than ionic tensides and possess a greater capacity to dissolve poorly soluble drugs. Additionally, in general, non-ionic surfactants are less cytotoxic and show superior compatibility with other ionic excipients or active agents. Examples of non-ionic surfactants include cetyl alcohol, cetyl stearyl alcohol, polyoxyethylene fatty acid esters (Myrjs®), polyoxyethylene fat alcohol ethers (Brijs®), polyoxyethylene sorbitan fatty acid esters (Tweens®), sorbitan fatty acid esters (Spans®), polyoxyethylene polyoxypropylene blockcopolymers (Pluronic®), polyoxyethylene fatty acid glycerides (e.g. Cremophor EL®) and vitamin E TPGS. Non-ionic surfactants are widely used in pharmaceutical technology as wetting agents, solubilizers, emulsifiers, foam stabilizers, antifoams and also as permeation enhancers in oral formulations. For many years, the permeation enhancing effect of non-ionic surfactants was mainly attributed to an increased solubility of lipophilic drugs, a perturbation of intestinal cell membranes or tight junctions and an interaction with metabolic enzymes [78-80].

However for some non-ionic surfactants it has been shown that the permeability enhancement is in large part due to inhibition of efflux systems such as P-gp or MRP.

A



B

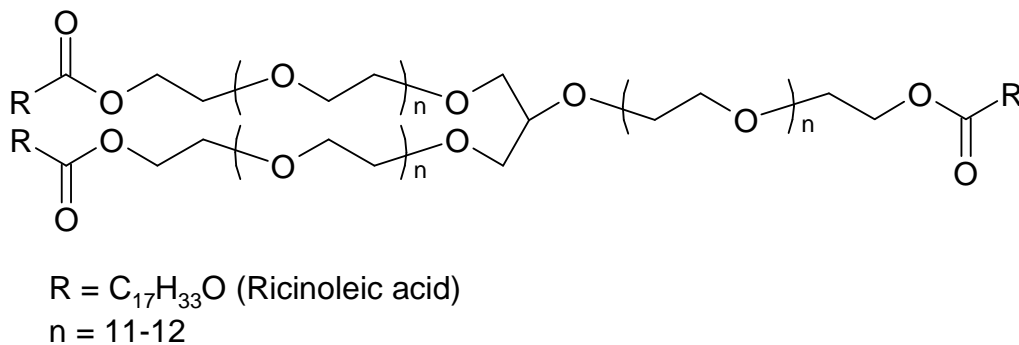


Figure 1-6 Structure of A: Tween 80 and B: Polyoxyl -35-castor oil (Cremophor EL).

1.3.2 Surfactants as oral absorption enhancers

Several studies investigated the inhibitory potential of different surfactants on efflux transporters and tried to elucidate specificity and mechanism of inhibition. Various excipients (e.g. Labrasol, Tween 20 and 80, TPGS 1000, Imwitor 742, Solutol HS15, Cremophor EL, different Pluronics, Softigen 767) were identified as more or less potent P-gp inhibitors [72, 81-84], whereas only few substances show MRP inhibition [85, 86]. Thus far, no reports can be found in the literature on surfactant interaction with BCRP. The inhibitory effect seems to be restricted to non-ionic surfactants as neither cationic (hexadecyltrimethylammonium bromide (CTAB)) nor anionic surfactants (SDS) modulate P-gp activity [74].

Currently, little is known about the mechanism of efflux pump inhibition. Besides a competitive inhibition of drug binding or an allosteric modulation of P-gp activity, where interaction occurs at one of the non-transport active binding sites, a non-specific alteration of the lipid membrane environment has been proposed as a possible inhibition mechanism. Surface active agents might become incorporated into the phospholipid bilayer, thereby either increasing or decreasing the microviscosity of the membrane. P-gp displays a tangled relationship with its membrane environment; P-gp recognizes its substrates within the cytosolic leaflet and also translocates some endogenous lipids to the exoplasmic leaflet [87]. Furthermore recent studies demonstrated an integral role of membrane cholesterol content and localization on P-gp functionality. Cholesterol membrane depletion was shown to inhibit activity of P-gp [87-89], which in some cell lines was found to be preferably located in cholesterol enriched membrane microdomains, so called 'lipid rafts' [90]. Therefore, it seems feasible that a rigidization and/or fluidization of the lipid membrane may alter cholesterol organisation and might influence conformation and/or conformational flexibility of P-gp and its nucleotide and substrate binding domains. However, findings on the membrane altering effects of non-ionic surfactants and their correlation to P-gp inhibition are contradictory. For example, in the case of Cremophor EL, different reports can be found in the literature suggesting either fluidization [91], rigidization [92], or no effect [73] on membrane fluidity. Inconsistencies, such as these, may be observed when different surfactants are compared: Rege *et al.* [72] observed a membrane fluidization for Tween 80 and Cremophor EL, whereas TPGS 1000 was found to be a membrane rigidifier. At the same time, cholesterol is known to rigidify the lipid membrane yet it does not modulate P-gp activity [72].

Studies on Pluronic P85 and other block copolymers have revealed an inhibition of P-gp ATPase, which alone or in combination with an intracellular energy depletion by disruption of mitochondria seems responsible for P-gp inhibition [93, 94]. The inhibition of the efflux pump ATPase could be due to a direct blocking of intracellular NBD's, sterical hindrance of drug, nucleotide binding or unspecific membrane effects, tying back to the aforementioned theory [93].

Altogether, the exact mechanism of action for P-gp inhibition by surfactants remains unclear and it seems questionable, if all surface active compounds share a common mechanism of inhibition.

In many cases, the bioavailability enhancing effect of TPGS is not restricted to a mere drug solubilization. Significant effects on bioavailability can already be observed at levels below the CMC, where no micellation of drug can occur [101]. Instead, the absorption enhancing effect of TPGS 1000 may also be attributed to an inhibition of P-gp mediated efflux [101, 102]. TPGS increases the sensitivity of P-gp expressing cells to several cytotoxic P-gp substrates *in vitro* and effectively blocks polarized transport of rhodamine 123 (RHO) and paclitaxel in transport assays [101]. P-gp inhibition by TPGS 1000 has also been demonstrated in a number of *in vivo* studies: TPGS 1000 increased bioavailability of paclitaxel in rats both via intravenous (iv) as well as oral (po) formulations [58, 103] and increased oral bioavailability of talinolol in humans [104].

Among surfactants TPGS 1000 is generally considered to be one of the most potent P-gp inhibitors [72, 77, 81, 84]; however, some groups report no significant influence of TPGS 1000 on P-gp [72, 75]. The inhibitory potency of TPGS 1000 (IC_{50} : 3.5 μ M) is only slightly weaker than that of the first generation P-gp inhibitor cyclosporine A (IC_{50} : 1.0 μ M), but falls considerably short to specifically synthesized inhibitors of the third generation, such as GF120918 (IC_{50} : 20 nM) [105] or LY335979 (IC_{50} : 50-60 nM) [106]. TPGS 1000 was shown to be relatively selective in its inhibition, not significantly modulating the activity of other efflux pumps such as MRP2, or uptake transporters such as hPeptT1 and MCT [84]. The membrane bound metabolizing enzyme CYP P450 3A4, that shares a broad range of substrates with P-gp, is also not affected by TPGS 1000 [107]. A second beneficial effect of TPGS for cancer chemotherapy may not be related to P-gp inhibition: Alpha-tocopherol succinate itself has been described to have anti-cancer properties, inducing cell apoptosis in leukaemia cells as well as human breast and prostate cancer cells [108-110]. The effect has been shown to be enhanced by esterification of alpha-tocopherol succinate with polyethylene glycol to TPGS 1000 [111].

A small number of products on the market already employ the solubilizing and permeability enhancing properties of TPGS 1000: For example, Agenerase® soft capsules and solution contain TPGS 1000 and the P-gp substrate and poorly water soluble HIV protease inhibitor amprenavir. In addition, some generic oral formulations

of the immunosuppressant cyclosporine A (Cicloral Hexal® capsules and solution, Ciclosporin-1A Pharma® capsules and solution) contain TPGS 1000.

In recent years, the potential of TPGS 1000 for oral drug delivery and cancer chemotherapy has also been utilized in the development of nanoscaled controlled drug delivery system.: TPGS 1000 can be used as an emulsifier [112, 113] or as a coating material [113, 114] in the preparation of poly-d,l-lactide-co-glycolide (PLGA) and polylactide (PLA) nanoparticles. The addition of TPGS 1000 as an emulsifier in the preparation of paclitaxel loaded PLGA nanoparticles, increased the AUC by a factor of three compared to Cremophor EL emulsified PLGA nanoparticles [103]. Alternatively, TPGS 1000 can represent the polymer-matrix itself. Copolymers of PLA-TPGS [115, 116] and PLGA-TPGS [117] showed higher paclitaxel drug loads and stronger sustained release compared to PLA/ PLGA controls.

Furthermore, polycaprolactone (PCL)-TPGS nanoparticles have been designed for nasal immunisation with diphtheria toxoid [118]. Liposomal systems employing TPGS 1000, such as the mixed micelles of poly(ethylene glycol)-phosphatidyl ethanolamine conjugate (PEG-PE) and TPGS 1000 for the delivery of the anti-cancer drug camptothecin [119], are also feasible.

1.4 Aim of the work

Originally, TPGS 1000 was developed as a water soluble form of Vitamin E and not with the aim to synthesize a new surfactant or even to act as a P-gp efflux inhibitor. The absorption enhancing properties of TPGS 1000 were more or less discovered by chance. Therefore it seems reasonable to assume that the structure of TPGS 1000 may not be optimized for either aim, and that a structural modification might yield more potent P-gp inhibitors. Commercially available TPGS 1000 was chosen as the chemical lead and two groups of analogues were synthesized by Eastman Chemical Company; analogues varied via PEG chain length or via a modified hydrophobic moieties replacing the vitamin E succinate portion.

In the first part of this thesis, the inhibitory potential and cytotoxicity of all analogues were determined by *in-vitro* assays and the results were correlated to physicochemical parameters in a structure activity relationship (SAR) study. Based upon these preliminary results, additional analogues of TPGS 1000 were synthesized and the SAR working hypothesis was further refined. To better understand the

mechanism of TPGS interaction with P-gp, and to compare and contrast results with findings from other labs, influence of experimental design (site of application, pre-incubation time) and purification of TPGS on the P-gp inhibition were investigated.

In the second part, more sophisticated mechanistic studies were conducted. To understand the observed SAR pattern and improve the rational design of new P-gp inhibitors, influence of TPGS on P-gp ATPase activity, cell membrane fluidity and conformational flexibility were investigated.

2 Structure-activity relationship of the interaction of vitamin E TPGS with P-glycoprotein

Parts of this chapter have been published in:

E.M. Collnot, C. Baldes, M.F. Wempe, J. Hyatt, L. Navarro, K.J. Edgar, U.F. Schaefer, C.M. Lehr, Influence of vitamin E TPGS poly(ethylene glycol) chain length on apical efflux transporters in Caco-2 cell monolayers, *J. Control Release* 111 (2006) 35-40.

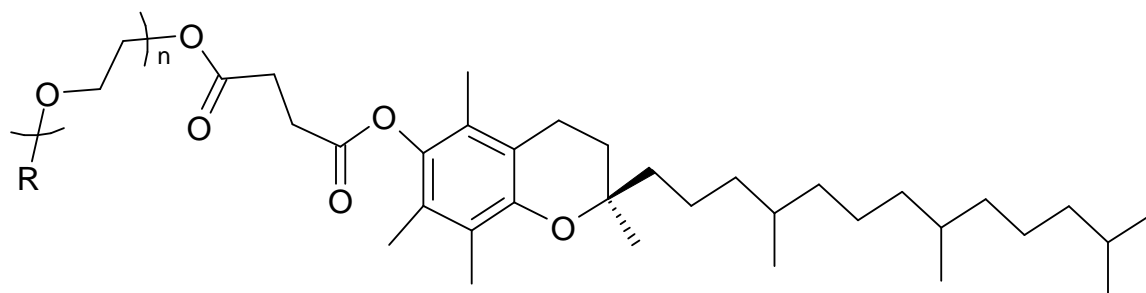
Copyright © 2006 Elsevier B.V

E.M. Collnot, C. Baldes, C. Wright, J.L. Little, U.F. Schaefer, C.M. Lehr, V.J. Wachter, K.J. Edgar, M. Wempe, Vitamin E TPGS modulation of P-gp efflux in Caco-2 cells: Significance of compound purity, pre-incubation time and application side, *Eur J Pharm Sci*, submitted

2.1 Introduction

The commercially available TPGS 1000 (D-alpha-tocopheryl poly(ethylene glycol 1000) succinate) was originally developed as a water-soluble form of vitamin E. It consists of a lipophilic alpha-tocopherol head, which is connected via a succinate linker to a hydrophilic polyethylene glycol tail. Due to its surface active properties, TPGS 1000 may be used as a solubilizer, as an emulsifier and as a vehicle for lipid based-drug delivery formulations. In recent years, TPGS 1000 has been described as an effective oral absorption enhancer for improving the bioavailability of poorly-absorbed drugs, an effect believed to be mediated via an inhibition of the apical efflux transporter P-gp. TPGS increased the sensitivity of P-gp expressing cells to several cytotoxic P-gp substrates *in vitro* and effectively blocked polarized transport of RHO and paclitaxel in transport assays [101]. In several studies, TPGS 1000 was found to be one of the most effective P-gp inhibitors among the surfactants [77, 81, 84]; however, other groups have reported no significant effect of TPGS 1000 [72, 75].

TPGS 1000 is a relatively weak P-gp inhibitor. Originally, TPGS 1000 was not developed as a P-gp inhibitor; thus it is reasonable to believe, that the structure of TPGS may be further optimized for P-gp inhibition. Hence, TPGS 1000 was chosen as the lead molecule and two different groups of analogues were prepared by Eastman Chemical Company, a supplier of commercially available TPGS 1000. In one analogue group, the alpha-tocopherol part was conserved and only the PEG chain length was altered, leading to a broad range of TPGS derivatives with PEG molecular weights between 200 and 6000 Da (TPGS 200, 238, 400, 600, 1500, 2000, 3350, 3500, 4000 and 6000; Figure 2-1). Two analogues (TPGS 750 OMe and TPGS 1100 OMe) contained a mono-methyl-ether group instead of a free hydroxyl group at the end of the PEG chain. The second group of TPGS analogues encompassed molecules with an average PEG chain length of 22 monomers (1000 Da) but varying hydrophobic moieties in exchange for alpha-tocopherol (Figure 2-2). In particular gamma-tocopherol, 4-octylphenol, phytol, cholesterol and thioctic acid were employed. Because thioctic acid is a carboxylic acid the formation of a direct ester with PEG 1000 via its carboxyl group negated the need for a succinate linker.



Analogue	n	R		Analogue	n	R
TPGS 200	4	H		TPGS 1500	33	H
TPGS 238	5	H		TPGS 2000	45	H
TPGS 400	9	H		TPGS 3350	76	H
TPGS 600	13	H		TPGS 3350	79	H
TPGS 750-OMe	16	CH ₃		TPGS 4000	91	H
TPGS 1000	22	H		TPGS 6000	136	H
TPGS 1100-OMe	24	CH ₃				

Figure 2-1 General structure of TPGS and novel analogues with modified PEG chain properties.

In this first part of the dissertation, the novel analogues were tested in a bidirectional Caco-2 transport assay conducted to investigate their ability to modulate efflux of the model P-gp substrates RHO, a fluorescent dye, and ³H-digoxin (DIG), a cardiac glycoside. Cytotoxicity indicators such as transepithelial electrical resistance (TEER) and lactate dehydrogenase (LDH) release were investigated. Moreover, physicochemical properties of the analogues were determined experimentally (CMC) or *in silico* and correlated to the inhibitory activity in a structure activity relationship (SAR) study. Based on the preliminary results, additional TPGS analogues were synthesized and the SAR working hypothesis further refined.

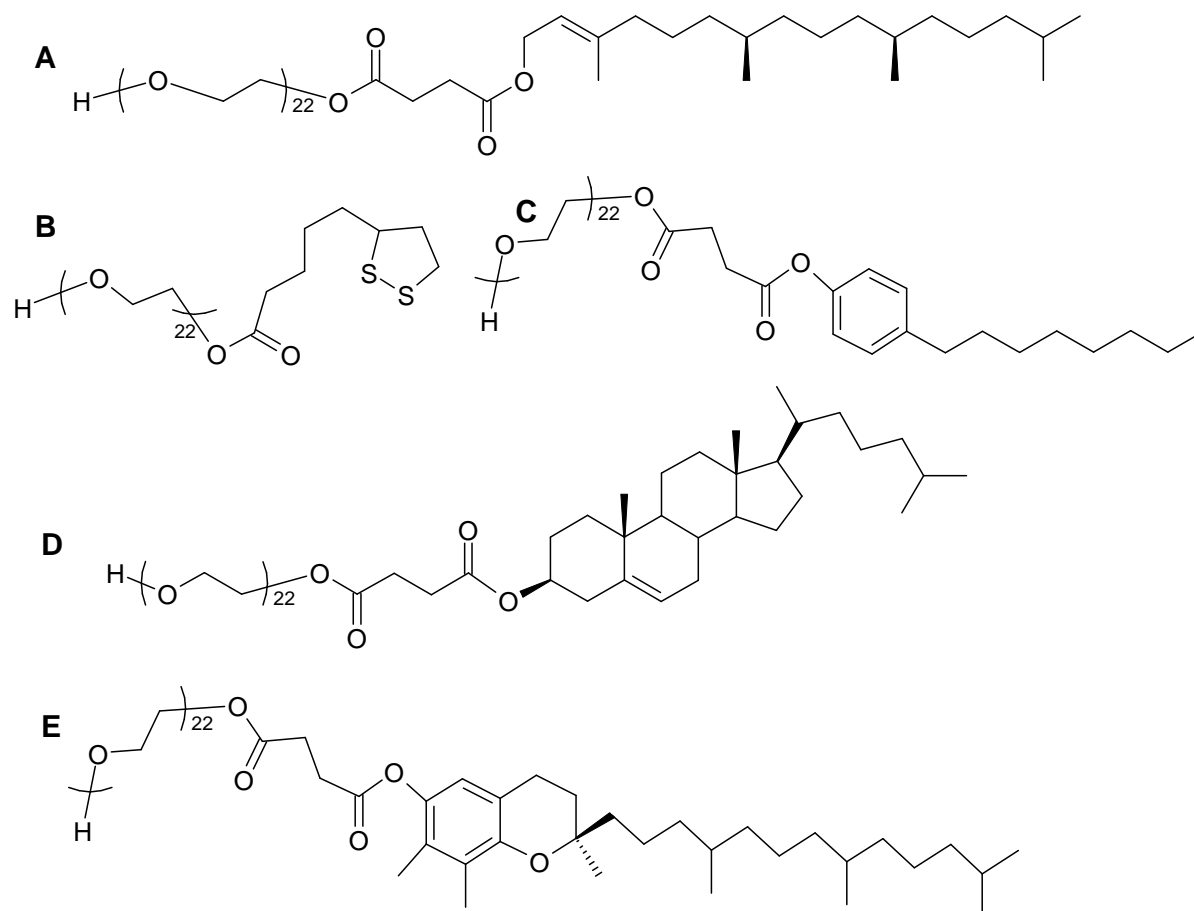


Figure 2-2 Structures of TPGS analogues with modified hydrophobic moieties: A Phytol PEG 1000 succinate, B Thioctic acid PEG 1000 ester, C 4-Octylphenyl PEG 1000 succinate, D Cholesteryl PEG 1000 succinate, E Gamma-tocopheryl PEG 1000 succinate.

2.2 Materials and methods

2.2.1 Materials

TPGS 1000, alpha-tocopherol, alpha-tocopherol succinate and all TPGS derivatives were obtained from Eastman Chemical Company (TN, USA). Transwell permeable filter inserts (3460, pore size 0.4 μM , 1.13 cm^2) were obtained from Corning B.V Life Sciences (Schiphol-Rijk, Netherlands). Dulbecco's modified Eagle's medium (DMEM), non-essential aminoacids (NEAA) and fetal bovine serum (FBS) were purchased from GIBCO (Invitrogen GmbH.; Karlsruhe, Germany). The "cytotoxicity detection kit (LDH)" was from Roche Diagnostics (Mannheim, Germany). Rhodamine 123 (RHO), ^3H -digoxin (specific activity 6.4 Ci/mmol), non-labelled digoxin, bovine serum albumin (BSA), PEG 1000 and all other chemicals were purchased from Sigma-Aldrich (Taufkirchen, Germany).

2.2.2 Synthesis of TPGS

All syntheses were performed at Eastman Chemical Company according to the following general synthetic procedure: UPS grade alpha-tocopherol succinate (3.25 g, 6.12 mMol) was dissolved in dichloromethane (20 ml) and 1.1 equivalents of the corresponding polyethylene glycol added and stirred at room temperature. DMAP (4-dimethylaminopyridine; 0.1 equivalents) and DCC (N, N'-dicyclohexylcarbodiimide, 1.1 equivalents) were sequentially added. The reaction vessel was capped and stirred overnight. The reaction mixture was Büchner filtered, and the filtrate concentrated under reduced pressure to afford crude product(s). Whenever indicated, products were then purified as their mono- and di-ester mixtures via preparative HPLC (Dynamax Microsorb C8, 250 x 41.4 mM I.d., 8 μM particles, 60 Å pore) using mobile phases (A, 25/75 methanol/acetonitrile (ACN); B, 25/75 iso-propyl alcohol (IPA)/ACN; C, IPA) with general gradient conditions of A for 24 min, B for 6 min and C for 12 min at a flow rate of ~80 ml/min.

2.2.3 Cell culture

Caco-2 cells, clone C2BBE1, were purchased at passage 60 from American Type Culture Collection (ATCC; Manassas, VA, USA) and experiments conducted using passages 70-92. Cells were grown to ~90% confluence in 75 cm^2 T-flasks with

DMEM supplemented with 10% FBS and 1% NEAA. Cells were grown at a temperature of $37.0 \pm 0.5^\circ\text{C}$ in an atmosphere of ~85 % relative humidity and ~5% CO_2 and culture medium was changed every second day. Cells were seeded on Transwell inserts (pore size $0.4 \mu\text{M}$, 1.13 cm^2) at a density of ~60,000 cells/ cm^2 . TEER was measured and only monolayers with a TEER $> 350 \Omega \cdot \text{cm}^2$ with background subtracted were used for transport studies.

2.2.4 Preparation of TPGS stock solutions

All TPGS analogue stock solutions (33 mM), except TPGS 200, 238, and 3350, were prepared immediately prior to experiments in Krebs Ringer Buffer pH 7.4 (KRB: 14 mM NaCl, 0.3 mM KCl, 1 mM HEPES, 0.4 mM glucose, 0.14 mM CaCl_2 , 0.25 mM MgCl_2 , 0.15_{mM} K_2HPO_4). TPGS 200, 238, and 3350 as well as vitamin E stock solutions were prepared using DMSO. Cholesterol and cholesterol succinate stock solutions were prepared in ethanol 96%. Stock solutions were diluted (1:1000) to give a final TPGS derivative concentration of $33 \mu\text{M}$. Both DMSO and ethanol 96% were found to have no influence on RHO/DIG transport in a 1:1000 dilution (data not shown). To generate dose-response curves, dilutions of the stock solutions with the corresponding solvent were prepared and then diluted 1:1000 with KRB/RHO/DIG to afford the final concentration.

2.2.5 Transport assay

Caco-2 monolayers were used 21-25 days after seeding. Transport of the P-gp model substrates RHO and DIG was assessed in absorptive (apical to basolateral, $\text{Ap} \rightarrow \text{Bl}$) and secretory (basolateral to apical, $\text{Bl} \rightarrow \text{Ap}$) directions. Prior to the transport experiments, unless otherwise denoted, monolayers were pre-incubated (1 h) with the respective TPGS analogue ($33 \mu\text{M}$ in KRB pH 7.4) on both sides. Subsequently, at $t = 0 \text{ min}$, the substrate solution, consisting of RHO ($13 \mu\text{M}$) or DIG ($1 \mu\text{M}$) in KRB pH 7.4, respectively, was added to the donor compartment. To study RHO transport pure KRB pH 7.4 was added to the receiver compartment; in the DIG experiments the receiver solution consisted of 1% BSA in KRB pH 7.4. All solutions also contained the TPGS analogue ($33 \mu\text{M}$).

In some experiments standard pre-incubation conditions were modified to study influence of experimental protocol: Overall pre-incubation time was always 60 min. However, pre-incubation with KRB containing TPGS was varied between 0 and 60 min, *i.e.* pre-incubation time 15 min means 45 min of pre-incubation with KRB, followed by 15 min incubation with KRB containing TPGS (33 μM). In experiments studying the influence of the side of surfactant application, pre-incubation took place for 60 min in pure KRB containing no TPGS. Before the experiment was commenced, TPGS was added to the apical side only, to the basolateral side only, or to both sides.

Throughout all experiments, monolayers were agitated using an orbital shaker (IKA®-Werke GmbH & CO KG; Staufen, Germany) at 100 ± 20 rpm. Samples were taken after 30, 60, 120, 180, 240, and 300 min from the receiver compartment. After each sampling, an equal volume of fresh transport buffer ($\sim 37^\circ\text{C}$) was added to the receiver compartment. Experiments were performed over 3 passages, each directional transport experiment comprising a total of $n = 18$, with the exception of the DIG experiments, dose-response curves and control experiments, where $n = 9$. To ensure integrity of the monolayers, TEER values were measured on the day of the experiment, after the pre-incubation, and at the end of the experiment.

2.2.6 Sample analysis

RHO was quantified using a CytoFluor-II fluorescence plate reader (Perseptive Biosystems; Weiterstadt, Germany) operating at excitation wavelength of 485 nm and emission wavelength of 530 nm. Fluorescence was linear in a range between 0.006 μM and 6.5 μM and the detection was reproducible with a standard deviation $< 2.0\%$. The limit of quantification (LOQ) was 0.006 μM . The detection was accurate with a relative standard deviation of 0.45%, 1.6%, and 3.5% at 6.5 μM , 0.5 μM and 0.01 μM , respectively. To take possible quenching into account, all calibration curves were generated in the presence of the respective tenside.

^3H labelled DIG samples were collected in scintillation vials and mixed with 2 ml of Ultima Gold scintillation cocktail (Perkin Elmer). Activity of these samples was assessed in a Tri-Carb liquid scintillation analyzer (Perkin Elmer).

2.2.7 Data processing and statistical analysis

Flux was determined using receiver compartment steady-state appearance rates of RHO/ DIG ($\Delta Q/\Delta t$; $\mu\text{g/s}$). Apparent permeability (P_{app}) was calculated according to:

$$P_{app} = (\Delta Q/\Delta t) * (1/A) * (1/C_0)$$

where A (cm^2) is the nominal surface area of the monolayer and C_0 ($\mu\text{g/ml}$) is the RHO concentration in the donor compartment at $t=0$.

Relative change of P_{app} (cm/s) was calculated according to the equation:

$$\begin{aligned} \text{rel. increase of absorptive transport} &= \left| (1 - P_{app}(\text{Ap} \rightarrow \text{BI})_{\text{test}} / P_{app}(\text{Ap} \rightarrow \text{BI})_{\text{control}}) * 100 \right| \\ \text{rel. decrease of secretory transport} &= \left| (1 - P_{app}(\text{BI} \rightarrow \text{Ap})_{\text{test}} / P_{app}(\text{BI} \rightarrow \text{Ap})_{\text{control}}) * 100 \right| \end{aligned}$$

where $P_{app \text{ control}}$ is the absorptive/ secretory transport in the absence of TPGS or any P-gp modulator and $P_{app \text{ test}}$ represents the respective values in the presence of the investigated substance.

Additionally, the degree of inhibition (DI) was calculated as a measure of the overall extent of P-gp inhibition. DI was defined as:

$$\text{DI} = (P_{app}(\text{BI} \rightarrow \text{Ap})_{\text{test}} - P_{app}(\text{Ap} \rightarrow \text{BI})_{\text{test}}) / (P_{app}(\text{BI} \rightarrow \text{Ap})_{\text{control}} - P_{app}(\text{Ap} \rightarrow \text{BI})_{\text{control}}) * 100$$

2.2.8 Cytotoxicity

LDH is a cytosolic enzyme that is readily released upon cell membrane damage. Hence, LDH may be used as a tool to monitor cellular toxicity. LDH released into the assay medium can be measured via a coupled enzymatic assay. Conversion of the yellow tetrazolium salt (2-[4-iodophenyl]-3-[4-nitrophenyl]-5-phenyltetrazolium chloride) into a red formazan salt is colorimetrically detected at 490 nm. Caco-2 cells were grown on 96-well tissue culture plates with a flat bottom (Greiner Bio-One GmbH; Frickenhausen, Germany) for 21 days as previously described. Monolayers were incubated (4 h) with 10 different concentrations ranging between 19.5 μM and 10 mM of the respective TPGS derivative in fresh Hank's balanced salt solution (HBSS) ($\sim 37^\circ\text{C}$) pH 7.4 containing 1% BSA. After the incubation, LDH release into the supernatant was determined using the cytotoxicity LDH kit as described by

Roche Diagnostics. Fresh HBSS/BSA (1%) pH 7.4 and Triton-X 100 (0.1%) in HBSS/BSA (1%) pH 7.4 were used as negative and positive controls, respectively. LDH release has been expressed (Fig. 5) relative to control values. Experiments were performed with an n=8 for each concentration.

2.2.9 Determination of the critical micelle concentration (CMC)

Using the Du Nouy ring method, CMC's were determined from surface tension measurements performed with an Interfacial-Tensiometer K8600 (Kruess, Germany). All measurements were conducted in KRB pH 7.4 at 37°C in the absence of cells. Two independent experiments were performed with 3 measurements per concentration (n=6).

2.2.10 Computational modelling

Computational modelling was conducted at Eastman Chemical Company using a Dell™ computer equipped with a Pentium(R) 4 CPU (2.40 GHz) containing 1.5 GB of RAM. Chemical structures were drawn with CS Chem-Draw Ultra® (version 6.0.1, Cambridge Soft Corporation) and copied into CS Chem3D Ultra® (version 6.0, Cambridge Soft Corporation). Gaussian 03W® (Version 6.0) was installed and used. The structures were initially inputted so that the repeating PEG chain length was linear. For each molecule, a molecular mechanics (MM) minimization was performed with a root-mean-square (RMS) of 0.01. Next, molecular dynamics was conducted (parameters: 2.0 fs step interval, 1 kcal/atom/ps, and 310 K) to afford structures containing coiled PEG units. Subsequently, Gaussian® molecular mechanics (UFF, 6-31G basis set) was conducted [29]; afterwards, the property server was used to compute theoretical Connolly Molecular Area (CMA), Connolly Solvent-Excluded Volume (SEV), and ClogP (octanol/water).

2.2.11 Data fitting and statistical analysis

Data was fitted empirically to respective equations using Sigma Plot 9.0 graphing software (Systat Software Inc.; Point Richmond, CA, USA).

Results are expressed as mean ± standard deviation (SD). Significance of difference in the P_{app} values was determined by one-way analysis of variances (ANOVA) followed by Neumann-Keuls-Student post-hoc tests.

2.3 Results

2.3.1 Transport assay

2.3.1.1 Analogues with modified PEG chain length

In the first set of transport experiments, TPGS analogues with modified PEG chain lengths and a free hydroxyl group at the end of the PEG chain were investigated (Figure 2-1). The original data set encompassed TPGS 200, 238, 400, 600, 1000, 2000, 3350, 3500, 4000 and 6000.

Among these analogues, TPGS 1000 had the greatest influence on RHO efflux (Figure 2-3). TPGS 1000 significantly ($P < 0.001$) increased the absorptive transport of RHO from $0.36 \pm 0.05 \cdot 10^{-6}$ cm/s (control) to $0.66 \pm 0.07 \cdot 10^{-6}$ cm/s (~82% increase). Resulting in an overall reduction of RHO efflux ratio (ER) from 18.0 ± 5.3 to 2.6 ± 1.0 (Table 2-2), secretory transport of RHO was likewise significantly ($P < 0.001$) reduced from $6.47 \pm 0.85 \cdot 10^{-6}$ cm/s in the control group to $1.71 \pm 0.29 \cdot 10^{-6}$ cm/s (~74% decrease). The effects were still noteworthy, but not as pronounced for TPGS 238, 400, 600, 2000, 3350, and 3500. No significant influence was observed for TPGS 200, 4000, and 6000. Furthermore, all analogues displayed comparable effects on absorptive (Ap→Bi) and secretory (Bi→Ap) RHO transport.

To further evaluate the influence of PEG chain length, the chain length was plotted against the observed results (increase of absorptive transport as well as decrease of secretory transport) and fitted empirically to different equations. In both cases, the activity pattern may be best described by a Weibull distribution (Figure 2-4) ($F(x) = 1 - \exp[-(x/b)^c]$, $0 < x$) with r^2 values of 0.94 and 0.91, respectively. Using these calculations, the predicted optimal PEG chain length for absorptive and secretory RHO transport resides between 1581 ± 209 and 1182 ± 476 Da, respectively.

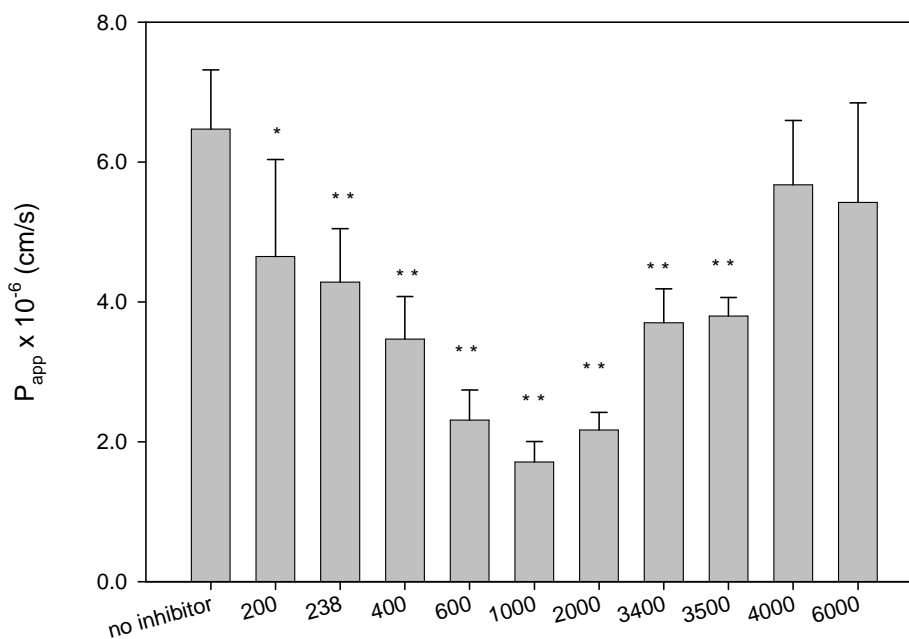
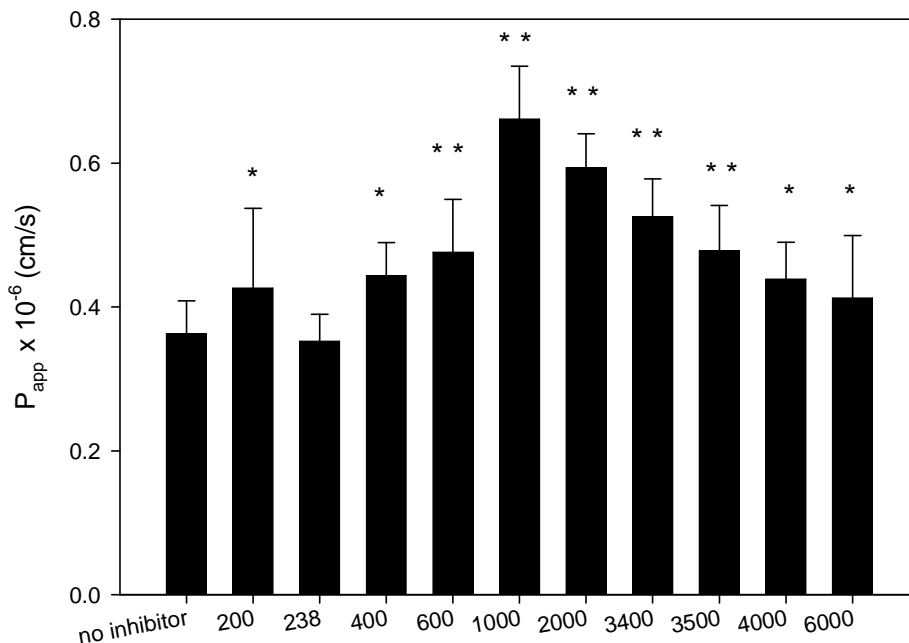


Figure 2-3 RHO transport across Caco-2 monolayers in the absence and presence of TPGS analogues possessing different PEG chain lengths; above: absorptive transport Ap→Bl; below: secretory transport Bl→Ap; mean \pm SD, n = 18; bars marked with * are significantly different from negative control. (P < 0.05) and ** are very significantly different (P < 0.001).

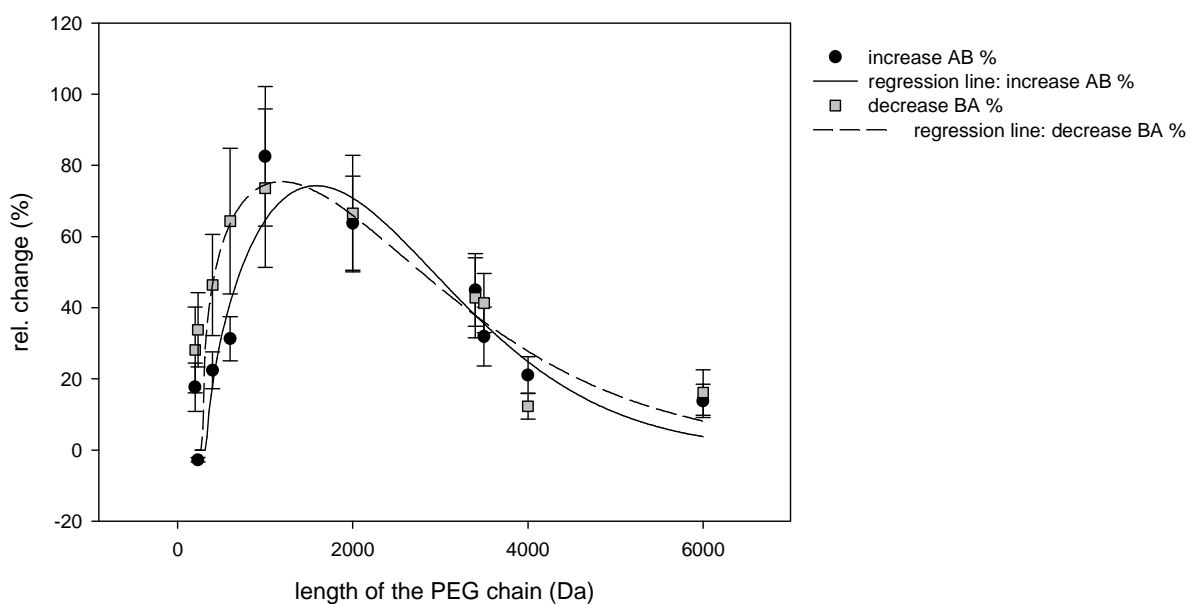


Figure 2-4 PEG chain length dependency of P-gp inhibitory effect of TPGS 1000 in absorptive as well as secretory direction; mean \pm SD, n= 18.

2.3.1.2 Testing of the PEG chain length hypothesis and influence of purification

After the first set of studies, the proposed PEG chain length theory (see 2.3.1.1), was tested in a head to head comparison of novel TPGS analogues; PEG chain lengths in the range of the predicted optima (TPGS 750-OMe, TPGS 1000, TPGS 1100-OMe, TPGS 1500, and TPGS 2000) were used. Two of these analogues, TPGS 750-OMe and TPGS 1100-OMe, differed in the terminal hydroxyl group of the PEG chain, which was capped off as a mono-methyl-ether.

Previous to the head to head comparison, the influence of TPGS analogue purification on the inhibitory potency was determined in a dose-response study (Figure 2-5) employing different concentrations of commercial TPGS 1000 (83-85%) and highly purified (>99%) TPGS 1000 as modulators of P-gp mediated RHO efflux.

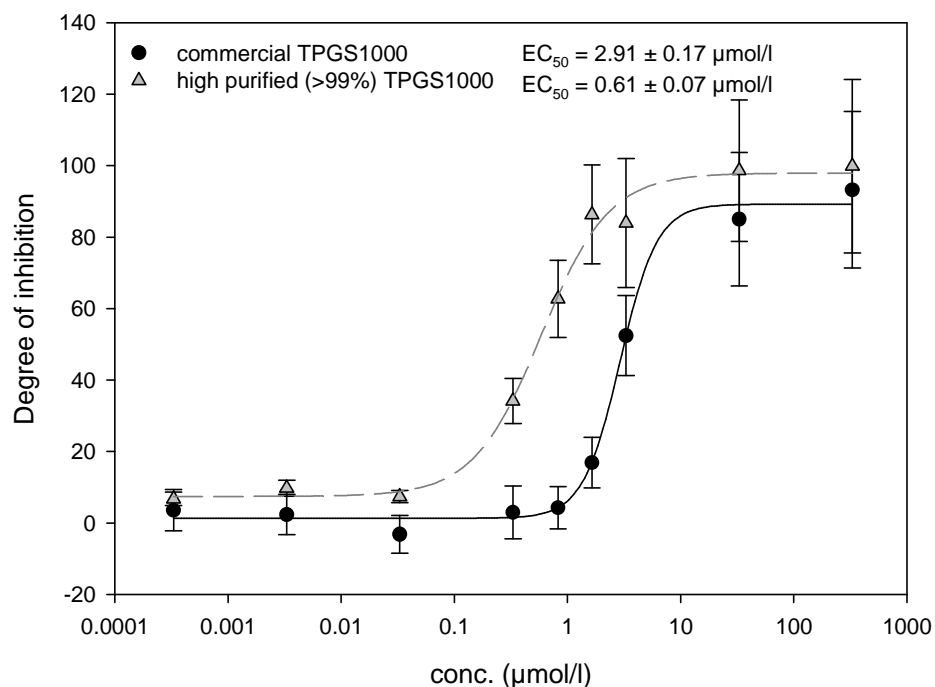


Figure 2-5 Dose response curve of commercial TPGS 1000 and high purified (>99%) TPGS 1000 in Caco-2 transport studies with the fluorescent dye RHO; mean \pm SD, $n = 9$.

At the highest concentrations tested (33 μM and 330 μM), both purified and non-purified TPGS 1000 achieved almost complete inhibition of P-gp with no statistically significant differences between both qualities. The inhibitory effect levelled out in this concentration range. However, as reflected in its EC_{50} value, the inhibitory values were slightly higher for purified TPGS 1000 and its onset of inhibitory action occurred at lower concentrations compared to the non-purified material, purified TPGS 1000 EC_{50} ($0.61 \pm 0.07 \mu\text{M}$) was about 5 times lower than the EC_{50} of commercially available, non-purified TPGS 1000 ($2.91 \pm 0.17 \mu\text{M}$). As a result, highly purified materials were used in the subsequent head to head comparison of the different second generation TPGS derivatives. As indicated in the reduction of RHO ER from 18.6 ± 4.1 to values ≤ 4.5 (Table 2-1), all tested analogues, including the two TPGS methyl-ethers, significantly reduced RHO efflux.

Experiment	Ap→BI $P_{app} \times 10^{-6} \text{ cm/s} \pm \text{SD}$	BI→Ap $P_{app} \times 10^{-6} \text{ cm/s} \pm \text{SD}$	Efflux Ratio (ER) $\pm \text{SD}$
Control	0.22 \pm 0.02	4.1 \pm 0.6	18.6 \pm 4.1
TPGS 750-OMe	0.36 \pm 0.07	0.96 \pm 0.29	2.7 \pm 1.3
TPGS 1000	0.39 \pm 0.05	1.0 \pm 0.14	2.6 \pm 0.7
TPGS 1100-OMe	0.39 \pm 0.11	0.97 \pm 0.14	2.5 \pm 1.1
TPGS 1500	0.45 \pm 0.08	0.84 \pm 0.17	1.9 \pm 0.7
TPGS 2000	0.42 \pm 0.03	1.9 \pm 0.3	4.5 \pm 1.0

Table 2-1 RHO absorptive transport (Ap→BI), secretory transport (BI→Ap), and efflux ratio (ER) across Caco-2 monolayers in the presence of different TPGS analogues (33 μM) on both apical and basolateral sides at pH 7.4; mean \pm SD, n=9.

Consistent with PEG chain hypothesis, TPGS 1500 was the most potent P-gp inhibitor, increasing absorptive RHO transport from $0.22 \pm 0.02 \times 10^{-6} \text{ cm/s}$ to $0.45 \pm 0.08 \times 10^{-6} \text{ cm/s}$ (102% increase) and reducing secretory RHO transport from $4.1 \pm 0.6 \times 10^{-6} \text{ cm/s}$ to $0.84 \pm 0.17 \times 10^{-6} \text{ cm/s}$ (79% decrease) (Table 2-1). For all of these purified analogues, the influence on P-gp mediated transport in both directions was stronger than was to be expected from the previous SAR study, placing the new data points above the previously fitted Weibull curve in the original PEG chain length plot (Figure 2-6, grey plot). However, the new data points still follow the predicted trend, allowing for a new fitting of curves to the same function. Compared to the old predictions (0.94 and 0.91), the new Weibull curve showed slightly improved r^2 values (0.98 and 0.97) and a noticeable but not statistically significant ($P > 0.05$) shift of the PEG chain length maxima ($1466 \pm 125 \text{ Da}$ and $1271 \pm 123 \text{ Da}$ for absorptive and secretory transport, respectively).

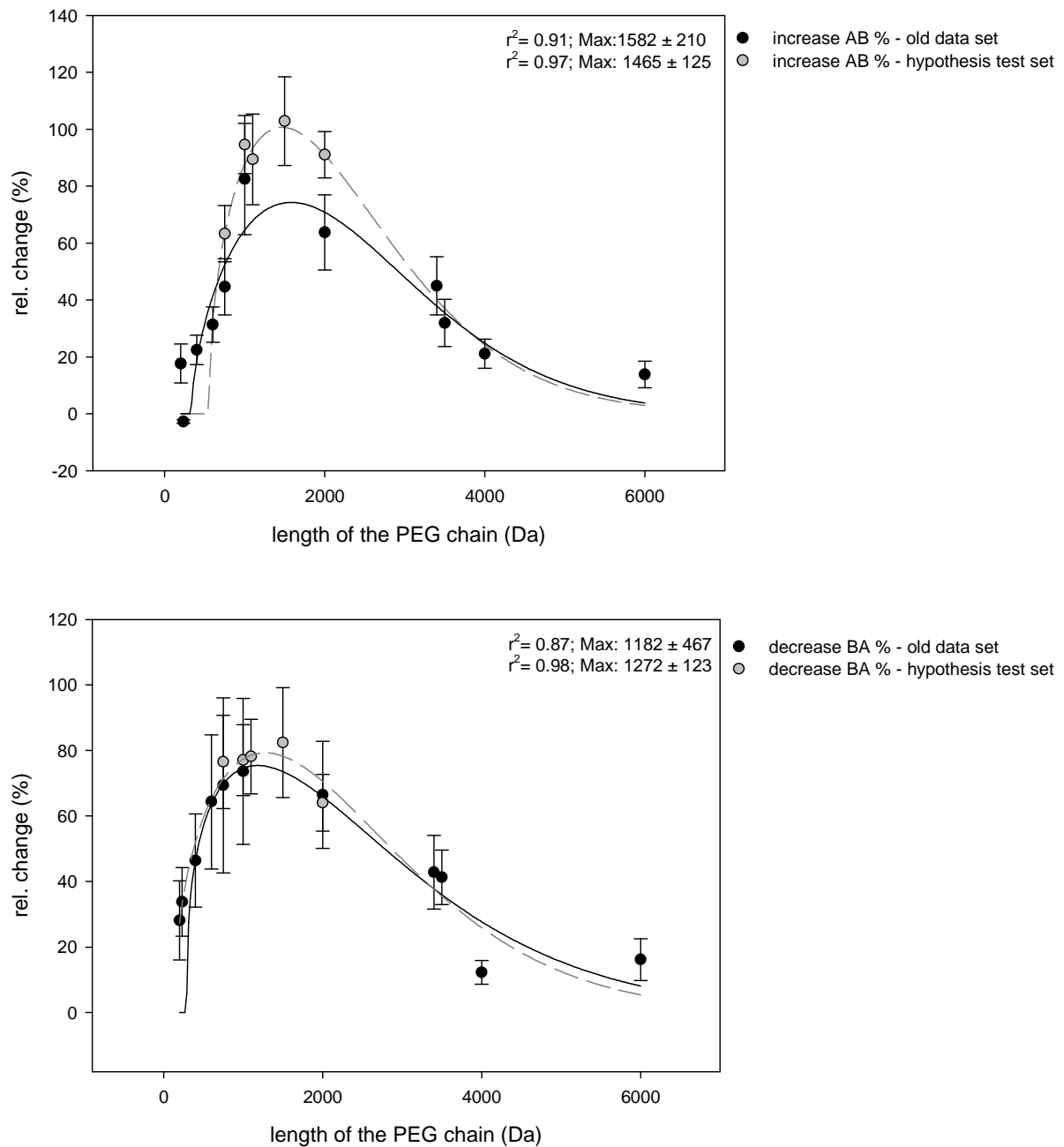


Figure 2-6 Dependence of TPGS PEG chain length: Weibull regression of relative absorptive transport increase (above) and relative secretory transport decrease (below); new data points and fit integrated into old plot; mean \pm SD; n = 18.

2.3.1.3 Variation of P-gp model substrate

Since little is known about the specificity of TPGS interaction with P-gp (and its different binding sites) and choice of substrate might influence the results, transport experiments were also conducted using ^3H -digoxin (DIG) as an alternative model P-gp substrate. Inhibitory effects of TPGS 1000 as a moderate P-gp inhibitor and TPGS 4000 as a non-modulator of P-gp activity were investigated. Furthermore the strong first generation P-gp inhibitor cyclosporine A (CsA, 15 μM) was included as a positive control.

		RHO (13 μM)	DIG (1μM)
Control	$P_{\text{app}}(\text{A} \rightarrow \text{B}) \times 10^{-6} \text{ cm/s}$	0.36 \pm 0.05	0.66 \pm 0.14
	$P_{\text{app}}(\text{B} \rightarrow \text{A}) \times 10^{-6} \text{ cm/s}$	6.47 \pm 0.85	11.41 \pm 0.54
	ER	18.0 \pm 5.3	17.3 \pm 4.4
CsA (15 μM)	$P_{\text{app}}(\text{A} \rightarrow \text{B}) \times 10^{-6} \text{ cm/s}$	0.80 \pm 0.05	1.45 \pm 0.11
	Increase (A \rightarrow B) %	121.2 \pm 20.2	118.7 \pm 32.6
	$P_{\text{app}}(\text{B} \rightarrow \text{A}) \times 10^{-6} \text{ cm/s}$	0.91 \pm 0.18	1.78 \pm 0.38
	Decrease (B \rightarrow A) %	86.0 \pm 28.4	84.3 \pm 11.9
	ER	1.1 \pm 0.3	1.2 \pm 0.2
TPGS 1000 (33 μM)	$P_{\text{app}}(\text{A} \rightarrow \text{B}) \times 10^{-6} \text{ cm/s}$	0.67 \pm 0.07	1.24 \pm 0.20
	Increase (A \rightarrow B) %	82.5 \pm 19.6	87.3 \pm 36.9
	$P_{\text{app}}(\text{B} \rightarrow \text{A}) \times 10^{-6} \text{ cm/s}$	1.71 \pm 0.29	4.23 \pm 0.58
	Decrease (B \rightarrow A) %	73.6 \pm 22.3	62.8 \pm 17.5
	ER	2.6 \pm 1.0	3.4 \pm 1.5
TPGS 4000 (33 μM)	$P_{\text{app}}(\text{A} \rightarrow \text{B}) \times 10^{-6} \text{ cm/s}$	0.44 \pm 0.05	0.76 \pm 0.11
	Increase (A \rightarrow B) %	21.1 \pm 5.1	13.9 \pm 5.2
	$P_{\text{app}}(\text{B} \rightarrow \text{A}) \times 10^{-6} \text{ cm/s}$	5.67 \pm 0.92	8.66 \pm 0.63
	Decrease (B \rightarrow A) %	12.3 \pm 3.6	24.1 \pm 2.9
	ER	12.9 \pm 3.8	11.4 \pm 2.7

Table 2-2 Comparison of inhibitory effect of CsA (15 μM), TPGS 1000 (33 μM) and TPGS 4000 (33 μM) on RHO and DIG efflux in Caco-2 monolayers; mean \pm SD, n = 18 for RHO data, n = 9 for DIG data.

Independent of transport direction, and the presence or absence of a P-gp modulator, P_{app} values for DIG were about 2 times higher than RHO permeability data. Nevertheless, the total effects of all three tested P-gp inhibitors were

comparable in both experimental setups. Both CsA and TPGS 1000 significantly ($P < 0.05$) reduced DIG efflux ratio from 17.3 ± 4.4 to 1.2 ± 0.2 and 3.4 ± 1.5 , respectively. TPGS 4000 had no significant effect, only slightly lowering ER to 11.4 ± 2.7 . As indicated by the differences in relative increase (87.3 ± 36.9) and decrease (62.8 ± 17.5) of transport, the inhibitory influence of TPGS 1000 was slightly but not statistically significantly ($P = 0.091$) stronger in the absorptive direction than in the secretory direction.

2.3.1.4 Analogues with modified hydrophobic moieties

The second set of TPGS analogues evaluated in the RHO transport assay consisted of analogues with modified hydrophobic moieties (Figure 2-2). In a head to head comparison, commercial TPGS 1000, cholesteryl PEG 1000 succinate and gamma-TPGS 1000 all showed significant inhibitory effects on P-gp activity (Figure 2-7). Inhibition was most pronounced for cholesteryl PEG 1000 succinate, which increased absorptive transport from $0.41 \pm 0.02 \cdot 10^{-6}$ cm/s to $0.79 \pm 0.11 \cdot 10^{-6}$ cm/s and reduced secretory transport from $4.43 \pm 0.44 \cdot 10^{-6}$ cm/s to $0.93 \pm 0.22 \cdot 10^{-6}$ cm/s. Phytol PEG 1000 succinate and 4-octyl-phenyl PEG 1000 succinate had weak effects on RHO transport, while thioctic acid PEG 1000 ester showed no significant influence at all.

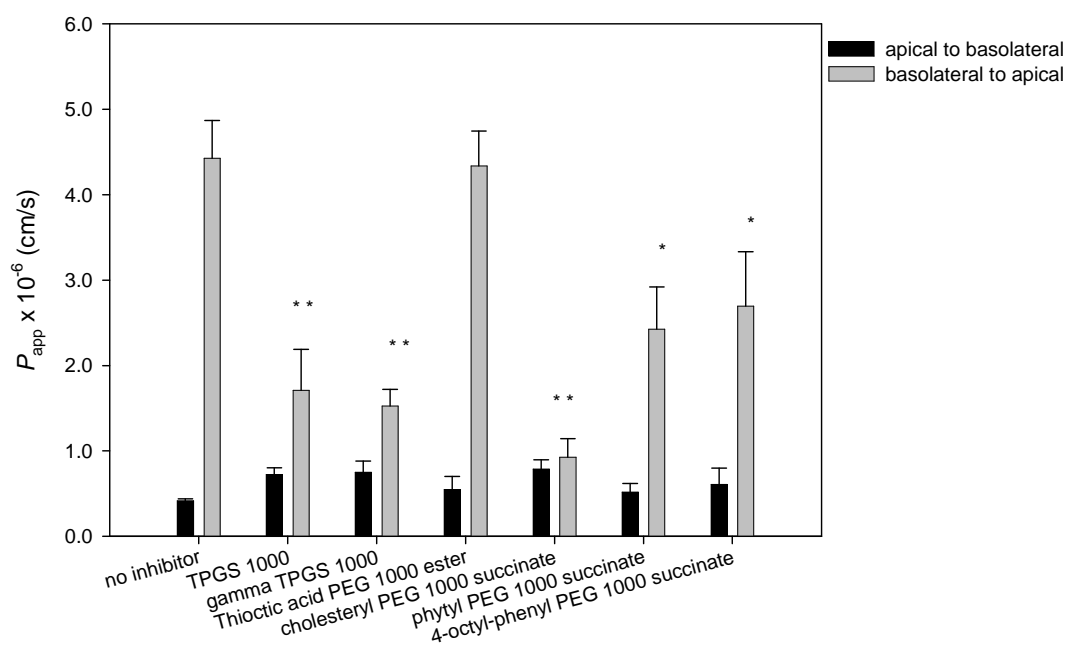


Figure 2-7 Influence of TPGS analogues with modified hydrophobic moieties on RHO transport across Caco-2 cell monolayers; mean \pm SD, $n = 18$.

To better quantify the differences in inhibitory potency between the two most potent P-gp modulators (TPGS 1000 and cholesteryl PEG 1000 succinate) a dose-response study with the two surfactants was conducted (Figure 2-8). At $0.47 \pm 0.05 \mu\text{M}$, the determined EC_{50} value for cholesteryl PEG 1000 succinate was significantly lower than the EC_{50} of commercial TPGS 1000 ($2.92 \pm 0.17 \mu\text{M}$). As was the case for the purified commercially available TPGS 1000, the inhibitory potency of the cholesterol derivative could be increased via purification of the monoester, i.e. by-products of its synthesis, such as the cholesteryl PEG 1000 succinate diester were removed. The purification of cholesteryl PEG 1000 succinate reduced the EC_{50} value to a level of $0.067 \pm 0.009 \mu\text{M}$.

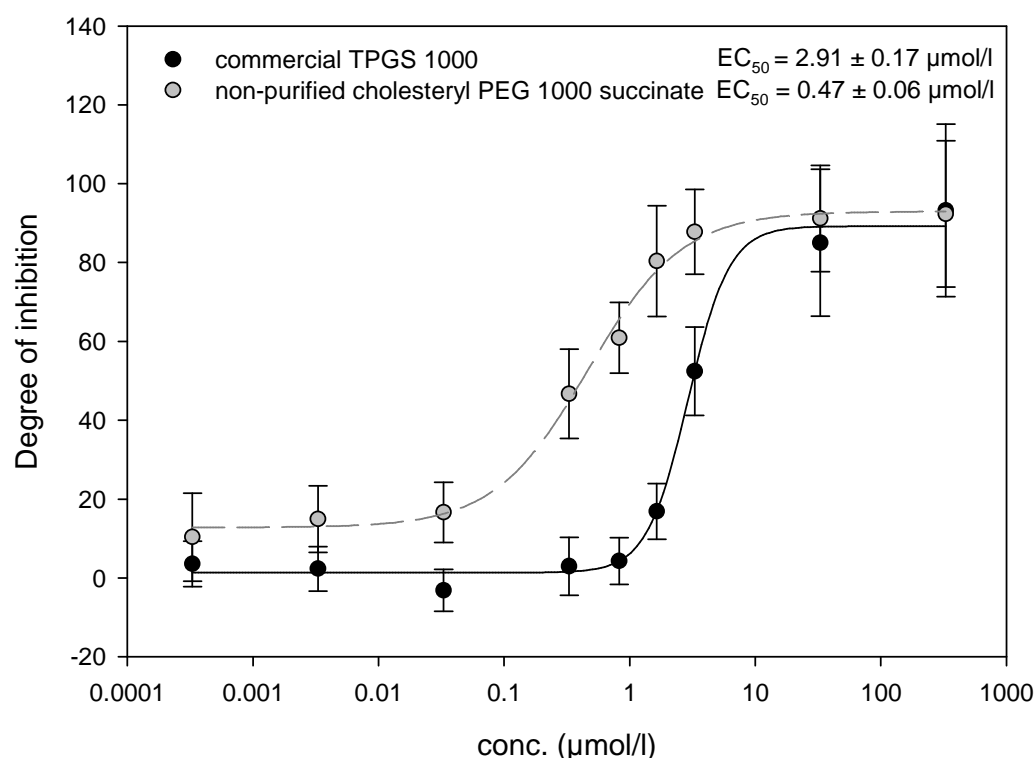


Figure 2-8 Dose response curve of commercial TPGS 1000 and non-purified and purified cholesteryl PEG 1000 succinate; mean \pm SD, $n = 9$.

2.3.1.5 Influence of pre-incubation time and side of application

Various investigators have reported differing results for effectiveness of *in vitro* P-gp inhibition by TPGS 1000 [58, 77, 101, 104]. Because the experimental conditions may account for these inconsistencies, we varied pre-incubation conditions,

surfactant application side and model substrate (RHO) concentration. Kinetics of RHO transport across Caco-2 cell monolayers were studied in the presence and absence of TPGS 1000 (33 μM) on both sides of the monolayer. In the absence of a P-gp modulator, absorptive RHO flux was linearly correlated to the employed RHO amount, while secretory RHO transport was saturable and followed a one-site saturation model ($F(x) = J_{\text{max}} * \text{abs}(x) / (K_M + \text{abs}(x))$) with a K_m value of $27.84 \pm 5.32 \mu\text{M}$ and J_{max} of $1.085 \mu\text{Mol/h/cm}^2$. On the addition of TPGS 1000, absorptive RHO transport increased, and secretory transport was reduced: both now followed linear kinetics over the tested RHO concentration range (0.1 to 50 μM).

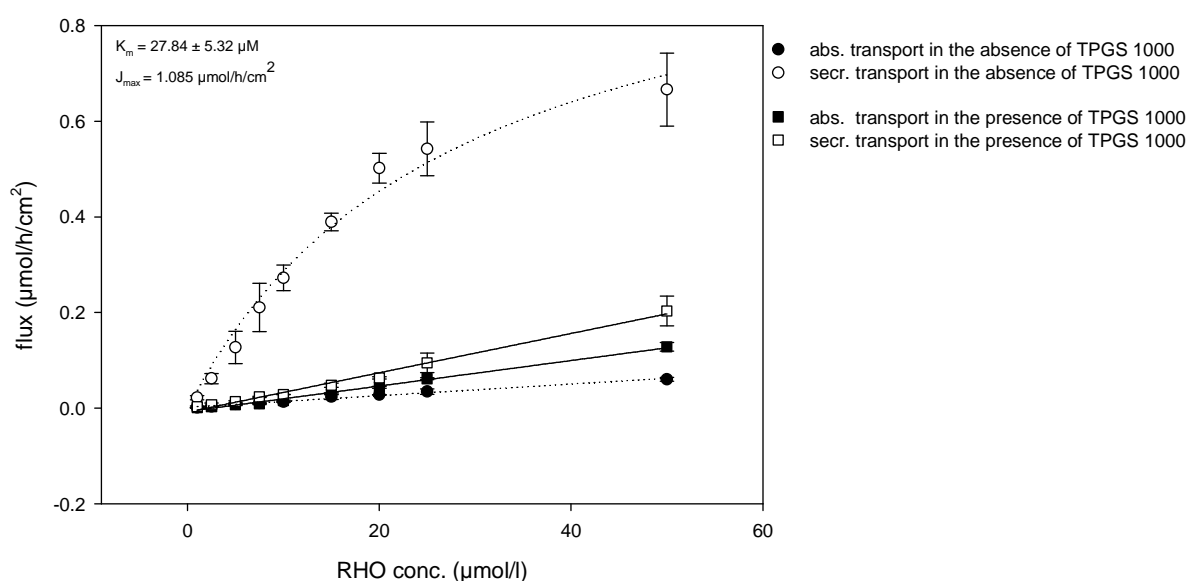


Figure 2-9 RHO kinetics in the presence and absence of TPGS 1000; mean \pm SD, $n = 9$; plots were fitted to linear curve for absorptive (Ap \rightarrow Bl) transport and secretory (Bl \rightarrow Ap) transport in the presence of TPGS 1000 and to a one site saturation model for secretory (Bl \rightarrow Ap) transport in the absence of TPGS 1000.

As represented in Figure 2-10 and Figure 2-11, bi-directional RHO transport was investigated using different pre-incubation times (0, 15, 30, 45 and 60 min) in the presence of TPGS 1000. The influence of TPGS 1000 on absorptive RHO transport was clearly time dependent: the shorter the pre-incubation time, the longer the delay in the onset of inhibition (Figure 2-10). As a result, if Caco-2 cell monolayers were pre-incubated for only 0, 15, or 30 min with TPGS 1000, the increase in absorptive permeability at the end of the experiment was weaker and steady state was never achieved, making the determination of meaningful P_{app} values nearly impossible. Optimum results with a maximal influence were reached after 45-60 min of pre-incubation.

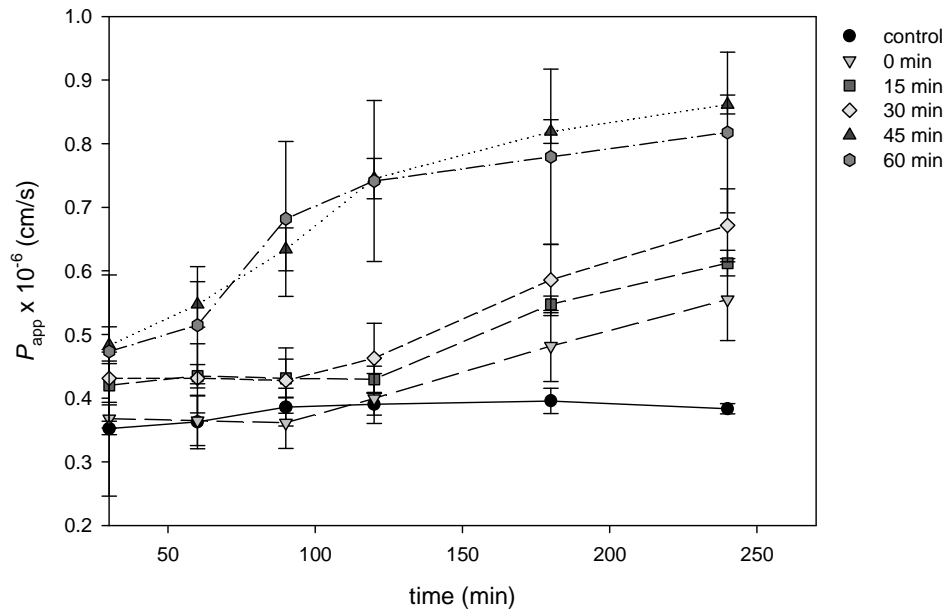


Figure 2-10 Influence of pre-incubation time on P-gp inhibitory effect of TPGS 1000: absorptive (Ap→BI) permeability of RHO in Caco-2 cell monolayers; mean ± SD, n = 9.

In the case of secretory RHO transport, regardless of the length of pre-incubation time, TPGS 1000 had a large effect relative to control (Figure 2-11). Yet, a clear increase in inhibition with pre-incubation time was noticeable.

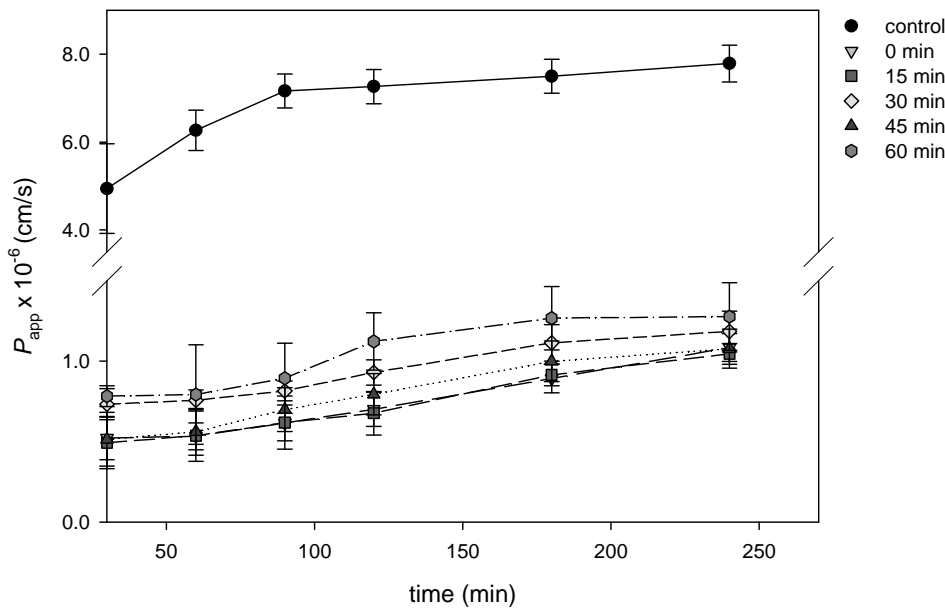


Figure 2-11 Influence of pre-incubation time on P-gp inhibitory effect of TPGS 1000: secretory (BI→Ap) permeability of RHO in Caco-2 cell monolayers; mean ± SD, n = 9.

In a next step the impact of application side of the inhibitor on absorptive and secretory RHO transport in the absence of pre-incubation was determined. In separate experiments, TPGS 1000 was placed on the apical side only, on the basolateral side only, and on both sides of the monolayer (Figure 2-12 and Figure 2-13). Independent of the application side, it took ~1.5-2.0 h to observe an enhancement in absorptive RHO transport rate. The effect was slightly delayed when TPGS 1000 was only placed on the basolateral side and also afforded lower, but not significantly different, permeability values after 300 min (Figure 2-12).

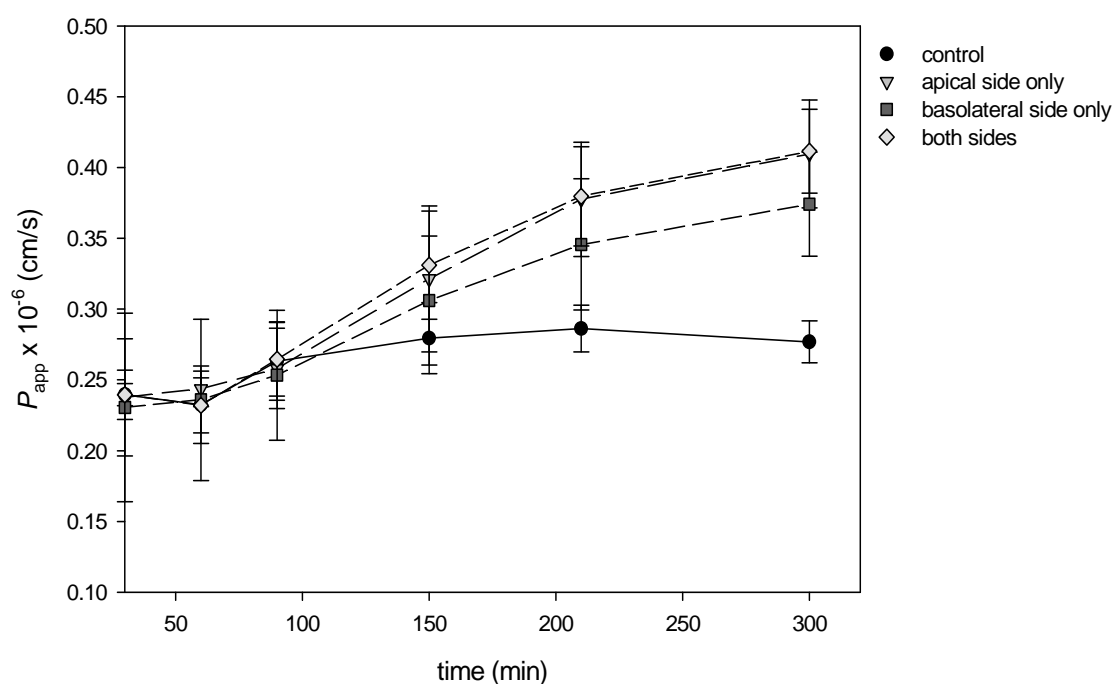


Figure 2-12 Influence of the application side on P-gp inhibitory effect of TPGS 1000; absorptive ($A_p \rightarrow B_l$) permeability of RHO in Caco-2 cell monolayers; mean \pm SD, $n = 9$.

The impact of TPGS 1000 on secretory RHO transport was instantaneous and showed the same time dependent behaviour as absorptive RHO transport. When TPGS 1000 was only placed on the basolateral side, significantly weaker effects on RHO efflux were observed. No differences could be found between applications on both sides versus only on the apical side of the monolayer (Figure 2-13).

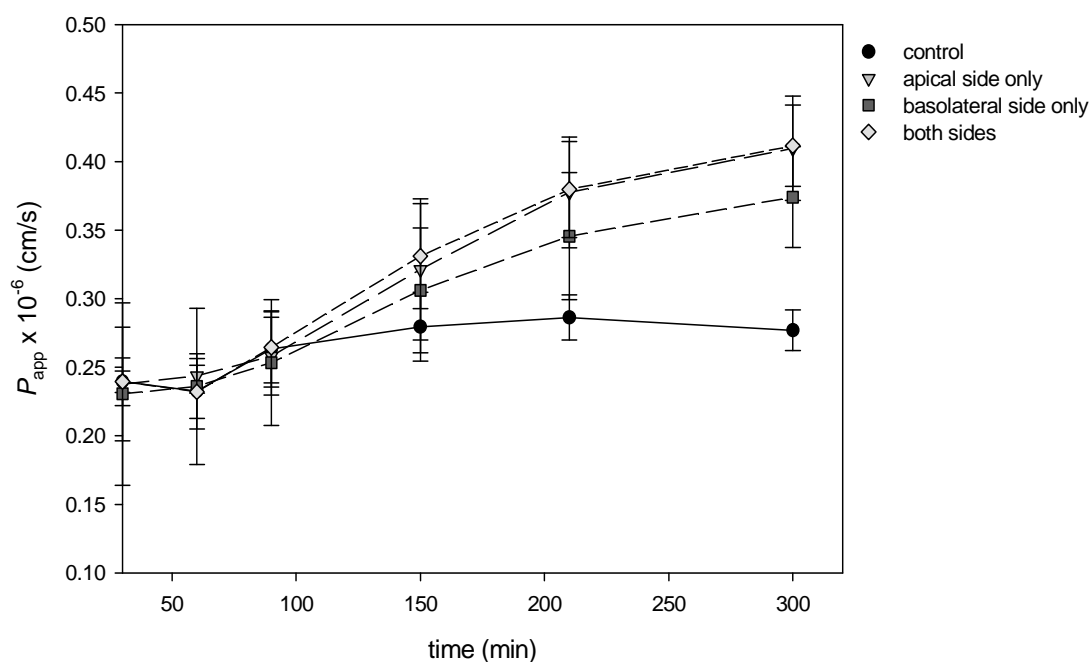


Figure 2-13 Influence of the application side on P-gp inhibitory effect of TPGS 1000; secretory (Bl→Ap) permeability of RHO in Caco-2 cell monolayers; mean \pm SD, n = 9.

2.3.1.6 Other surfactants

As examples of other non-ionic surfactants previously described to modulate P-gp activity, Tween 80 and Cremophor EL were included in the transport experiments. To compare their inhibitory properties to TPGS 1000, EC_{50} values were determined from dose-response curves (Table 3-4). The study revealed TPGS 1000 to be the strongest P-gp modulator of the three surfactants. Tween 80 and Cremophor EL both performed significantly worse at $18.4 \pm 6.5 \mu\text{M}$ and $24.7 \pm 10.2 \mu\text{M}$, respectively.

2.3.1.7 Control experiments with degradation products

Control experiments were performed. TPGS 1000 and cholesteryl PEG 1000 succinate degradation products (alpha-tocopherol, alpha-tocopherol succinate, cholesterol, and cholesterol succinate) and polyethylene glycol 1000 were tested at a concentration of $33 \mu\text{M}$ for their ability to inhibit RHO efflux (Figure 2-14). All 5 substances had no significant effects on RHO efflux, neither in absorptive nor in secretory direction. ER, as an overall indicator of efflux activity, therefore remained unchanged on addition of the degradation products ($ER > 11.5$). ER was very significantly reduced in the presence of TPGS 1000 (2.5 ± 1.1) and cholesteryl PEG 1000 succinate (1.4 ± 0.5).

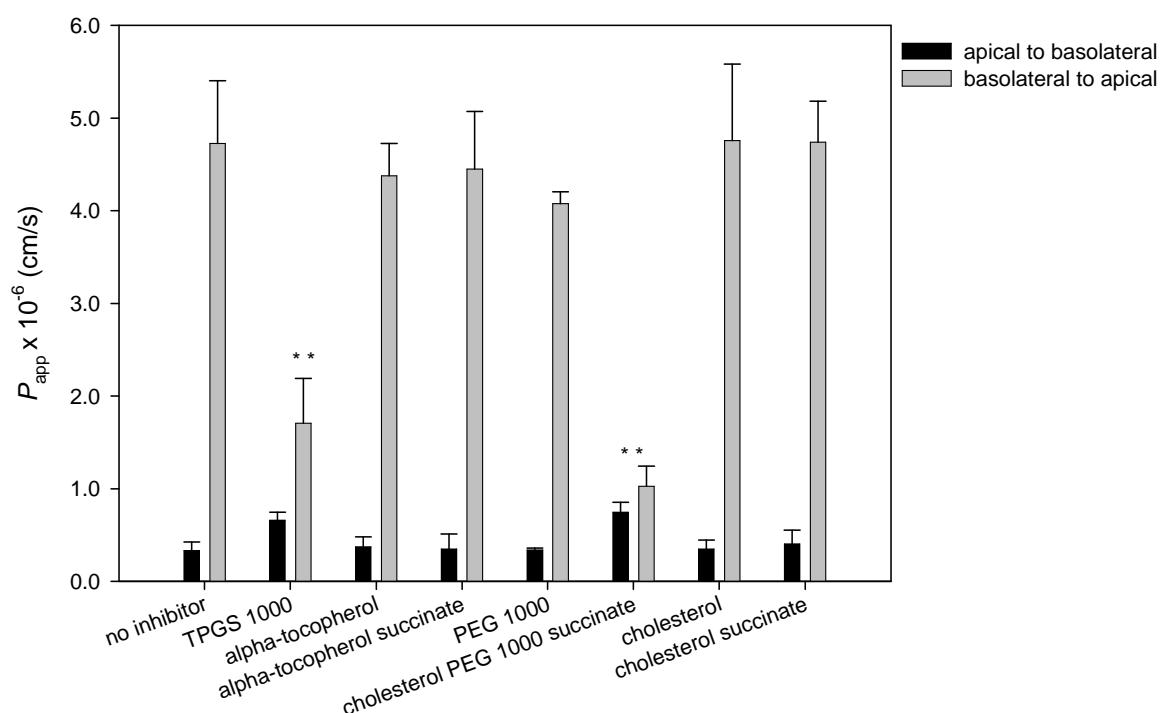


Figure 2-14: Influence of alpha-tocopherol, alpha-tocopherol succinate, cholesterol, cholesterol succinate and PEG 1000 on RHO transport across Caco-2 monolayers; mean \pm SD, n=9; bars marked with ** are very significantly different from control ($P < 0.001$).

2.3.2 Cytotoxicity

As compared to control values, none of the TPGS analogues, whether with modified PEG chains or hydrophobic cores, showed relevant LDH cytotoxicity at 33 μ M, the concentration employed in the transport assay. TPGS 200, 232, 400, 600, 750-OMe, 3350, and 4000 had no significant effect at any of the tested concentrations and never reached a relative LDH release of 20% or higher (Figure 2-15). TPGS 2000, 3500 and 6000 slightly raised the LDH release at concentrations > 5 mM. However, compared to a 1% Triton X-100 solution, relative cytotoxicity was still at a reasonably low level between 20 and 42%. TPGS 1000 showed the highest increase in LDH release among the analogues with conserved alpha-tocopherol cores, starting at a concentration of 625 μ M and reaching a maximum cytotoxicity of 82 (\pm 32)% at a concentration of 10 mM.

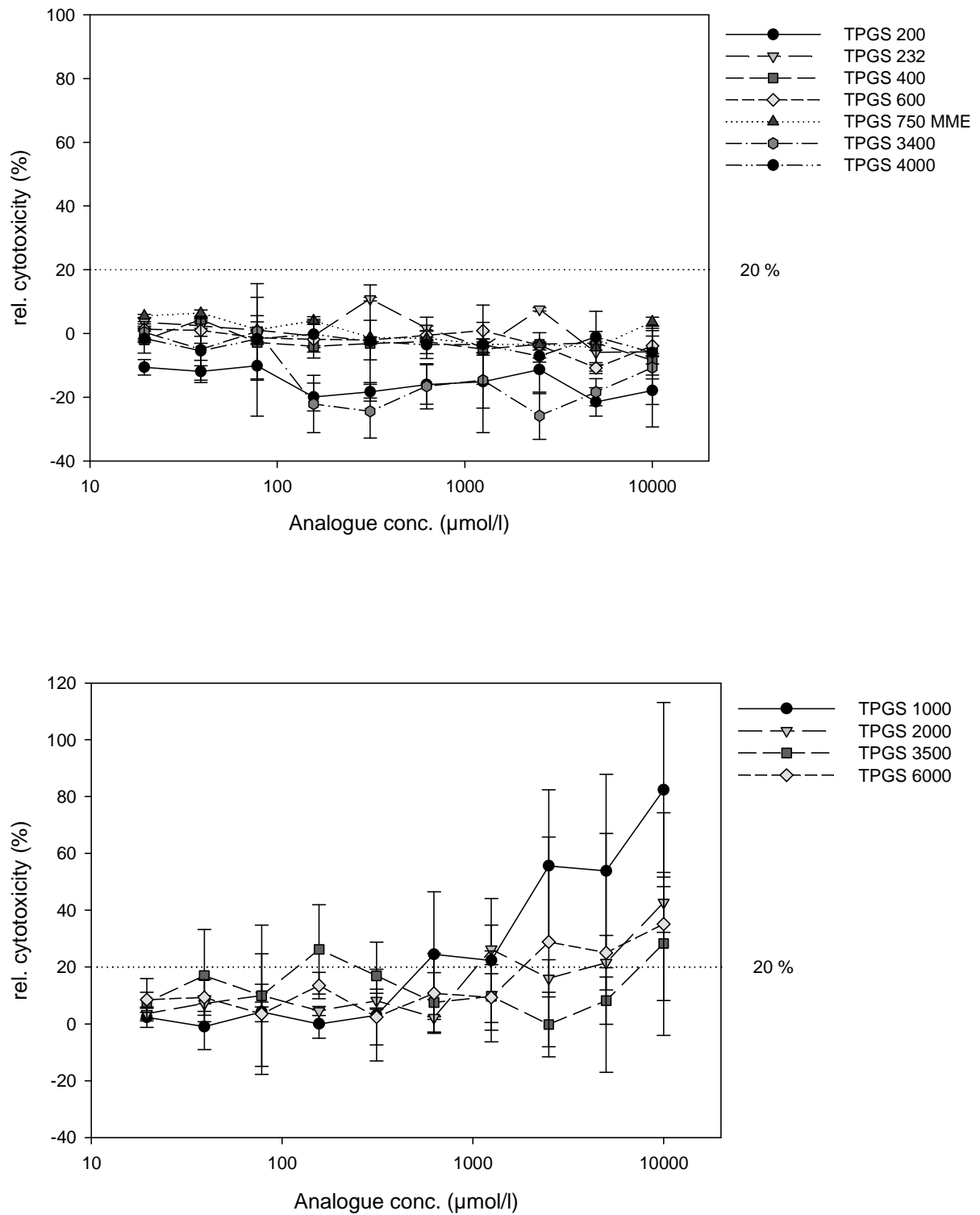


Figure 2-15 Rel. cytotoxicity of TPGS analogues with modified PEG chain length compared to positive control (0.1% triton X-100) in the LDH release assay; mean \pm SD; n = 12.

In general, analogues with modified hydrophobic moieties generally demonstrated higher LDH cytotoxicity (Figure 2-16). Among these surfactants, 4-octyl phenyl PEG 1000 succinate had the highest cytotoxic potential, reaching half maximal cytotoxic effect at a concentration of 0.24 ± 0.03 mM. Cholesteryl PEG 1000 succinate and phytol PEG 1000 succinate also showed significant cytotoxic effects, but at higher concentrations with IC_{50} values of 0.89 ± 0.09 mM and 0.97 ± 0.11 mM, respectively. The other analogues displayed only slightly increased LDH release with an overall ranking of 4-octyl-phenyl PEG 1000 succinate > cholesteryl PEG 1000 succinate = phytol PEG 1000 succinate > TPGS 1000 = gamma-TPGS 1000 > thioctic acid PEG 1000 ester.

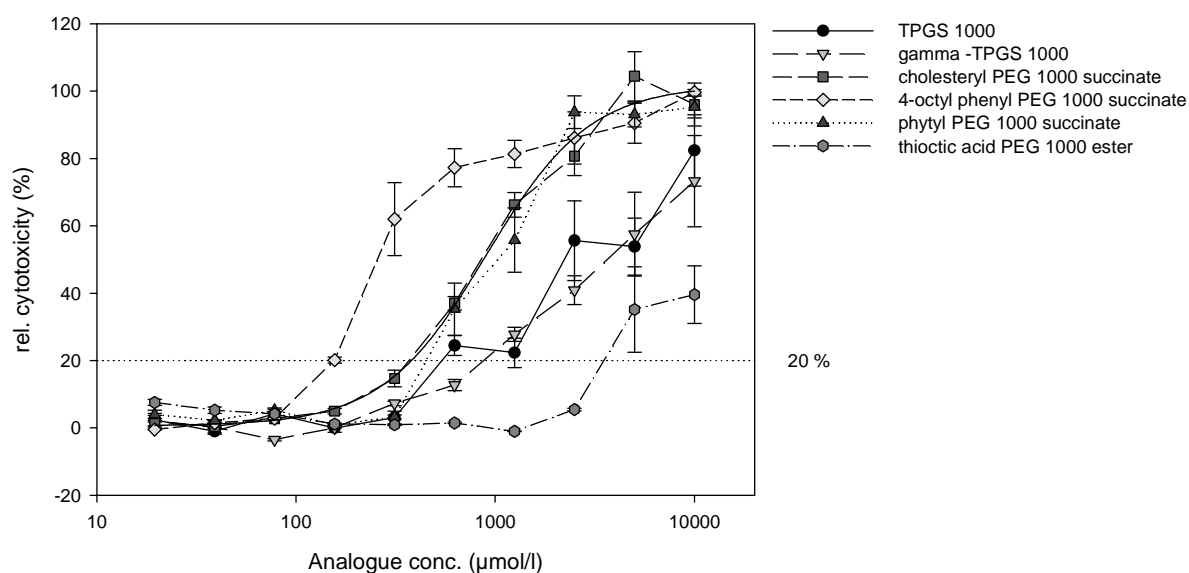


Figure 2-16 Rel. cytotoxicity of TPGS analogues with modified hydrophobic moieties compared to positive control (0.1% triton X-100) in the LDH release assay; mean \pm SD; n = 12.

In accordance with the LDH release data, TEER values were constant throughout the transport experiment, consistent with viable intact monolayers, when Caco-2 cells were incubated with TPGS 1000 or PEG chain length analogues (Table 2-3). Moreover, no loss of tight junction functionality could be observed in the presence of gamma-TPGS 1000, cholesteryl PEG 1000 succinate, and thioctic acid PEG 1000 ester (Table 2-3). However, TEER dropped significantly on incubation with phytol PEG 1000 succinate. The decrease of barrier resistance was most pronounced for 4-octyl phenyl PEG 1000 succinate, which reduced TEER from $605 \pm 45 \Omega \cdot \text{cm}^2$ to $63 \pm 20 \Omega \cdot \text{cm}^2$ after 6 hours.

	Start of the experiment	After 60 min of preincubation	End of the experiment
No TPGS analogue	507 ± 49	557 ± 50	541 ± 125
TPGS 200	573 ± 66	522 ± 42	526 ± 61
TPGS 238	502 ± 93	499 ± 61	533 ± 62
TPGS 400	529 ± 20	512 ± 24	531 ± 38
TPGS 600	452 ± 40	432 ± 68	431 ± 101
TPGS 750-OMe	609 ± 90	612 ± 64	636 ± 87
TPGS 1000	505 ± 76	502 ± 36	549 ± 41
TPGS 1100-OMe	591 ± 86	562 ± 121	604 ± 126
TPGS 1500	600 ± 39	582 ± 58	618 ± 48
TPGS 2000	590 ± 67	534 ± 88	601 ± 42
TPGS 3350	501 ± 68	432 ± 62	461 ± 87
TPGS 3500	510 ± 88	513 ± 143	480 ± 145
TPGS 4000	490 ± 51	509 ± 90	502 ± 88
TPGS 6000	574 ± 38	522 ± 46	526 ± 60
Cholesteryl PEG 1000 succinate	577 ± 67	467 ± 24	457 ± 34
Phytol PEG 1000 succinate	523 ± 40	503 ± 26	208 ± 77 *
4-octyl phenyl PEG 1000 succinate	605 ± 45	486 ± 25 *	63 ± 20 **
Thioctic acid PEG 1000 ester	471 ± 87	421 ± 87	505 ± 109
Gamma-tocopheryl PEG 1000 succinate	482 ± 30	413 ± 56	536 ± 97

Table 2-3 Development of TEER values in the presence of TPGS analogues during the course of transport experiments; mean ± SD, n = 18; * = significantly different to start of the experiment (P < 0.05).

2.3.3 Determination of physicochemical properties

The surface tensions of the TPGS analogues in KRB at 37 ± 1°C were measured and their CMC values determined. All TPGS analogues possessing the alpha-tocopherol moiety and modified PEG chain lengths presented CMC's of 0.02 ± 0.019% wt (Table III-4). Variances were greater between analogues with modified hydrophobic moieties. The cholesterol, phytol, and 4-octyl-phenol analogues (0.01 ± 0.01% wt) were comparable to TPGS 1000 in their solubilizing potential, while gamma-TPGS 1000 at 0.001 ± 0.001% wt had a considerably lower CMC. Thioctic acid PEG 1000 ester had the lowest solubilizing capacity at a CMC of 0.1 ± 0.09% wt.

Analogue	MW (Da)	CMC (% wt)	ClogP	CMA (Å ²)	SEV (Å ³)
TPGS 200	713.0	0.02 ± 0.019	11.9	668	762
TPGS 232	745.0	0.02 ± 0.019	11.9	763	805
TPGS 400	913.0	0.02 ± 0.019	12.2	850	987
TPGS 600	1113.0	0.02 ± 0.019	12.4	949	1199
TPGS 750-OMe	1278.0	0.02 ± 0.019	13.3	964	1396
TPGS 1000	1513.0	0.02 ± 0.019	13.0	1213	1667
TPGS 1100-OMe	1627.0	ND	13.8	1221	1908
TPGS 1500	2013.0	ND	13.8	1530	2420
TPGS 2000	2513.0	0.02 ± 0.019	ND	1719	3011
TPGS 3350	3863.0	0.02 ± 0.019	ND	2496	4911
TPGS 3500	4013.0	0.02 ± 0.019	ND	2522	5027
TPGS 4000	4513.0	0.02 ± 0.019	ND	3100	5676
TPGS 6000	6513.0	0.02 ± 0.019	ND	4268	8231
Gamma-tocopheryl PEG 1000 succinate	1503.0	0.001 ± 0.001	12.5	1135	1675
Cholesteryl PEG 1000 succinate	1472.6	0.01 ± 0.009	11.4	1178	1562
Phytyl PEG 1000 succinate	1382.5	0.01 ± 0.009	10.4	1161	1510
Thioctic acid PEG 1000 ester	1206.3	0.1 ± 0.1	3.5	986	1209
4-octyl phenyl PEG 1000 succinate	1292.0	0.01 ± 0.009	6.6	1026	1381

Table 2-4 Physicochemical properties of TPGS 1000 and its analogues; CMC was determined experimentally, while ClogP, CMA and SEV were calculated *in silico* using Chem 3D Ultra; ND = not determined.

Other physicochemical parameters to depict molecule size and lipophilicity were derived from *in silico* modelling of the molecule structure. Each TPGS analogue was initially drawn using Chem-Draw® with the corresponding linear PEG chain. A molecular mechanics (MM) followed by a molecular dynamics process was then conducted. Next, Gaussian® molecular mechanics (UFF, 6-31G basis set) was conducted to afford a local minimized gas-phase structure (Figure 2-17). In addition a semi-empirical calculation was conducted. Using the property server, Connolly Molecular Area (CMA), Connolly Solvent-Excluded Volume (SEV), and octanol/water partition coefficient (ClogP) were computed. Due to computational limitations, calculations were in part impeded by TPGS molecule structure: the high number of

atoms for TPGS analogues with a molecular weight > 2500 Da made ClogP values for these molecules unobtainable.

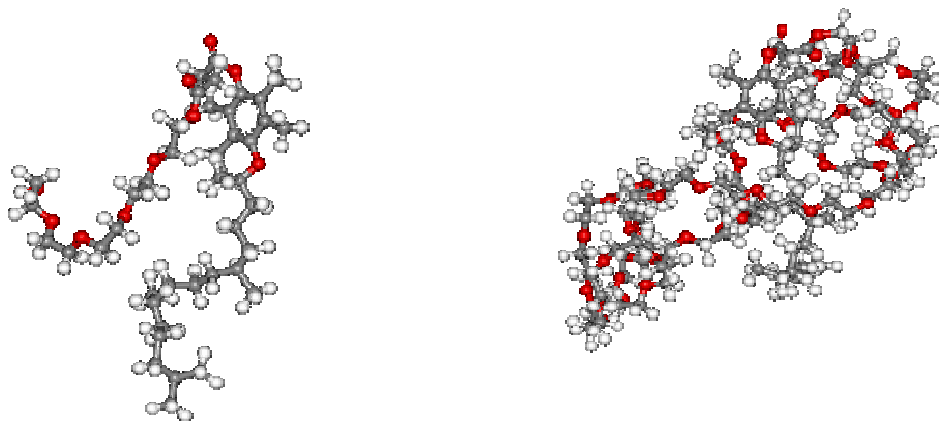


Figure 2-17 3D structure of TPGS 200 (left) and TPGS 2000 (right) as optimized by molecular dynamics calculations.

Molecule volume, which may be described by CMA and SEV, increased linearly with molecular weight/PEG chain length. The computational analysis did not reveal an optimum PEG chain length or a threshold value for a non-linear increase of molecule volume (Figure 2-18). The existence of such a threshold value would indicate a drastic change in molecular folding or mobility.

In the same way, ClogP, a measure of lipophilicity, increased linearly with the length of the PEG chain, the exception being the two ether analogues, whose increase in lipophilicity was more pronounced due to the capping of the terminal hydroxide functional group (Table 2-4). In consequence, if the degree of inhibition in the Caco-2 transport assay is plotted against the ClogP, the corresponding curve follows the same trend as in the original Weibull curve (Figure 2-19). Even though no actual ClogP values were obtainable for the rest of the TPGS analogues with PEG chains > 1500 Da, it can be assumed that their ClogP would continue to increase linearly, the ClogP vs. DI plot thus mirroring also the declining part of the Weibull distribution.

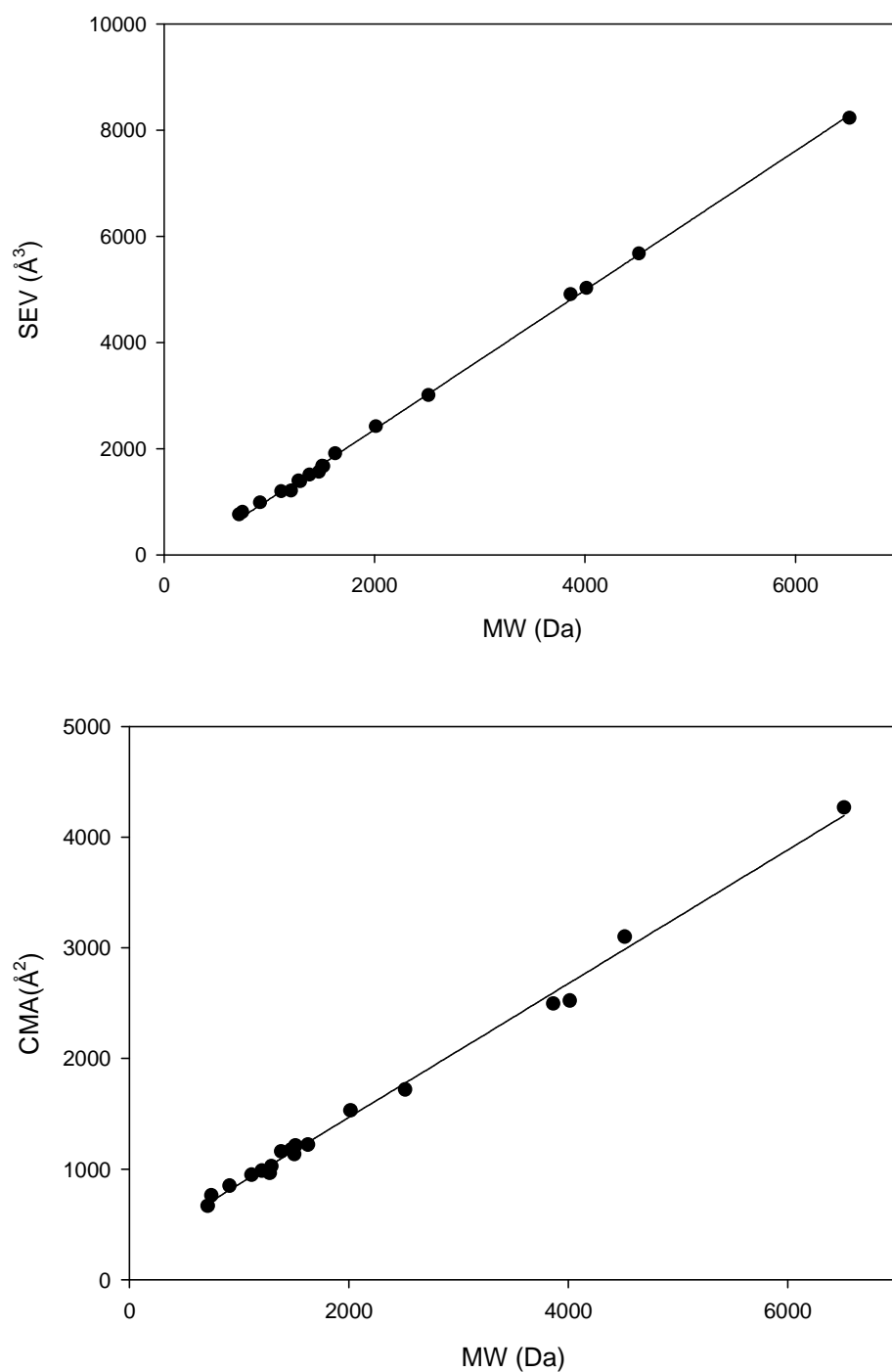


Figure 2-18 Correlation of computational data with molecule weight of the TPGS analogues: above: SEV, below: CMA.

A sufficient lipophilicity increases membrane penetration of a molecule and clearly facilitates its reaching the propagated site of action. However, a ClogP value of > 13.5 can't be a prerequisite for effective P-gp modulation, as the most potent P-gp modulator cholesteryl PEG 1000 succinate has a lower ClogP value of 11.4 (Table 2-4). The ClogP values of the TPGS analogues with modified hydrophobic moieties increase in the order thioctic acid PEG 1000 ester $<$ 4-octyl phenyl PEG 1000 succinate $<$ phytol PEG 1000 succinate $<$ cholesteryl PEG 1000 succinate $<$ gamma TPGS 1000, thus also demonstrating the relation between lipophilicity and effectiveness of inhibition. If combined however, the two groups of analogues are too divergent to make general predictions for optimal ClogP values.

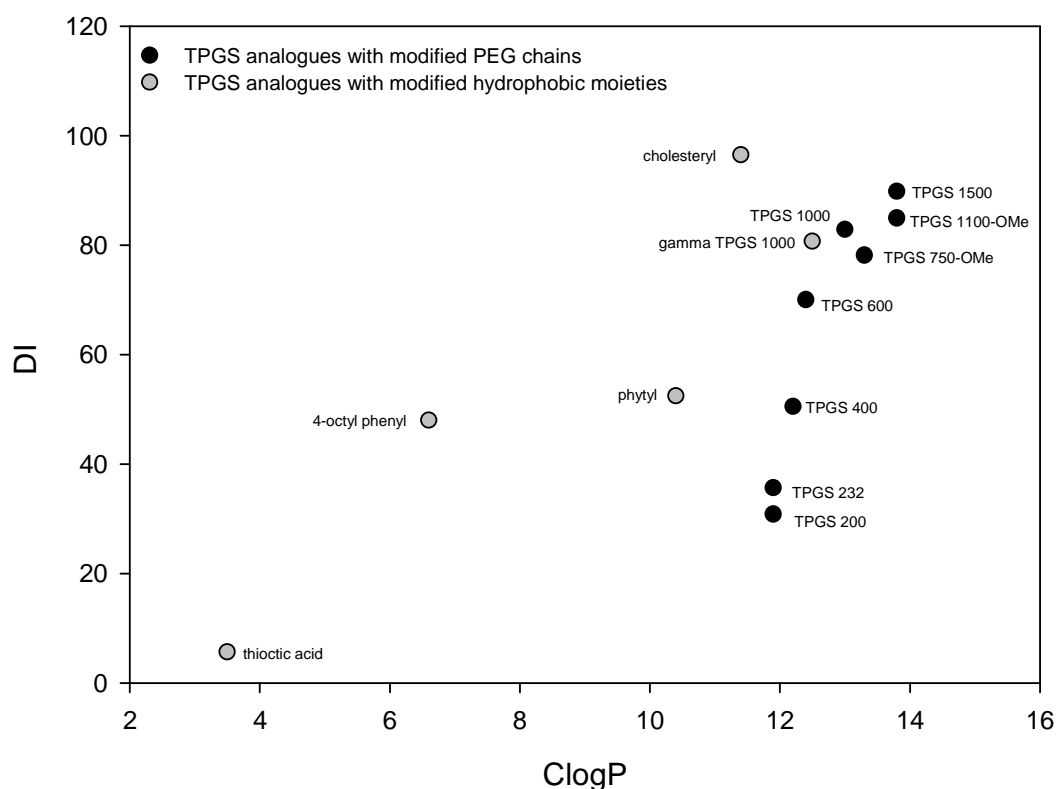


Figure 2-19 Correlation of ClogP with degree of inhibition.

2.4 Discussion

In recent years, several studies have presented effect(s) of different commonly used pharmaceutical excipients on P-gp efflux activity [75, 81, 120-122]. However, these studies discuss structurally diverse surfactants. The current work focuses on two groups of homologous TPGS analogues. In a TPGS structure-activity relationship (SAR) study, TPGS derivatives with varying PEG chain lengths or modified hydrophobic moieties were synthesized and evaluated *in vitro* for their ability to modulate P-gp mediated efflux.

2.4.1 Analogues with modified PEG chains

Among the tested analogues with modified PEG chain lengths, commercial TPGS 1000, whose P-gp modulating properties were merely discovered by chance, performed amazingly well: it was the most potent P-gp modulator in the original data set. All analogues with shorter or longer PEG chain length demonstrated weaker P-gp inhibition in both transport directions (Figure 2-3).

The astounding P-gp inhibitory properties of commercial TPGS 1000 are mirrored by the low EC_{50} value of TPGS 1000 compared to other surfactants such as Tween 80 and Cremophor EL (Table 3-4). The determined EC_{50} values for TPGS 1000 and Cremophor EL are comparable to literature results for the inhibition of RHO efflux in *mdr1* overexpressing P388/*mdr1* mouse lymphocytes ($3.92 \pm 0.60 \mu\text{M}$ and $33.5 \pm 22.4 \mu\text{M}$ for TPGS 1000 and Cremophor EL, respectively) [84]. However, in the case of Tween 80, the determined value here varies from previous findings which were reported with a higher EC_{50} at $152.7 \pm 229.0 \mu\text{M}$ [84]. The discrepancies may be explained by the use of different cell lines: P-gp expression levels may be assumed to be much higher in P388/*mdr1* cells than in Caco-2 cells, thus allowing for a better differentiation of inhibitory properties. On the other hand, Caco-2 cells were chosen for this study, as they present one of the best *in vitro* – *in vivo* correlations [123, 124]. In particular, Caco-2 cells express a vast array of efflux transporters known to influence *in vivo* oral absorption [125]. A comparative study performed in our lab, ranked the TPGS analogues according to their inhibitory potential in a calcein AM assay using

The TPGS 1000 monoester represents the active compound in this mixture, as its degradation products PEG 1000 and alpha-tocopherol succinate were shown not to influence *in vitro* P-gp activity (Figure 2-14) and a head to head comparison of TPGS 1500 diester, TPGS 1000 diester and TPGS 2000 diester, also failed to reveal a modulation of RHO transport in absorptive or secretory direction for either compound (study conducted at Eastman Chemical Company, data not shown). Interestingly, the difference in EC₅₀ values between the two TPGS qualities (commercial and purified TPGS 1000) is higher than can be attributed to the varying monoester content. A 'dilution' of the active component content would only afford a theoretical EC₅₀ value of ~2.5 μM. Instead, TPGS synthesis by-products, most likely the TPGS diester, interfere with the P-gp inhibitory mechanism of the monoester, providing additional reasons for the use of purified materials.

It is important to point out that the purification doesn't affect the ranking of the analogues' inhibitory potential. The same activity pattern can be observed in both the old and new data set. Consequently a fitting of the new data to the Weibull function only slightly alters the quality of the fit and doesn't significantly shift the predicted maxima (Figure 2-6). However, it can be noted, that the refinement of the maxima for secretory and absorptive transport leads to a converging of the predicted values and suggests the existence of a common optimum for both transport directions (as seems reasonable from a mechanistic point of view) at a length between 1466 ± 125 Da and 1271 ± 123 Da.

The two methyl ether compounds also followed the Weibull trend, demonstrating that the free hydroxyl group at the end of the PEG chain is not essential for the P-gp inhibitory function of TPGS. Furthermore, the ether derivatives present an interesting alternative to non-ether TPGS 1000. The use of a capped PEG in the TPGS synthesis allow for a much easier preparation of pure, more active material. Unlike non-ether PEGs, PEG 750-OMe and PEG 1100-OMe contain a reactive hydroxyl group at only one end of the polyethylene glycol polymer chain. Therefore esterification with vitamin E succinate can only occur on this end of the PEG chain, leading to the sole formation of TPGS monoesters and avoiding the formation of diesters.

2.4.2 Influence of experimental conditions

RHO kinetic in Caco-2 cells was investigated to determine substrate affinity to P-gp (Figure 2-9). Secretory RHO transport followed a one-site saturation model with a J_{\max} of $1.085 \mu\text{mol}/\text{h}\cdot\text{cm}^2$ and a K_m of $27.84 \pm 5.32 \mu\text{M}$, which is comparable to literature values ($16.5 \pm 2.0 \mu\text{M}$) [127]. This K_m value places RHO in the group of P-gp substrates with moderate affinity to the efflux pump, similar to vinblastine ($K_m = 36.5 \mu\text{M}$ [128]), but with markedly lower affinity than the HIV protease inhibitor ritonavir ($K_m = 0.06 \mu\text{M}$ [129]) and significantly higher affinity than the topoisomerase II inhibitor etoposide ($K_m = 276 \mu\text{M}$ [128]). At a RHO concentration of $13 \mu\text{M}$ (approximately half of the determined K_m value) no saturating effects can be observed, as RHO kinetic in this part of the curve is still linear, making it a suitable concentration for P-gp inhibition experiments. The lack of a saturating effect in absorptive direction where RHO transport follows simple linear kinetics may be explained by differing transport pathways of RHO across cell monolayers. According to the model of Troutman and Thakker (Figure 2-21), absorptive RHO transport is limited to the paracellular route, while secretory RHO transport is thought to mainly occur via a basolaterally located uptake transporter and subsequent apical P-gp efflux [130]. Consequently, in absorptive directions only low RHO concentrations can reach the efflux pump due to the longer diffusion distance, not reaching levels high enough to saturate the efflux transporter.

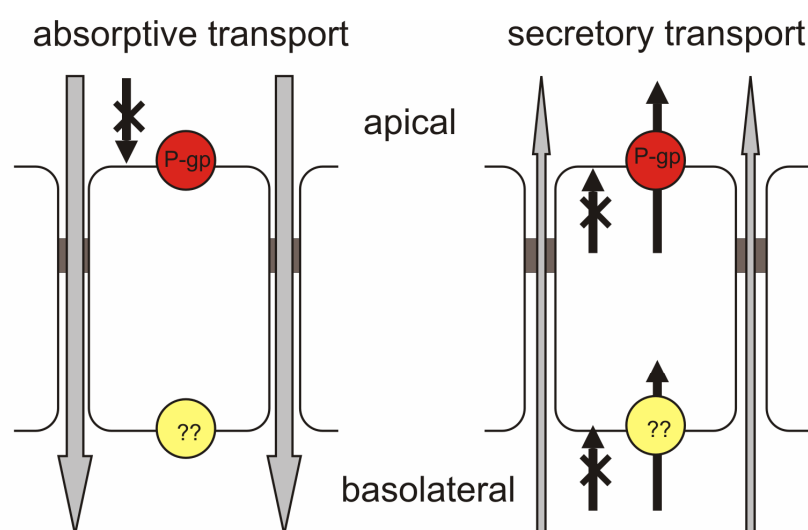


Figure 2-21 RHO transport routes across epithelial monolayers, according to Troutman and Thakker; adopted from [130]

In the presence of TPGS 1000 (33 μM), almost complete P-gp inhibition is achieved. In consequence RHO transport in both transport directions is controlled by passive diffusion, following linear kinetics. As the applied TPGS 1000 concentration was quite high, no information can be derived regarding the inhibitory mechanism of TPGS: only an incomplete P-gp inhibition would allow for a fitting of RHO data to a Michaelis-Menten model and a comparison of V_{max} and K_{m} data in the presence and absence of the P-gp modulator.

Due to the postulated differing transport routes between absorptive and secretory direction, the use of RHO for evaluating P-gp efflux activity was criticized in recent publications [130, 131]. In absorptive direction RHO is claimed to be transported solely via the paracellular diffusion, thus by-passing the efflux pump and yielding no information on actual 'absorption enhancement' by efflux pump inhibition. Instead of RHO, the use of other model substrates such as DIG is propagated, which are thought to be transported by transcellular diffusion in both transport directions. A comparison of the relative effect of TPGS 1000, TPGS 4000 and the first generation P-gp inhibitor CsA on P-gp efflux activity revealed no differences in the extent and ranking of the inhibitory effects between DIG and RHO as P-gp model substrates (Table 2-2): Due to its higher lipophilicity DIG permeability data was higher than RHO data. However, efflux ratios and the relative changes of transport were comparable in both experimental setups. Contrary to Troutman's substrate theory, the DIG data as well as the RHO data demonstrated no differences in the influence of the P-gp modulators on absorptive versus secretory transport. A stable experimental setup with a replacement of sample volume (instead of a complete exchange of receptor buffer) in an otherwise closed system and sufficient equilibration periods may negate the impact of the contrasting transport pathways. This also stresses the importance of experimental design for the evaluation of P-gp modulators in bidirectional transport experiments.

Differences in experimental protocol may help explain the discrepancies observed when comparing P-gp inhibition results for TPGS 1000 among different groups: while most in agreement with the above mentioned findings observe strong P-gp inhibitory effects of TPGS in both transport directions, others report a polarity of effect with a pronounced secretory inhibition, but no influence in the absorptive direction [72, 132].

RHO micellar sequestering by TPGS 1000 was proposed as a possible explanation for this phenomenon [72]. However, this seems unlikely as effects could in part be observed at concentrations well below the CMC of TPGS 1000 (0.02% wt) and the sequestering would affect both transport directions to a similar degree.

Instead, pre-incubation in the presence of TPGS proved to strongly influence the effectiveness of the P-gp inhibition. A polarity of effect was observed, as absorptive RHO transport was very pre-incubation time dependent, while secretory transport was less impacted by changes in the experimental protocol. The maximum increase of absorptive transport was observed after ~45 min of pre-incubation, while decrease of secretory RHO transport was instantaneous (Figure 2-10 and Figure 2-11). The distinct transport pathways for RHO may explain the discriminative effect of TPGS 1000 on RHO transport. In the absorptive direction a certain period of time (during which RHO enters the cells via the “backdoor”) has to pass before P-gp is exposed to significant amounts of RHO and efflux activity and inhibition of such can be observed. In the case of secretory RHO transport exposure occurs much faster and effects on P-gp activity become apparent immediately. The inhibitory potential of TPGS 1000 on P-gp is the same in both transport directions and optimal pre-incubation conditions of ~45-60 min apply for both experimental setups; however, the magnitude of the pre-incubation effect may vary depending on transport direction (*i.e.* the compartment to which RHO is administered). Besides providing a possible explanation for observed differences in inhibitory activity of TPGS 1000, the time-dependence of the inhibition offers new possibilities to optimize P-gp inhibition by TPGS. A delayed release of the P-gp substrate drug in relation to TPGS might increase the efficacy of *in vivo* P-gp inhibition.

A similar variation in sensitivity to changes in the protocol could be observed when the application side of TPGS 1000 was altered (Figure 2-12 and Figure 2-13): Independent of its side of application, TPGS 1000 affected absorptive as well as secretory RHO transport, although the effect was slightly weaker in both transport directions when the surfactant was placed only in the basolateral compartment. As in the previous experiments with zero min of pre-incubation time, it took up to 1.5-2.0 hours to observe an effect on absorptive transport. In addition, the effect was further delayed when TPGS 1000 was only added to the basolateral side, indicating that

TPGS 1000 has to first traverse the cell monolayer to reach its site of action in the apical cell membrane and subsequently inhibit P-gp mediated efflux. Consequently, P-gp inhibition by TPGS 1000 seems to be the result of a direct interaction of the tenside with the efflux pump rather than indirect effects that are translated through the cell membrane.

2.4.3 Analogues with modified hydrophobic moieties

A second possibility to influence the P-gp modulating properties of TPGS was demonstrated in the variation of the hydrophobic part of the molecule. Of the five novel structures with modified hydrophobic moieties, only cholesteryl PEG 1000 succinate surpassed TPGS 1000 in its P-gp modulating effect, with a slightly stronger inhibition of RHO efflux in the head to head comparison at 33 μM and a significantly lower EC_{50} value ($0.47 \pm 0.06 \mu\text{M}$). Similar to TPGS 1000, the amphiphilic cholesteryl PEG 1000 succinate monoester was shown to be the active component and the inhibitory potency could therefore be further increased via purification ($\text{EC}_{50} = 0.067 \pm 0.009 \mu\text{M}$). Gamma-TPGS 1000 performed similar to commercial alpha-TPGS 1000 in the head to head comparison, suggesting that a small change in the molecule structure, such as the addition of a methyl-group to the hydrophobic core, is not sufficient to drastically alter P-gp modulation potential. On the other hand, the exchange of alpha-tocopherol for 4-octyl-phenol and phytol decreased the P-gp activity. However, the evaluation of meaningful P_{app} values for these two analogues was hindered by their relatively high cytotoxicity: 4-octyl-phenyl PEG 1000 succinate and phytol PEG 1000 succinate compromised the Caco-2 monolayer integrity and made it impossible to reach steady state transport conditions. Thioctic acid PEG 1000 ester completely lacked P-gp modulating properties. As this is the only derivative to miss the succinate linker, the loss of activity can't be clearly ascribed to the change of the hydrophobic core. A reduced conformational flexibility of the molecule structure and/ or an increased susceptibility to hydrolysis may also account for this phenomenon.

2.4.4 SAR and mechanism of P-gp inhibition by TPGS

The head to head comparison results have implications for the understanding of the inhibitory mechanism of TPGS. TPGS 1000 and the analogues with modified hydrophobic moieties (with the exception of thioctic acid PEG 1000 ester) do not greatly differ in their physicochemical properties (*i.e.* ClogP, molecular weight, or molecule volume) yet they show markedly different extents of influence on the efflux pump. This indicates a more specific interaction of the surfactant molecule(s) with P-gp rather than an unspecific alteration of the membrane environment. The latter theory was suggested because of the amphiphilic structure of TPGS 1000, which allows for an intercalation of the molecules into the lipid bilayer of the cell membrane. Looking at the cytotoxicity and TEER data, a complete rupture of the cell membrane at P-gp active levels (~ 33 μ M) may be ruled out, although more subtle changes in membrane fluidity, might not be apparent from the LDH results and need to be excluded, *e.g.* via electron spin resonance spectroscopy (ESR).

No explanation can be derived for the observed Weibull activity pattern of analogues with varying PEG chain lengths from their physicochemical parameters computed in the molecular modelling study. Hydrophilicity and molecule volume are linearly related to molecule/ PEG chain weight and therefore don't correlate with P-gp activity. It might be inferred that at PEG chain lengths greater than ~1500 Da, the surfactant molecules simply become too large and/or hydrophilic to enter/cross the cell membrane and reach the site of action, thus explaining the declining part of the Weibull curve. None the less, the increased P-gp inhibitory potential with moderate PEG chain lengths remains unexplained, as the inhibitory mechanism of TPGS is not yet understood.

From the control results, it is clear that the formation of an amphiphilic structure by the PEG chain and the hydrophobic moiety is essential to influence RHO efflux. The importance of the PEG component for the inhibitory activity of several P-gp modulators had been suggested in previous studies [73, 75, 133]. Hugger *et al.* [121] illustrated that PEG 300 itself can inhibit P-gp function, but only at concentrations of $\geq 20\%$ v/v. Following this trend, PEG 1000 alone (at 33 μ M) was not sufficient to influence P-gp activity.

It was previously proposed that the permeability enhancing effect of tensides, amongst them TPGS 1000, was likely due to micelle formation [62, 134]. However, TPGS 1000 has been reported to influence efflux well below its CMC of 0.02% wt [101]; the current results using a TPGS 1000 concentration of 33 μ M (0.005% wt) are consistent with the 'below CMC' conclusion. Surface tension measurements of analogues with varying PEG chain lengths showed their CMC's to be similar to commercial TPGS 1000 ($0.02 \pm 0.019\%$); the variances were greater among analogues with modified hydrophobic moieties. Still, all derivatives, with the exception of thioctic acid PEG 1000 ester, showed sufficient to good solubilizing properties and would allow for their use as emulsifiers and/or solubilizers in pharmaceutical formulations. The high CMC standard deviations may be explained from the use of the non-purified crude products in the measurements; all analogues consisted of 80-85% mono-ester and 14-19% diester. The general trend clearly suggests no correlation between CMC values and P-gp modulatory activity. A RHO sequestering as the cause for the decline in the P-gp inhibitory activity for TPGS analogues with longer PEG chain length is questionable, as quenching was taken into account during the experimental setup and the decrease in activity became apparent while operating below the CMC.

Interestingly, the presented results demonstrate novel excipient potential in more than one way. Besides an optimization of TPGS structure for P-gp inhibition, the synthesis of new TPGS analogues with strong drug solubility capacity (e.g. TPGS 400) but little influence on efflux, could be demonstrated. Such detergents may be quite advantageous to drug-delivery, especially as new formulations get developed that show only minimal to no interactions with other drugs, formulations or nutrients.

2.4.5 *In vivo* impact of TPGS

Toxicity aspects are only a minor concern in the evaluation of TPGS. In clinical studies conducted in the 1980's (when TPGS was investigated as a water soluble vitamin E source), no toxicity from TPGS was found as measured by hemogram, urinalysis, osmolality, renal function, and liver function [135]. Only a small portion of TPGS is absorbed from the intestine as intact molecules. The majority is hydrolysed in the enterocytes to PEG and vitamin E succinate, which is then further degraded to

vitamin E. The absorbed PEG is rapidly cleared by glomerular filtration [135]; problems may only arise in patients with renal insufficiency, as they may develop a hyperosmolar state. The active component of TPGS, the TPGS monoester, doesn't reach the systemic circulation. Therefore interactions of TPGS with hepatic MDR1 and other metabolic transporters and enzymes can be excluded. This clearly represents an advantage of TPGS over other (small molecular) P-gp inhibitors, as a modulation of the interplay of the various hepatic transport systems could have unpredictable consequences on the pharmacokinetics of drugs.

TPGS concentrations reached *in vivo* via the formulations on the market are sufficient to completely inhibit P-gp, as Brouwers *et al.* [136] were able to demonstrate for Agenerase® soft gelatine capsules. The capsules contain 280 mg of TPGS in addition to the HIV protease inhibitor and P-gp substrate amprenavir. In human intestinal fluid from both duodenum and jejunum, high TPGS concentrations in the mM range were found, a TPGS concentration high enough to completely inhibit P-gp and at the same time increase amprenavir solubility from the μM to the mM range. However the high TPGS concentration also negatively affected amprenavir permeability: micellation of the drug reduced the free amount that could cross the intestinal epithelium.

The actual *in vivo* impact of TPGS for oral drug delivery, in particular the extent to which the P-gp inhibition contributes to the absorption enhancement, is still being discussed. The solubilizing effect of TPGS and other excipients may be the main cause for increasing bioavailability of P-gp substrates. The significance of the efflux phenomenon is most pronounced for poorly soluble, but highly permeable drugs in BCS class II. Drastically increasing their solubility allows the substrates to saturate the efflux systems, thus minimizing the efflux effect and the importance of P-gp modulation. Furthermore, endogenous substances such as bile salts and phospholipids might provide similar effects as TPGS and other non-ionic surfactants, as they are known to have both solubilizing and P-gp modulatory properties. The additional beneficial effect of adding a weak P-gp inhibiting surfactant to the formulation may therefore be only minimal.

2.5 Conclusion

Based on the PEG chain length hypothesis, TPGS 1500 was synthesized as a novel TPGS analogue with improved P-gp modulating properties. New P-gp inhibitors could also be developed via modification of the hydrophobic moiety. Cholesteryl PEG 1000 succinate represents the most potent P-gp inhibitor amongst TPGS analogues, so far. Furthermore, TPGS ether derivatives were introduced as an interesting alternative to synthesize purer, and thus more active, TPGS analogues. On the other hand the PEG chain length dependency of the inhibitory effect also suggests that new solubilizers without any P-gp inhibitory properties can be logically constructed (e.g. TPGS 400 or TPGS 4000). These new surfactants may greatly reduce formulation-formulation, drug-formulation, and/or formulation-food interactions associated with inhibition of P-gp and/or other drug transport proteins. They could broaden the spectrum of excipients for pharmaceutical formulations and open up a new series of useful solubilizers for *in vitro* drug permeability screening. Sensitivity of TPGS activity to exposure time (and to a lesser degree application side) may help explain the differing reports on TPGS ability to inhibit P-gp *in vitro*, and could have dramatic influence on its performance as an *in vivo* P-gp inhibitor and bioavailability enhancer. Delivery systems, which allow for a delayed release of the drug in relation to TPGS, could further improve the circumvention of P-gp mediated drug efflux. Thus far, the mechanism for the observed structure activity patterns has not been elucidated, although an unspecific alteration of the membrane environment does seem increasingly unlikely.

3 Mechanism of Vitamin E TPGS interaction with P-glycoprotein

Parts of this chapter have been published in:

E.M. Collnot, C. Baldes, M. Wempe, R. Kappl, J. Huettermann, J. Hyatt, K.J. Edgar, U.F. Schaefer, C.M. Lehr, Mechanism of inhibition of P-glycoprotein mediated efflux by Vitamin E TPGS: Influence on ATPase activity and membrane fluidity, *Mol Pharm* in press

Reproduced in part with permission from *Molecular Pharmaceutics*, in press. Unpublished work, © 2007 American Chemical Society.

3.1 Introduction

Although it was possible to improve the P-gp inhibition by TPGS through modifications of the hydrophilic PEG chain or the hydrophobic moiety, the rationale behind the superior inhibitory properties of the new surfactants has not been understood. Therefore it can not be predicted whether or not the potential for further structural improvement has been exhausted. A mechanistic understanding of inhibition of P-gp by surfactants should give new insights into the structure activity relationships and vastly improve the rational design of more potent P-gp inhibitors.

In the last years, a vast amount of research effort has been focussed on P-gp, yet the exact inhibitory mechanism of non-ionic surfactants remains unclear. Three mechanisms are currently being proposed in the literature: i) a sterical hindering of substrate binding [137], ii) an alteration of membrane fluidity [72, 73], and iii) an inhibition of efflux pump ATPase in combination with a possible intracellular ATP depletion [93, 138, 139]. Findings from the previous SAR studies suggest a more specific interaction of TPGS with the efflux pump instead of an unspecific alteration of membrane fluidity: Only some variations to the hydrophobic part of the molecule resulted in increased inhibitory activity, while others significantly reduced affectivity. Furthermore, to a certain degree, the P-gp inhibitory effect was side specific and could not be directly translated from the basolateral side of the monolayer to the apical side, where the efflux pump is located. However, all things considered evidence is tentative and necessitates more specific investigations into the state of the P-gp membrane environment.

Therefore, in this second part of the thesis the mechanism of TPGS interactions with P-gp in its membrane environment was investigated. Alterations in membrane fluidity in the presence of the surfactant were studied via electron spin resonance spectroscopy (ESR). Modulation of ATPase activity was measured in the absence and presence of P-gp substrates using an ATPase assay. Furthermore, conformational changes in P-gp due to the addition of TPGS were studied through the reactivity with the monoclonal antibody UIC2. Results were compared and correlated to findings from our previous P-gp inhibition experiments in the Caco-2 transport system.

3.2 Materials and methods

3.2.1 Materials

Commercial Vitamin E TPGS 1000, Vitamin E, Vitamin E succinate, cholesterol, cholesterol succinate and all TPGS derivatives were obtained from Eastman Chemical Company (TN, USA). Vitamin E TPGS and all analogues were prepared and purified according to the method previously described [140]. Dulbecco's modified Eagle's medium (DMEM), non-essential amino acids (NEAA) and fetal bovine serum (FBS) were purchased from GIBCO (Invitrogen GmbH, Karlsruhe, Germany). Reduced β -nicotinamide dinucleotide (NADH), sodium azide, ethylene glycol-bis (2-aminoethylether)-*N,N,N',N'*-tetraacetic acid (EGTA), and phosphoenol-pyruvate were from Fluka (Neu-Ulm, Germany). Monoclonal CD243 P-gp antibody clone UIC2 was from Immunotech (Marseille, France), Alexa Fluor® 488 conjugated anti-mouse IgG was purchased from Molecular Probes (Leiden, Netherlands). 5-doxy stearic acid, ouabain, nifedipine, R+-verapamil, quinidine, progesterone, lactic dehydrogenase (LDH)/ pyruvate kinase, bovine serum albumin (BSA), PEG 1000, SDS, Triton-X 100, procaine hydrochloride and all other chemicals were purchased from Sigma-Aldrich (Taufkirchen, Germany).

3.2.2 Cell culture

Caco-2 cells, clone C2BBE1, were purchased at passage 60 from American Type Culture Collection (ATCC; Manassas, VA) and used at passages 70-92. Cells were grown to ~90% confluence in 75 cm² T-flasks with DMEM supplemented with 10% FBS and 1% NEAA. Culture media were changed every second day and cells were grown at a temperature of $37 \pm 0.5^\circ\text{C}$ in an atmosphere of ~85% relative humidity and ~5% CO₂.

3.2.3 ESR spectroscopy

ESR was chosen as a convenient method to study the membrane environment of P-gp in the absence and presence of TPGS 1000 and its different analogues. ESR is a form of absorption spectroscopy that is used in various fields of application, e.g in solid-state physics, for the identification and quantification of radicals, in chemistry, to

identify reaction pathways, and in biology or medicine for tagging biological spin probes (see 6).

Trypsinized Caco-2 cells were spin labelled by incubating a suspension (2.0×10^7 cells/ml) in Krebs Ringer Buffer (KRB; pH 7.4) for 30 min at $37 \pm 0.5^\circ\text{C}$ with 0.50 mM of a spin label stock solution (10 mM 5-doxy stearic acid (5-SA) in ethanol). Different test compound concentrations were added to the cell suspensions and incubated for 60 min. After suspension centrifugation (4 min at 1200 g), supernatant was removed and the cell pellet was washed and resuspended in KRB to give a final concentration of $\sim 1.0 \times 10^8$ cells/ml. To quench residual free spin label, chrome oxalate (final concentration 2.0 mM) was added and the ensuing cell suspension (100 μl) was filled into the test tube (WG806A Tissue cell; Rototec-Spintec, Biebesheim, Germany) and placed in a 4103 TM/ 8609 cavity (Bruker, Karlsruhe, Germany).

ESR measurements were performed at room temperature using a Bruker ESP300 E spectrometer with an ER081 (90/30 C5) magnet (Bruker, Karlsruhe, Germany). The following conditions were used: microwave power 1mW, modulation amplitude 2 G, sweep width 100 G, modulation frequency 100 kHz, scanning time 40.96 s and time constant 10.24 ms. ESR measurements were performed at room temperature using a Bruker ESP300 E spectrometer with an ER081 (90/30 C5) magnet (Bruker, Karlsruhe, Germany).

Using the equation proposed by Gaffney and Lin (see below)[141], cell membrane fluidity may be depicted via the cell membrane order parameter S . S can be derived from the ESR spectral line splitting. Briefly, the spin active nitroxide group of 5-SA is situated within four carbon atoms of the polar carboxyl group of the lipid acid. Reporting on molecular dynamics occurring near the membrane surface, 5-SA is located in the membrane close to the membrane head groups and the nitroxide functionality unveils molecular dynamic changes that may occur near the membrane surface. Normally, a free nitroxide radical in solution will produce a characteristic three line (isotropic) ESR spectrum because of rapid tumbling of the molecule; whereas in biological membranes, the restricted mobility of the spin label is causing an anisotropic (or powder-like) spectrum. The spin probe 5-SA becomes intercalated into the membrane bilayer and aligns itself along an axis parallel to the membrane

normal. In that case the maximal hyperfine component a_{zz} of the NO-moiety is oriented parallel to the long molecular axis of 5-SA and parallel to the membrane normal, the minimal hyperfine component a_{xx} is oriented perpendicular to it. The anisotropic motion of the spin label with respect to membrane normal then leads to the experimentally observed largest hyperfine interaction $a_{||}$ ($\leq a_{zz}$) and minimal splitting a_{\perp} ($\geq a_{xx}$) which thus are monitoring the dynamic behaviour (Figure 3-3). Comparing the observed $a_{||}$ and a_{\perp} values to the theoretical principal values, a_{zz} and a_{xx} , allows one to calculate S ; defined as the ratio of the observed hyperfine anisotropy ($a_{||} - a_{\perp}$) to the 25 gauss theoretical maximum $a_{zz} - a_{xx} = 25$ G when the spin label is rigidly immobilised.

$$S = (a_{||} - a_{\perp}) / (a_{zz} - a_{xx}); 0 \leq S \leq 1$$

When $S = 0$, molecular mobility is unhindered and fluidity is maximal. When $S = 1$, molecular motion is negligible and rigid glass spectra are obtained. In biological membranes, a membrane order gradient may be observed [142]. The gradient typically stretches from a highly ordered zone (0.60-0.80) in the polar-non-polar interface region to the non-polar membrane core where it may approach 0.20. As the solvent terms such as polarity are not included, the expression for S is only an approximation. However, in this study only relative changes in the Caco-2 system are measured and the absolute values for S are not essential.

3.2.4 ATPase assay

Since it may be affected by TPGS analogues, ATPase activity was measured in the presence and absence of different P-gp substrates (verapamil (50 μ M), quinidine (50 μ M), progesterone (100 μ M), and nifedipine (0.5 μ M)). We used a modified version of a high-throughput screening assay developed by Garrigues *et al.* [143] with commercially available human P-gp membranes from Sf9 insect cells (BD Gentest, Heidelberg, Germany). Briefly, membrane vesicles were preincubated for 30 min at $37 \pm 0.5^{\circ}\text{C}$ in assay buffer that contained: i) MgATP (1.0 mM); ii) an ATP regenerating system consisting of pyruvate kinase (0.7 units/ml) and phosphoenolpyruvate (1.0 mM); and iii) a coupled system using LDH (1.0 unit/ml) and NADH (0.5 mM). Ouabain (0.5 mM), sodium azide (10 mM) and EGTA (1.0 mM) were added as inhibitors of unspecific ion pump ATPases.

The surfactant and – depending on the experimental setup – the respective P-gp substrate were added from stock solutions and vesicles were incubated for 60 min at $37 \pm 0.5^\circ\text{C}$. NADH consumption, corresponding stoichiometrically to the produced ADP, was measured with a UV-VIS plate reader (Spectra SLT III, TECAN, Crailsheim, Germany) at 340 nm.

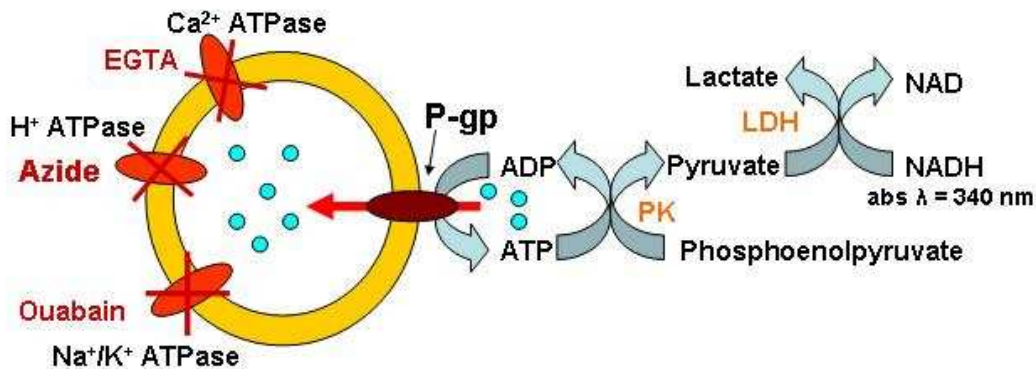


Figure 3-1 Schematics of a coupled enzymatic ATPase assay, adapted from [143].

3.2.5 Immunocytochemical staining

Caco-2 cell monolayers were stained three weeks after seeding on Transwell permeable filter inserts. Cells were washed and preincubated for 15 min at 37°C with pure KRB or KRB containing $10 \mu\text{M}$ CsA, respectively. Preincubation solution was removed and cells were fixed at room temperature for 10 min with 2% paraformaldehyde (PFA). Cells were washed and residual PFA was blocked for 10 min with 50 mM NH_4Cl , followed by permeabilization for 8 min with 0.1% triton X-100. UIC2 mouse monoclonal antibody stock solution ($50 \mu\text{g}/\text{ml}$) was diluted 1:50 in phosphate buffered saline (PBS) containing 1% BSA and cells were incubated for 60 min with the UIC2 primary antibody at 37°C . Mouse IgG1 κ was used as isotypic control and diluted 1:100 with PBS containing 1% BSA. The monolayers were then washed three times with PBS before being reacted with 1:100 dilution of Alexa Fluor[®] 488 conjugated goat anti-mouse $\text{F}(\text{ab}')_2$ fragment in PBS containing 1% BSA. $1 \mu\text{g}/\text{ml}$ of propidium iodide was added for counterstaining of cell nuclei. After 30 min of incubation at 37°C , cells were washed three times with PBS and embedded in FluorSave anti-fade medium (Calbiochem, Bad Soden, Germany).

Images were obtained using a confocal laser scanning microscope (MRC-1024, Biorad, Munich, Germany) with the instrument settings adjusted that no positive signal was observed in the channel corresponding to green fluorescence of the isotypic control.

3.2.6 UIC2 shift assay

UIC2 is a monoclonal antibody that can recognize human P-gp on the cell surface and strongly inhibits P-gp mediated drug efflux [144]. In contrast to other similar P-gp antibodies, UIC2 reactivity is sensitive to the functional state of P-gp, thus allowing to monitor P-gp conformational changes via its binding. UIC2 binding to P-gp is increased upon substrate binding or in cells whose ATP levels are depleted or whose nucleotide binding sites are inactivated by mutation [145]. On the other hand UIC2 binding is decreased in the presence of vanadate, which traps P-gp in a transition state by forming an irreversible ternary complex with ADP and P-gp [146, 147]. The differences in UIC2 reactivity are ascribed to differing numbers of P-gp molecules presenting the epitope recognized by UIC2 at the cell surface, thus reflecting conformational changes of the efflux pump during its catalytic cycles (Figure 3-2). Residues in the extracellular loop between TM5 and TM6 are directly involved in the display of the UIC2 epitope [148]. TM6 has been shown to be actively involved in the drug transport process and the proximity of this region to TM6 may help explain why UIC2 binding is sensitive to the functional state of P-gp and why binding of UIC2 inhibits P-gp mediated drug transport.

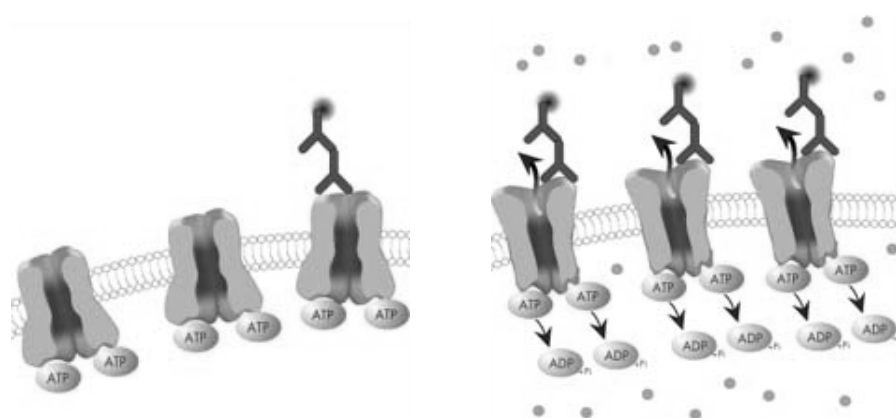


Figure 3-2 Principle of the UIC 2 shift assay: A Binding of UIC2 to inactive P-gp in the absence of a substrate; B: increased binding of UIC2 to P-gp paratopes exposed in active P-gp; adapted from www.chemicon.com.

For the UIC2 shift assay, Caco-2 cells, grown on Transwell permeable filter inserts, were harvested by trypsinization, washed and resuspended in KRB supplemented with 1% BSA. The number of viable cells was determined by trypan blue staining. 0.5×10^6 of viable cells in a total volume of 400 μ l KRB + 1% BSA were incubated for 30 min at 37°C with 5 μ g of primary monoclonal anti body UIC2. Wherever mentioned, cells were pre-incubated for 15 min (45 min in the case of TPGS 1000) at 37°C with 5 μ M of CsA, 1 mM sodium orthovanadate, 50 μ M verapamil, or 33 μ M of TPGS 1000 prior to antibody addition. With the exception of CsA, which was dissolved in ethanol 96%, all test compound stock solutions were prepared using bidistilled water. Sodium orthovanadate had to be activated for use in the UIC2 shift assay by depolymerization of vanadate. For this purpose a 100 mM stock solution of sodium orthovanadate was adjusted to pH 10.0, boiled and cooled down. The three steps were repeated until a stable, colourless solution was received. The activated orthovanadate stock solution was stored in aliquots at -20°C.

After incubation with the UIC2 antibody, cells were diluted with ice cold KRB to 2 ml and the suspension was centrifugated at 1000 g for 5 min. The cell pellet was washed two times with 2 ml of ice cold KRB. Cells were then resuspended in 400 μ l of KRB + 1% BSA containing 4 μ l of Alexa Fluor[®] 488 conjugated anti-mouse IgG and incubated for 30 min at 37°C in the dark. After wards, cells were diluted again to 2 ml and secondary antibody was removed by centrifugation. Cells were washed two times with 2 ml of ice cold KRB, before the cell pellet was resuspended in 1 ml of ice cold PBS to be analyzed in a BD FACS Calibur fluorescence-assisted cell sorter (BD Biosciences, Heidelberg, Germany). The fluorescence intensity associated with cells was expressed on a log scale.

3.2.7 Statistical analysis

All results are expressed as mean \pm standard deviation (SD). Correlation of data with results from previous Caco-2 transport experiments was conducted using Sigma Plot 9.0 graphing software (Systat Software Inc.; Point Richmond, CA, USA). Significance of difference in order parameters and ATPase activity values was determined by one-way analysis of variances (ANOVA) followed by Holm-Sidak post-hoc tests.

3.3 Results

3.3.1 ESR

The influence of TPGS 1000, and other analogues, on bilipid cell membrane fluidity was investigated using the lipid soluble spin label 5-doxyyl stearic acid (5-SA). Figure 3-3 shows a typical ESR spectrum obtained when 5-SA was incorporated into Caco-2 cell membranes in the absence of any modulators of membrane fluidity or P-gp activity.

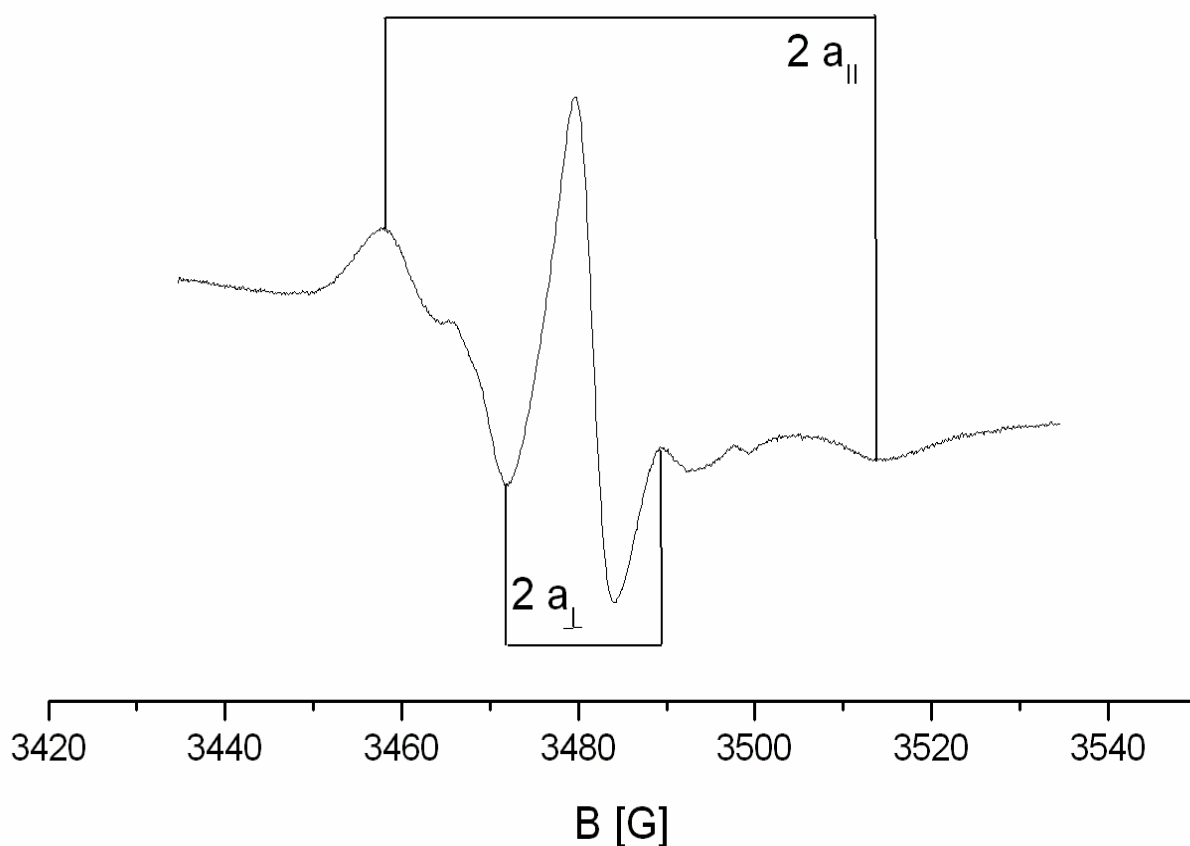


Figure 3-3 Typical ESR spectrum of 5-doxyylstearic acid incorporated into Caco-2 cells: $a_{||}$ and a_{\perp} are derived from spectral line splitting as indicated.

Incubating with the spin label and brief exposure to hypoxic conditions during the ESR measurements, had no negative effect on cell viability; trypan blue viability staining results for ESR treated and untreated trypsinized Caco-2 cells revealed $72.2 \pm 4.8\%$ and $75.4 \pm 3.9\%$ viable cells, respectively (mean \pm SD, $n = 3$).

Indicating a highly organized Caco-2 cell membrane in the head group region, the spin probe 5-SA in untreated cells gave an average S value of 0.789 ± 0.007 (Table 3-1). The results are in line with literature values describing an S value between 0.60 and 0.80 in the head group region of the lipid membrane bilayer.

To validate the Caco-2 ESR technique, we studied the influence of the surfactants SDS and Triton-X 100, which are both commonly used in molecular biology to fluidize and enhance the permeability of cell membranes, and have already been shown to fluidize membranes of prokaryotic and eukaryotic cells [149-151]. SDS showed a concentration dependent effect on membrane fluidity. Compared to control, 1.0 mM SDS significantly reduced S to 0.728 ± 0.014 (Table 3-1). A similar effect was observed for Triton-X 100 0.1%, which afforded an S value of 0.732 ± 0.006 (Table 3-1). Cholesterol succinate (1.0 mM) was used as a model membrane rigidifying compound [152-154]. The moderate but significant ($P < 0.05$) rigidification of the cell membrane in the presence of cholesterol succinate ($S = 0.813 \pm 0.005$) was comparable to the effect observed in the presence of 0.37 mM of the local anaesthetic procaine hydrochloride ($S = 0.805 \pm 0.005$; Table 3-1). For a long time, local anaesthetics were believed to fluidize cell membranes [155, 156]. However, it could be shown that they exert an amphiphilic effect on cell membrane fluidity, fluidizing the hydrocarbon core region but rigidifying the head group region [157, 158]. Overall, the extent of change in the order parameter S observed in the validation studies is well in the “normal range” compared to findings from previous ESR studies on other membrane active substances [70, 149].

Membrane Fluidizer/ Rigidizer	Order parameter S
Control	0.789 ± 0.007
SDS 0.10 mM	$0.784 \pm 0.070^*$
SDS 1.0 mM	$0.728 \pm 0.014^*$
Triton-X 0.1%	$0.732 \pm 0.006^*$
Procaine hydrochloride 37.0 mM	$0.813 \pm 0.005^*$
Cholesterol succinate 1.0 mM	$0.805 \pm 0.005^*$

Table 3-1 Order parameter 'S' of the spin label 5-SA incorporated into untreated Caco-2 cells and cells preincubated with potential membrane rigidizers and fluidizers; mean \pm SD, n = 3-5; * = significantly different from untreated control ($P < 0.05$).

TPGS 1000 at a concentration between 3.3 μM and 1.65 mM had no statistically significant ($P < 0.05$) effect on Caco-2 cell membrane fluidity (Figure 3-4). As the concentration of TPGS 1000 was continuously increased, a progressive fluidization of the cell membrane was observed. At the highest TPGS 1000 concentration (16.5 mM), 'S' was reduced from control (0.807 ± 0.005) to 0.727 ± 0.019 , corresponding to a 12.9% reduction of the order parameter.

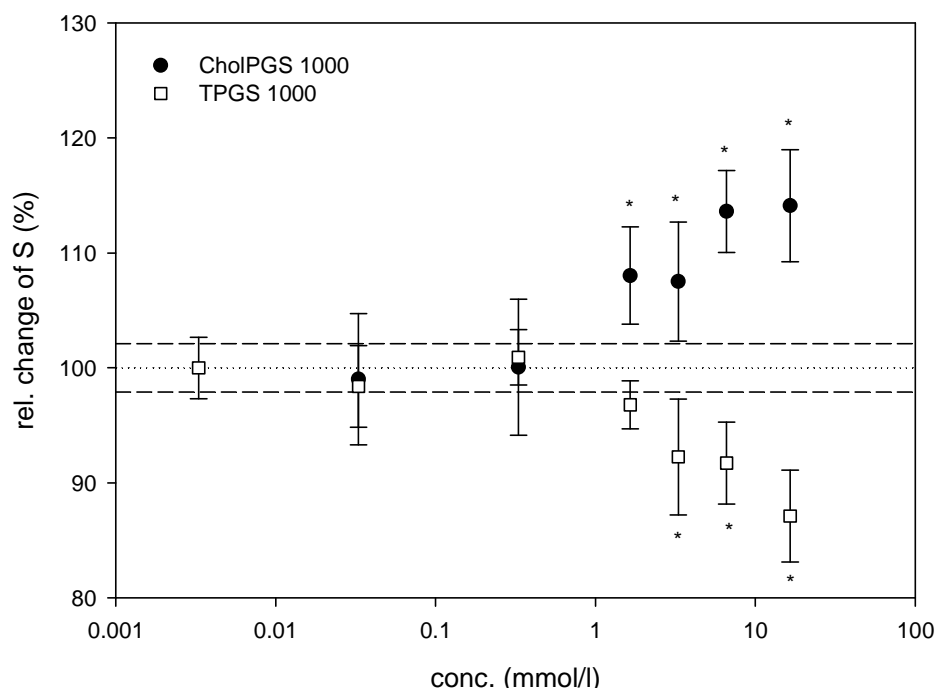


Figure 3-4 Relative change of the order parameter 'S' of the spin label 5-SA in Caco-2 cells under the influence of different concentrations of TPGS 1000 and cholesteryl PEG 1000 succinate ; mean \pm SD, $n = 3-4$; * = significantly different from untreated control ($P < 0.05$).

In contrast to TPGS 1000, cholesteryl PEG 1000 succinate rigidified the membrane in a dose dependent manner (Figure 3-4). The effect was statistically significant ($P < 0.05$) at a concentration of 1.65 mM onward. At the highest concentration, cholesteryl PEG 1000 succinate (16.5 mM) increased 'S' from control (0.790 ± 0.026) to 0.902 ± 0.003 , a 14.1% increase of the degree of order. For a head to head comparison of different TPGS analogues with varying PEG chain length (Table 3-2), concentrations of 33 μM and 3.3 mM were chosen, as they produced a maximal TPGS 1000 influence in the Caco-2 P-gp inhibition transport assay and the first

significant fluidizing effects in the ESR studies, respectively. At 33 μM , all of the tested TPGS analogues had only minimal influence on rigidity. At 3.3 mM, TPGS 200 was the only analogue that slightly, although not statistically significantly ($P = 0.279$) rigidified the membrane, while S for TPGS 600 was comparable to control. Similar to the previous dose response curve (Figure 3-4), TPGS 1000 (3.3 mM) significantly ($P < 0.05$) decreased S from 0.780 ± 0.016 to 0.746 ± 0.004 . TPGS 2000, 4000 and 6000 all showed similar extents of fluidization as TPGS 1000; the fluidizing effect appears to level off at a PEG chain length of 1000 Da. The membrane fluidization by TPGS 3500, though notable, was not statistically significant ($P = 0.17$).

	Order parameter S \pm SD	
Control	0.780 \pm 0.016	
Test compounds	At 3.3 mM	At 33 μM
TPGS 200	0.791 \pm 0.010	0.788 \pm 0.008
TPGS 600	0.779 \pm 0.016	0.784 \pm 0.031
TPGS 1000	0.746 \pm 0.004 *	0.783 \pm 0.002
TPGS 2000	0.747 \pm 0.011 *	0.790 \pm 0.001
TPGS 3500	0.754 \pm 0.016	0.778 \pm 0.008
TPGS 4000	0.749 \pm 0.019 *	0.793 \pm 0.014
TPGS 6000	0.752 \pm 0.004 *	0.776 \pm 0.002

Table 3-2 Order parameter 'S' of the spin label 5-SA incorporated into Caco-2 cell membranes in the presence of different TPGS analogues (at 33 μM and 3.3 mM); mean \pm SD, n = 3-5; * = significantly different from untreated control. ($P < 0.05$)

3.3.2 ATPase assay

To quantify changes in the P-gp ATPase activity by surfactants, especially TPGS 1000, a coupled enzymatic assay using artificial human MDR1 enriched membrane vesicles was employed [143]. Varying TPGS 1000 concentrations were tested for ATPase activity modulation; experiments were conducted in the absence and presence of different P-gp substrates known to induce efflux pump action and thereby ATPase activity. TPGS 1000 did not significantly influence ATPase activity on its own, neither inducing additional ATPase activity nor inhibiting basal ATPase function (Figure 3-5, open circles).

However, in the presence of verapamil (50 μM), which stimulated ATPase activity to a level of 39.89 ± 3.79 nmol/(mg*min), a dose dependent inhibition of this activation was observed with a TPGS 1000 EC_{50} value of 3.18 ± 1.97 μM (Figure 3-5, closed circles and Table 3-3).

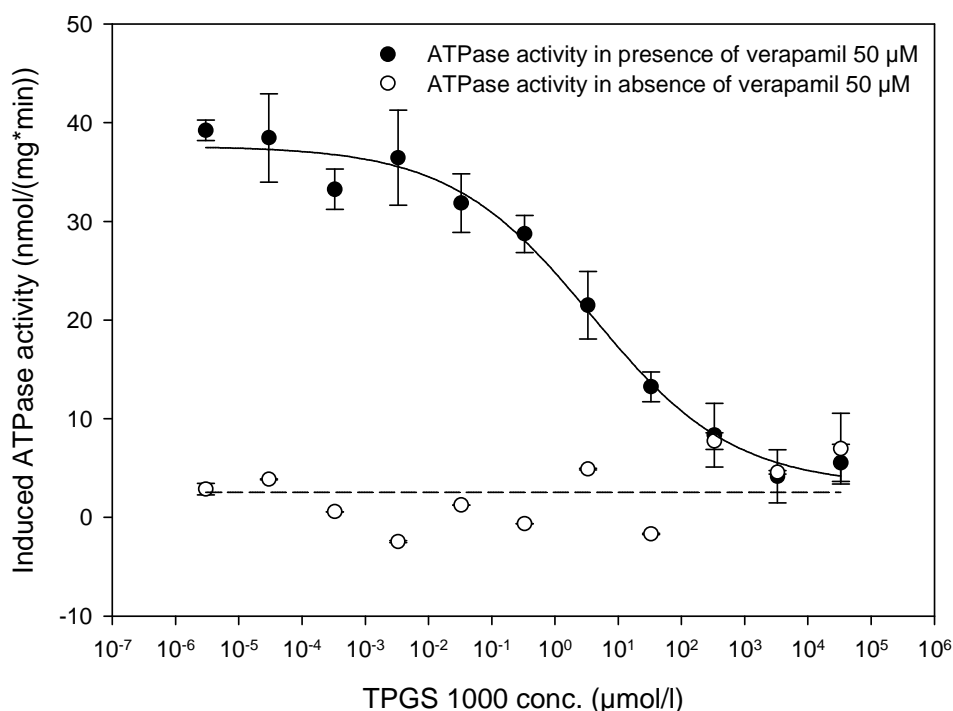


Figure 3-5 Influence of TPGS 1000 on P-gp ATPase activity in the absence and presence of verapamil (50 μM).

EC_{50} values were also determined in the presence of other P-gp substrates known to induce ATPase activity (Table 3-3). The ATPase activating effect (44.48 ± 2.69 nmol/(mg*min)) and the EC_{50} value determined for TPGS 1000 (3.25 ± 1.29 μM) were comparable to verapamil results if progesterone (100 μM) was instead used as the model substrate. The EC_{50} values in the presence of quinidine (50 μM) and nifedipine (1.0 μM) were about 4-8 times lower at 0.82 ± 0.47 μM and 0.40 ± 0.17 μM , respectively. Nifedipine induced the highest ATPase activity in the absence of TPGS 1000 (46.72 ± 6.67 nmol/(mg*min)), while quinidine was the weakest inducer amongst the tested substrates at 17.00 ± 3.96 nmol/(mg*min)).

Inductor of ATPase activity	Level of induced ATPase activity (nmol/(mg*min))	IC 50 (TPGS 1000) (μ M)
Verapamil (50 μ M)	39.89 \pm 3.79	3.18 \pm 1.97
Quinidine (50 μ M)	17.00 \pm 3.96	0.82 \pm 0.47
Progesterone (100 μ M)	44.48 \pm 2.69	3.25 \pm 1.29
Nicardipine (1 μ M)	46.72 \pm 6.67	0.40 \pm 0.17

Table 3-3 Induction of ATPase activity and EC₅₀ values of TPGS 1000 in the presence of different P-gp substrates; mean \pm SD, n = 8.

In order to try and expand the findings from TPGS 1000 to other non-ionic surfactants, EC₅₀ values in the ATPase assay using verapamil (50 μ M) as an ATPase inducer were also determined for Tween 80 and Cremophor EL. The determined EC₅₀ value for Tween 80 at 2.21 \pm 0.65 μ M was in the same concentration range as the TPGS 1000 value, but markedly lower than the EC₅₀ previously determined for the same compound in the Caco-2 transport assay. Cremophor EL performed best with an EC₅₀ value of 0.35 \pm 0.05 μ M.

	TPGS 1000 EC ₅₀ (μ M)	Tween 80 EC ₅₀ (μ M)	Cremophor EL EC ₅₀ (μ M)
Caco-2 transport assay	2.91 \pm 0.17	18.4 \pm 6.5	24.7 \pm 10.2
ATPase assay (verapamil 50 μ M)	3.18 \pm 1.97	2.21 \pm 0.65	0.75 \pm 0.10

Table 3-4 EC₅₀ values of TPGS 1000, Tween 80 and Cremophor EL as determined in the bidirectional Caco-2 transport assay (2.3.1.6) and in the ATPase assay, using verapamil 50 μ M as an inductor of ATPase function; mean \pm SD, n = 9 (transport assay), n = 12 (ATPase assay).

Using the same experimental setup, we expanded our findings by comparing the modulating effect of different TPGS analogues on ATPase activity. Both groups of TPGS derivatives with varying PEG chain length and modified hydrophobic moiety, but conserved PEG chain of 1000 Da, were evaluated. The derivatives did not influence ATPase activity in the absence of P-gp substrates, but they were able to inhibit verapamil induced ATPase activity. The head to head comparisons showed that the cholesterol and phytol derivatives had the strongest inhibitory influence on verapamil induced ATPase activity at the two tested concentrations of 3.3 μ M and

33 μM (Figure 3-6). Compared to the negative control in the absence of any TPGS analogue, verapamil induced ATPase activity was reduced by 30.28 ± 2.75 nmol/(mg*min) and 29.61 ± 2.75 nmol/(mg*min), respectively.

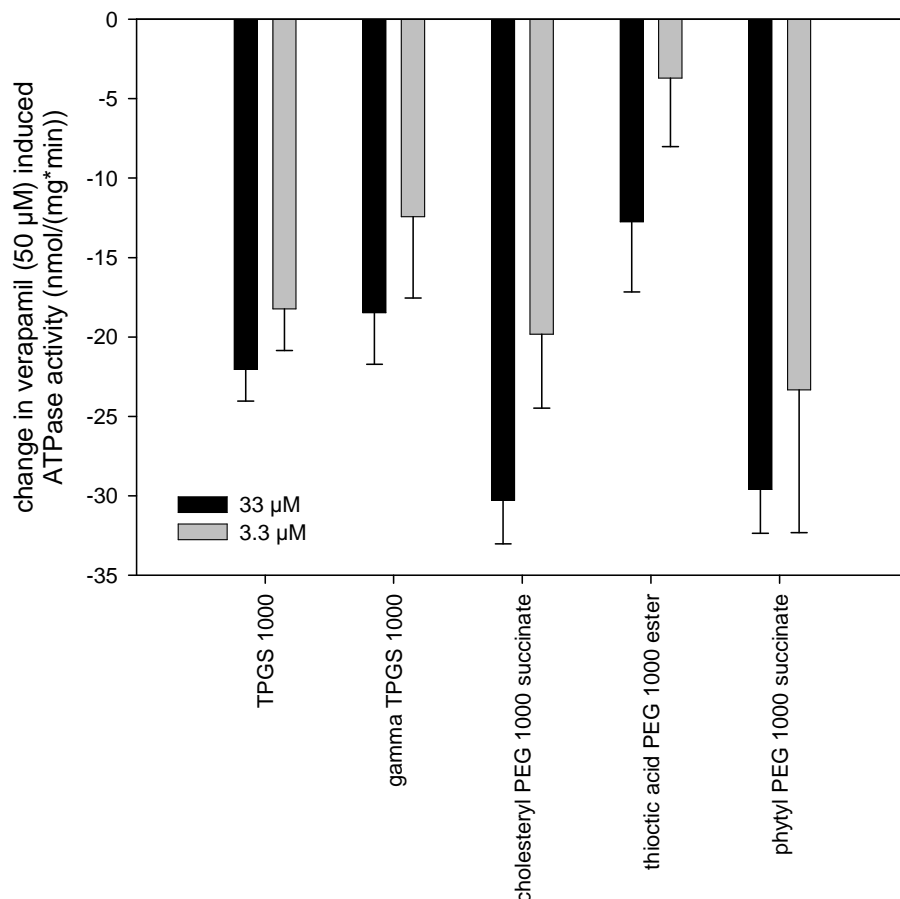


Figure 3-6 Change of verapamil (50 μM) induced ATPase activity in the presence of different TPGS analogues (33 μM) with modified hydrophobic moieties; mean \pm SD, n = 8; * = significantly different from untreated control (P < 0.05).

Among the derivatives with alternative hydrophobic moieties, thioctic acid PEG 1000 ester was the weakest ATPase activity modulator. Gamma-TPGS behaved similarly to commercially available alpha-TPGS 1000. Among the TPGS analogues that varied in PEG chain length (Figure 3-7), commercially available TPGS 1000 was the most efficient ATPase activity inhibitor. Analogues with longer or shorter PEG chain lengths gradually showed weaker inhibitory potential on ATPase function. In the case of TPGS 6000, a reverse effect was observed with a slight but significant (P < 0.05) induction of ATPase activity.

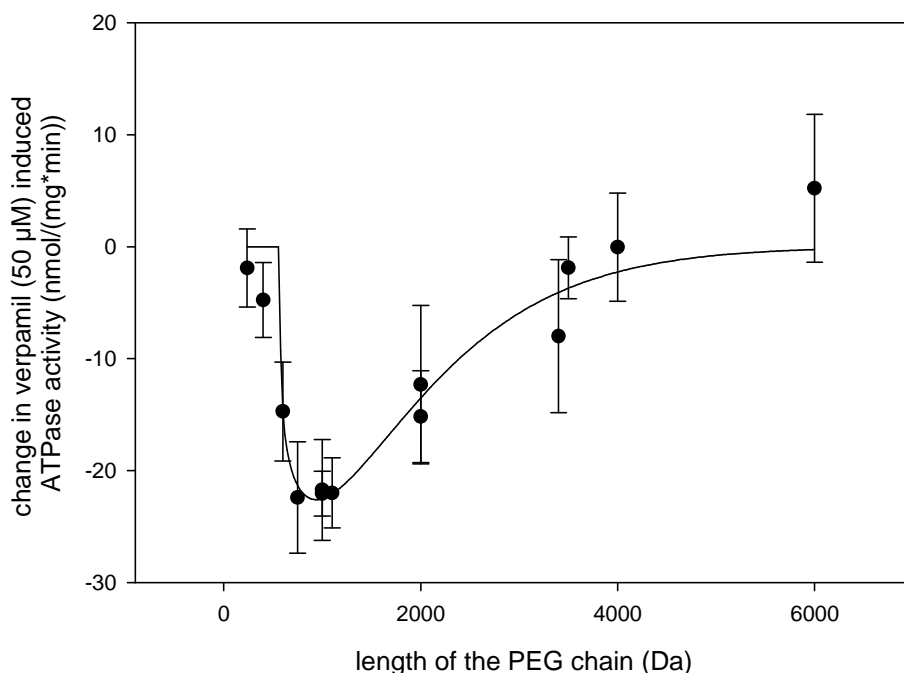


Figure 3-7 Change of verpamil (50 µM) induced ATPase activity in the presence of different TPGS analogues (33 µM) with varying PEG chain lengths; mean \pm SD, n = 8; * = significantly different from untreated control (P < 0.05).

Furthermore, as control experiments in the ATPase assay, ATPase inducing and/or inhibiting activity was investigated using vitamin E, vitamin E succinate, cholesterol, cholesterol succinate and PEG 1000. No significant (P < 0.05) influence on ATPase activity was observed over a concentration range from 0.0033 nM to 330 µM neither in the presence nor absence of P-gp substrate verpamil.

3.3.3 UIC2 shift assay

UIC2 reactivity shift assay was used to study P-gp conformational transitions in the presence of different concentrations of TPGS 1000. The known P-gp substrates and competitive inhibitors CsA and verpamil were included as references as well as sodium orthovanadate which traps the efflux pump in a transition state.

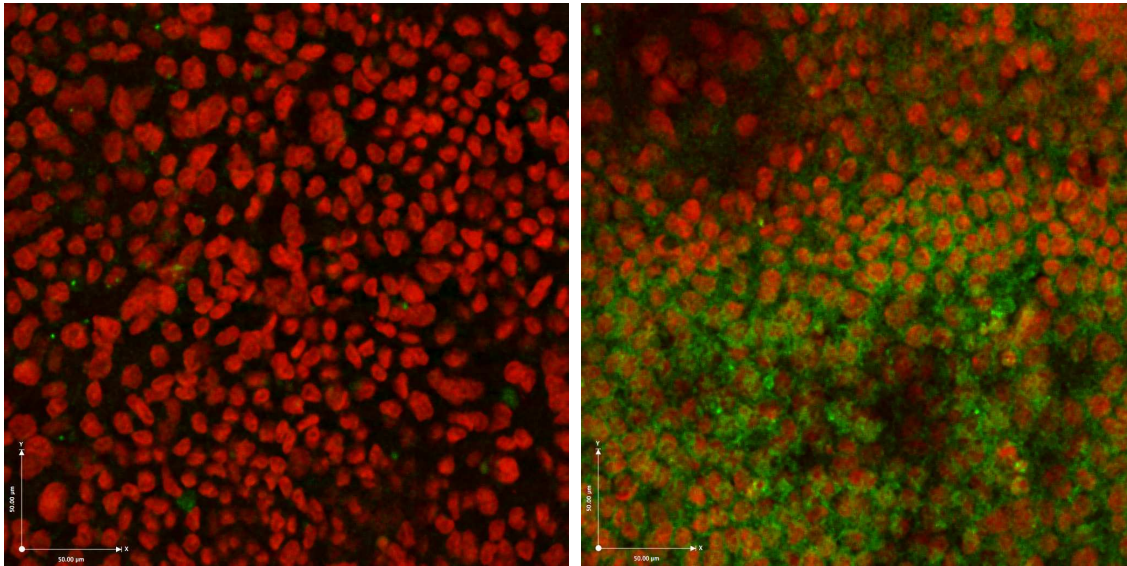


Figure 3-8 Immunofluorescence staining of P-gp in Caco-2 cells using the UIC2 antibody, cell nuclei are counterstained with propidium iodide left: in the absence of a P-gp substrate, right: in the presence of CsA 10 μM ; microscope settings were kept constant in both pictures; the scale bar in the lower left corner represents 50 μm

Binding of the UIC2 antibody to P-gp was shown by immunocytochemical staining (Figure 3-8). Intensity of the fluorescence can be quantified in a fluorescence activated cell sorter. Indicating increased reactivity of UIC2 with its epitope in P-gp, both CsA (10 μM) and verapamil (50 μM) shifted intensity of the fluorescence to higher levels (Figure 3-9 A and B, respectively). The shift was stronger for CsA, which raised the mean fluorescence intensity F_{mean} from 21.8 ± 4.3 FU in the control to 106.2 ± 9.2 FU, while verapamil only increased F_{mean} to a level of 45.4 ± 4.7 . In contrast, 1.0 mM sodium orthovanadate induced a profound reduction in UIC2 binding ($F_{\text{mean}} = 4.0 \pm 1.3$ FU). The presence of TPGS 1000 did not significantly affect UIC2 reactivity, although F_{mean} was slightly reduced to 18.6 ± 3.9 FU.

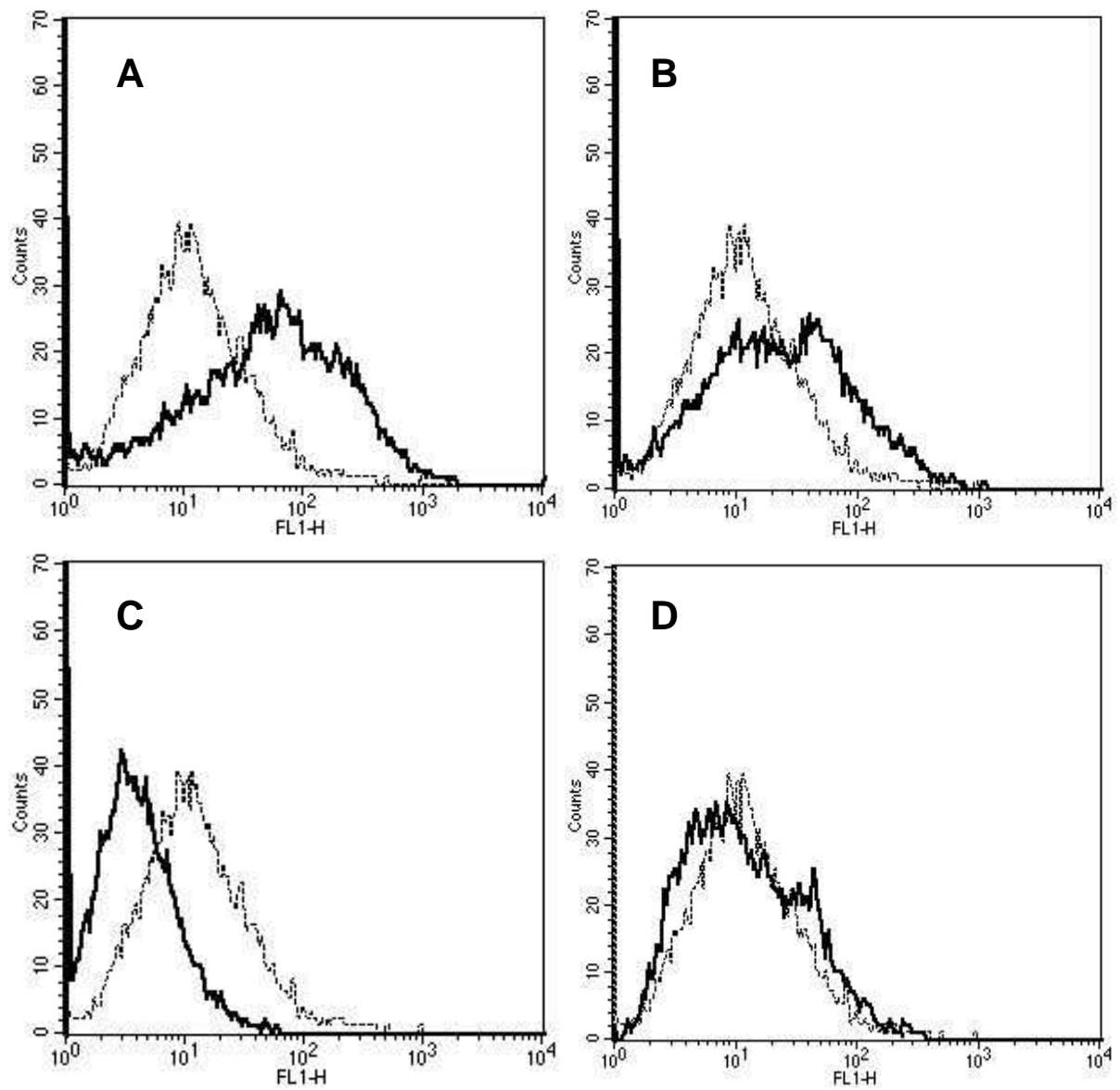


Figure 3-9 Monoclonal antibody UIC2 reactivity with P-gp in Caco-2 cells. Caco-2 cells were incubated with UIC2 antibody in the absence (dotted line) and presence of P-gp substrates/ modulators (fat lines); A: 10 μ M CsA, B: 50 μ M verapamil, C: 1.0 mM vanadate, D: 33 μ M TPGS 1000.

3.4 Discussion

3.4.1 Influence on membrane environment

In recent years, interest in surfactant interaction with efflux pumps such as P-gp has steadily increased. A number of studies have attempted to evaluate inhibitory potential of different surfactants and the exact nature of their interaction with efflux transporters [72, 73, 81, 84]. A fluidization/rigidification of the membrane environment [72, 73, 159, 160], sterical hindrance of substrate binding [137], and inhibition of efflux pump ATPase activity [93, 138, 139] are among the various mechanisms that have been proposed. However, so far there is no clear answer; results from different studies are contradictory and systematic studies with homologous groups of surfactants are lacking.

In an attempt to correlate our results with data from the previous SAR study (see 2), we focused on TPGS 1000 and two groups of homologous analogues with either modified PEG chain lengths or modified hydrophobic moieties. Using ESR as our method of choice, we investigated the influence of TPGS 1000 and its analogues on membrane fluidity. The ESR technique was already previously used to study membrane fluidizing effects of bile salts and verapamil in viable MDR1 over-expressing Chinese hamster ovary (CHO) cells [70].

At low concentrations (up to 0.33 mM) TPGS 1000 had only negligible effects on Caco-2 membrane fluidity, not statistically significantly ($P > 0.05$) reducing the membrane microviscosity (Figure 3-4) Our findings contradict previous results which showed TPGS 1000 (0.025 and 0.10 mM) to rigidify Caco-2 cell membranes [72]. Those measurements were performed using a fluorescence anisotropy method where the rigidifying effect of TPGS 1000 was restricted to the lipophilic fluorescent dye 1,6-diphenyl-1,3,5-hexatriene (DPH). DPH was incorporated into the non-polar side chain regions of Caco-2 cell membranes, whereas its cationic derivative 1-(4-trimethylammoniumphenyl)-6-diphenyl-1,3,5-hexatriene (TMA-DPH) measured membrane effects in the polar head group region and was unaffected by the presence of TPGS. DPH measurements often present highly variable results, as can be seen when comparing studies using other known P-gp surfactant modulators (e.g. Cremophor EL®). Hugger *et al.* [73] reported no effect of Cremophor EL® on DPH or

TMA-DPH membrane fluidity in Caco-2 and MDCK-MDR1 cells; yet, other groups reported either a significant fluidization of the cell membrane in the presence of Cremophor EL® [91], or a rigidifying effect of the surfactant on KB 8-5-11 (human epidermoid carcinoma) cells [92]. Besides the use of different cell lines with varying lipid compositions and protein content, the distribution of fluorescent dyes into intracellular organelles may help explain the experimental discrepancies. DPH is not only plasma membrane specific, but is known to distribute to other cell organelles within the cell, such as mitochondrial membranes. Therefore, the net polarization value is a product of all these effects [161]. Furthermore, variable placement of the fluorescent dye into the lipid bilayer may also contribute to the contradictory findings. Altogether, the shortcomings of the fluorescence anisotropy method necessitate the use of alternative techniques, such as ESR. Spin probes, such as 5-SA, are derived from lipidic acids and are much more lipophilic than fluorescent dyes (e.g. DPH and TMA-DPH). Relative to fluorescent dyes, spin probes incorporated into cell membranes are more stable and have not been reported to access intracellular membranes. The spin probe position within the membrane is highly defined and by adjusting the position of the spin active group, different regions of the cell membrane may be selectively studied.

Significant membrane fluidizing via TPGS 1000 was only observed above 3.3 mM (Figure 3-4). This concentration is about 100 times higher than the concentration at which full inhibition in Caco-2 transport studies was observed, and almost 1000 times higher than the IC_{50} value determined for TPGS 1000 in the transport ($5.86 \pm 2.17 \mu\text{M}$, data not shown) and ATPase assays. Instead the findings match better with results from previous cytotoxicity studies, which measured the release of the intracellular enzyme LDH as an indicator of cell membrane damage. Increased LDH release (> 20% cytotoxicity compared relative to positive control 1% Triton-X 100) which reflects a destabilization of the cell membrane, was observed with a TPGS 1000 concentration of $\geq 2.5 \text{ mM}$ [140]. The discrepancy between membrane fluidization and effective inhibitory concentration weakens the argument that surfactants (e.g. TPGS 1000) afford an unspecific membrane perturbation that modulates P-gp activity.

Furthermore, cholesteryl PEG 1000 succinate, which performed as good as commercial TPGS 1000 in the ATPase inhibition assay and surpassed its inhibitory potential in the Caco-2 transport assay (see 2.3.1.3), demonstrates opposite behaviour to TPGS 1000. Instead of fluidizing the cell membrane, cholesteryl PEG 1000 succinate significantly ($P < 0.05$) rigidified the cell membrane (≥ 1.65 mM; Figure 3-4). It seems highly unlikely that two opposing phenomena (e.g. membrane rigidification and fluidization) mediated by two related substances would lead to identical changes in P-gp conformational mobility, a factor believed to be responsible for efflux pump inhibition.

We previously [140] established that different TPGS analogues with varying PEG chain lengths afford different P-gp inhibitory potential *in vitro*. The ESR head to head comparison data also support the notion that P-gp inhibition via TPGS 1000 is not directly correlated to cell membrane fluidization (Table 3-2). TPGS analogues were tested at 33 μ M and 3.3 mM; these concentrations produced a maximum TPGS 1000 influence in the Caco-2 P-gp inhibition transport assay and the first significant fluidizing effects in the TPGS 1000 dose-response ESR studies, respectively. At 33 μ M, all TPGS analogues, regardless if they were previously shown to be P-gp active or non-active in Caco-2 transport experiments, had only negligible influence on rigidity. These findings are consistent with the non-effect in the TPGS 1000 dose response curve at this concentration. No correlation of PEG chain length with cell membrane fluidization or rigidification was observed. At the higher concentration of 3.3 mM, a significant ($P < 0.05$) fluidization of the cell membrane was noted for TPGS 1000 and all other derivatives with higher molecular weights. It appears that a certain PEG chain length, or rather molecular size, is required to mediate a significant fluidizing effect. However, higher molecular weight TPGS analogues, such as TPGS 4000 and TPGS 6000 – non-active in previous P-gp inhibition assays – resulted in a similar decrease in 'S'; surfactant sequestering into the cell membrane apparently levels off or may be reduced.

3.4.2 Influence on P-gp ATPase

Besides possible unspecific alterations in membrane microviscosity, inhibition of efflux pump ATPase resulting in energy source depletion was investigated via an ATPase assay. In an attempt to consistently maintain a high amount of P-gp expression and selectively study a single efflux pump, artificial P-gp enriched membranes were used. Four different P-gp substrates (verapamil, quinidine, nicardipine, and progesterone) known to interact with different binding sites of the efflux pump, and/or occupy different regions of the large drug binding pocket [32, 162], were chosen as inducers of ATPase activity (see 1.2.2).

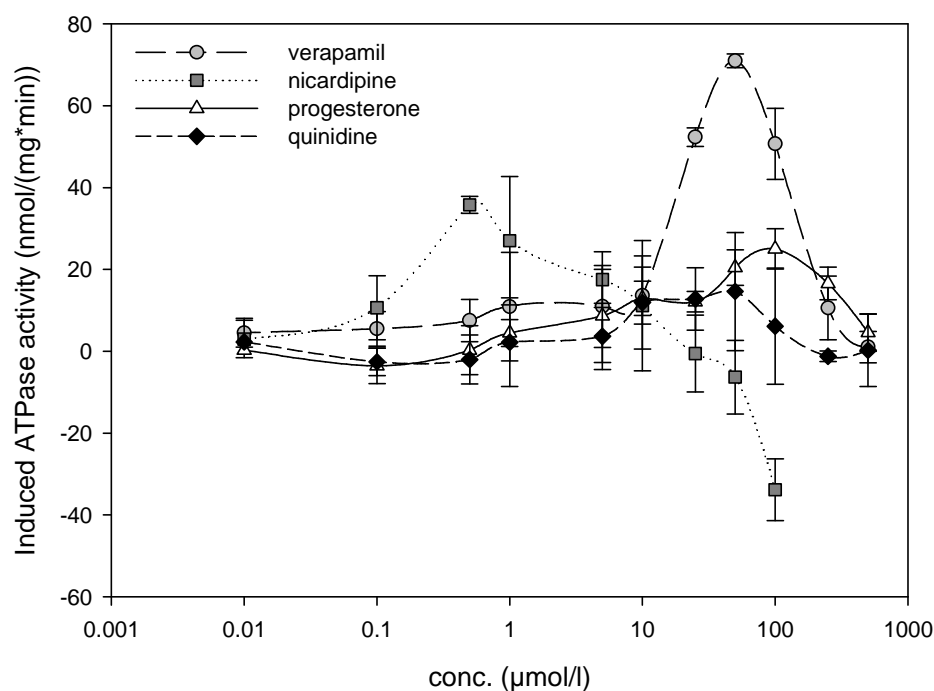


Figure 3-10 Determination of optimal substrate concentrations in the ATPase assay with commercially available MDR1 enriched Sf9 insect membranes; mean \pm SD, n = 4.

Optimal P-gp substrate concentrations were determined via standard dose response experiments. In accordance with previous studies [32, 143], verapamil, progesterone, quinidine and nicardipine all gave bell shaped dose response curves with maximum induction of ATPase activity at 50 μ M, 100 μ M, 50 μ M, and 1.0 μ M, respectively (Figure 3-10).

Dose response curves for TPGS 1000 were generated in the presence and absence of P-gp substrates. When incubated on its own with artificial P-gp containing

membranes (Figure 3-5), TPGS 1000 neither induced significant ATPase activity nor inhibited basal ATPase function over a concentration range from 0.0033 nM to 330 μ M, indicating no direct interaction between the transport sites and the surfactant. TPGS 1000 appears not to be a substrate of P-gp, making a competitive inhibition of substrate binding unlikely. However, a significant dose-dependent inhibition of P-gp substrate induced ATPase activity was observed. The determined EC_{50} values for inhibition of verapamil and progesterone induced ATPase activity ($3.18 \pm 1.97 \mu$ M and $3.25 \pm 1.29 \mu$ M, respectively) are comparable to the EC_{50} value determined in a transport assay with the fluorescent dye RHO ($2.91 \pm 0.17 \mu$ M), indicating a correlation between inhibition of substrate transport and energy depletion. EC_{50} values for inhibition of quinidine and nifedipine induction of ATPase activity were about 10 times lower ($0.82 \pm 0.47 \mu$ M and $0.40 \pm 0.17 \mu$ M, respectively).

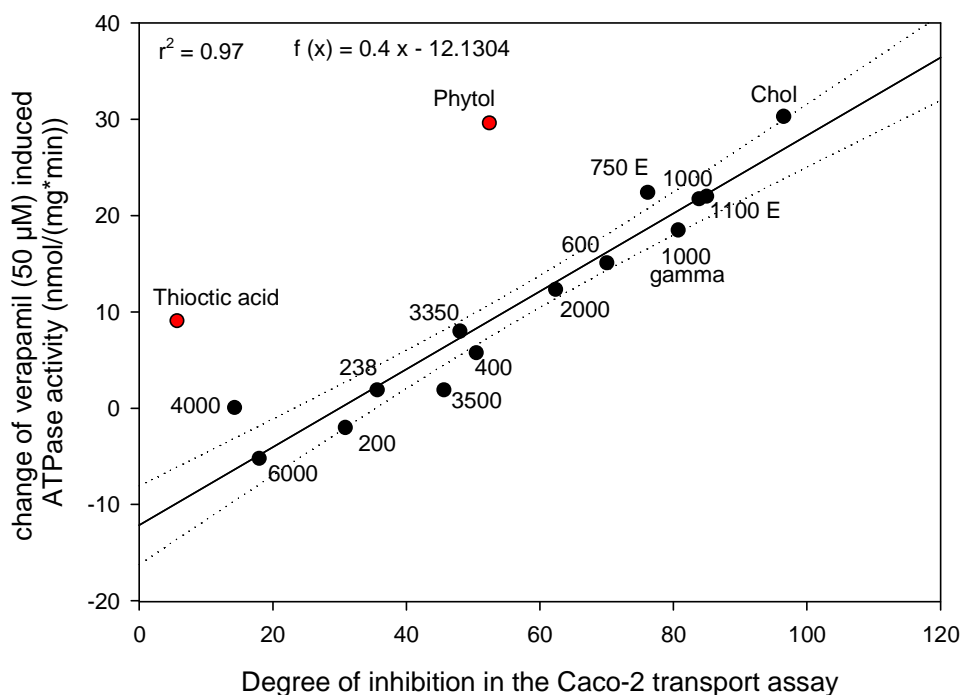


Figure 3-11 Correlation of change in induced ATPase activity mediated by different TPGS analogues and their degree of inhibition in the Caco-2 cell monolayer efflux assay.

As summarized in Figure 3-11 a correlation was observed when the change of verapamil (50 μ M) induced ATPase activity was plotted versus degree of inhibition observed in the Caco-2 transport assay. The degree of inhibition was calculated from the Caco-2 raw data. Generally, a good correlation ($r^2 = 0.97$) was found between the inhibitory potency of the various TPGS analogues and their effect on verapamil induced ATPase activity.

Consistent with findings from previous transport experiments, cholesteryl PEG 1000 succinate showed the strongest inhibition of verapamil induced ATPase activity. Cholesteryl PEG 1000 succinate, as well as phytyl PEG 1000 succinate, surpassed commercially available TPGS 1000 (Figure 3-6). However, phytyl PEG 1000 succinate performed considerably worse in the bidirectional Caco-2 transport assay and therefore lies outside the correlation (Figure 3-11). Besides phytyl PEG 1000 succinate, thioctic acid PEG 1000 ester is the only derivative that lies outside the correlation. Its effect in the transport assay was markedly lower than would be expected by the extent of energy depletion. In the case of phytyl PEG 1000 succinate this result could be attributed to its strong cytotoxic effect; as shown by increased LDH leakage and a massive drop off of TEER values during the transport experiment (see 2.3.2), while the discrepancy for thioctic acid PEG 100 ester may be due to increased hydrolysis of the ester during the longer course of the transport experiment (6 hours compared to 1.5 hours in the ATPase assay).

A slight induction of ATPase activity was observed in the presence of TPGS 6000. This phenomenon may be explained via micelle sequestration of inhibitors of unspecific ATPases (ouabain, EGTA, and sodium azide). A concentration of 33 μM was used, which lies above the CMC of 0.02% wt. Altogether, the ATPase assay data suggest that ATPase activity inhibition is a major part in the mechanism of P-gp inhibition by TPGS, and maybe non-ionic surfactants in general. Pluronic block copolymers have been shown to inhibit efflux pump ATPases [137]. Pluronic copolymers with intermediate lengths of hydrophobic PO (propylene oxide) chains and relatively short hydrophilic EO (ethylene oxide) segments, a model representative being Pluronic P85, were shown to have the highest MDR modulating potential [163]. Their modulatory influence on P-gp, and other ABC transporters, was attributed to a so called “double punch” effect of intracellular energy depletion by disruption of mitochondria and membrane fluidization, which directly affects P-gp ATPase activity [93].

As discussed above, we could not show relevant membrane fluidizing effects for TPGS analogues at P-gp active concentrations. Therefore, alternate hypotheses may be proposed: i) merely incorporating large surfactant molecules into the cell membrane affords a reduction of ATPase activity as substrate can not be bound because of a sterical blocking of the binding site; and ii) a direct interaction of the

surfactant with allosteric sites – not with a transport site – in the P-gp efflux pump. There is strong evidence for the existence of several allosteric sites in P-gp, such as the cis-(Z)-flupentixol binding site [164, 165] and the SR33557 binding site [166]. Both explanations appear consistent with the varying EC_{50} values for progesterone/verapamil and quinidine/ nicardipine determined in the ATPase assay. Sterically blocking substrate binding may not encompass all binding sites, or portions of the binding pocket, to the same extent. Alternatively, an allosteric modulation of P-gp may influence different binding sites to varying extents. A direct interaction of surfactant molecules with the efflux pump intracellular ATP binding domains is considered unlikely, since such a modulation of ATPase activity would influence all P-gp substrates to a similar extent and would be expected to perturb basal ATPase activity.

In an attempt to try to transfer the mechanistic findings for TPGS to other non-ionic surfactants, EC_{50} values for inhibition of verapamil induced ATPase activity were determined for Tween 80 and Cremophor EL. Tween 80 at $2.21 \pm 0.65 \mu\text{M}$ performed comparable to TPGS 1000, while Cremophor EL surpassed the other two non-ionic surfactants with an EC_{50} value of $0.35 \pm 0.05 \mu\text{M}$ (Table 3-4). The high affectivity for Tween 80 and Cremophor EL is in disagreement with the results from the Caco-2 transport assay and in consequence the ranking of the inhibitory potential for all three surfactants differs between both assays. The use of different cell systems (Caco-2 vs. P-gp enriched Sf9 cell membranes) and substrates in both assays might account for varying values. Still, the contradictory inhibitory potentials for the different surfactants infer that although a modulation of ATPase function is mediated by all three surfactants, Tween 80 and Cremophor EL affect additional transport systems (e.g. the postulated basolateral uptake transporter for RHO) thus negating their overall efficiency in the Caco-2 transport assay. Only further investigations can uncover if the structurally diverse group of non-ionic surfactants shares a common mechanism of action for P-gp modulation.

3.4.3 Influence on P-gp conformation

To further narrow down possible mechanisms of TPGS interaction with P-gp, the conformational changes in the efflux pump in the presence of TPGS were investigated using the UIC2 shift assay. The monoclonal UIC2 antibody inhibits the activity of MDR1 by binding to an epitope on the proposed extracellular loop between TM5 and TM6 [148]. As the display of the UIC2 epitope depends on the functional state of P-gp, the binding affinity of UIC2 reflects conformational changes in the efflux pump. In the absence of substrate, only a portion of P-gp molecules can react with UIC2. Addition of P-gp substrates or ATP depleting agents increases UIC2 reactivity. On binding of the drug, ATP is hydrolysed, which is coupled with movement in TM6 and TM12 [167], thus shifting position of the extracellular loop linked to TM6 and converting UIC2 non-recognizable P-gp molecules to UIC2-recognizable molecules.

As has been previously described [145], the known P-gp substrates and competitive inhibitors, CsA and verapamil, both significantly increased reactivity of UIC2 with P-gp in Caco-2 cell (Figure 3-9). In contrast, the presence of TPGS 1000 did not statistically significantly affect UIC2 binding, although a slight shift to lower affinities can be noted. Hence, TPGS doesn't bind to one of the substrate active drug binding sites of P-gp, neither as a substrate nor as a competitive inhibitor. Furthermore, an intracellular ATP depletion by TPGS can be excluded. Such a mechanism of action was previously proposed for Pluronic P85, an other non-ionic surfactant known to inhibit P-gp [139], but would increase the number of UIC2 recognizable molecules [145].

The slight reduction of UIC2 binding in TPGS treated Caco-2 cells shows similarities to the trapping of P-gp in a transition state in the presence of orthovanadate. Vanadate forms a ternary complex with ADP and the NBD of P-gp [146], inhibiting nucleotide dissociation and reducing the number of UIC2-recognizable P-gp molecules. As an alternative to the formation of an intracellular complex, an allosteric modulation of P-gp might be proposed. Cis(Z)-flupentixol, an allosteric inhibitor of P-gp, has been demonstrated to reduce UIC2 reactivity with P-gp by blocking substrate translocation and dissociation [165].

An allosteric inhibition of P-gp by TPGS would go with the sensitivity of P-gp inhibition to changes of the hydrophobic moiety (see 2.4.4) and the variation in EC_{50} values observed for substrates with varying drug binding sites (see 3.4.2). On the other hand a non-effect of TPGS 1000 on UIC2 binding would be in line with a proposed sterical blocking of substrate binding, as no direct binding with the efflux pump would occur and the number of UIC2-recognizable molecules would be neither increased nor decreased.

Altogether, the UIC2 results for TPGS 1000 have to be considered inconclusive as the observed shift to lower affinities is weak compared to the reduction induced by vanadate and can not be considered statistically significant. The overall UIC2 binding in Caco-2 cells, probably due to only moderate P-gp expression levels, is too low to better differentiate changes in the conformational state.

3.5 Outlook

Thus far, the results don't allow us to definitively identify the inhibitory mechanism of TPGS and additional studies are required. The synthesis of new TPGS analogues with further modified hydrophobic moieties may help to narrow down the specificity of the TPGS interaction with P-gp that was already hinted at in the results for the first generation TPGS analogues with modified hydrophobic cores.

A greater variety of TPGS analogues could lead to the development or rejection of a pharmacophore model, thus allowing to approve or to decline the 'sterical blocking of substrate binding' theory. Interesting candidates for the synthesis of these new TPGS analogues might be flavonoid or bile salt derivatives (e.g. naringenin PEG succinate, silybin PEG succinate, or chendesoxy cholic acid PEG succinate; Figure 3-12). These are molecules that have been described to modulate P-gp activity and subsequent PEGylation might increase or decrease the inhibition potency. According to the PEG chain length theory, the molecular weight of the PEG moiety should be adjusted to 1500 Da. Alternatively, other polymer chains could be evaluated, e.g. polyethyleneimine, although cytotoxicity aspects have to be taken into account.

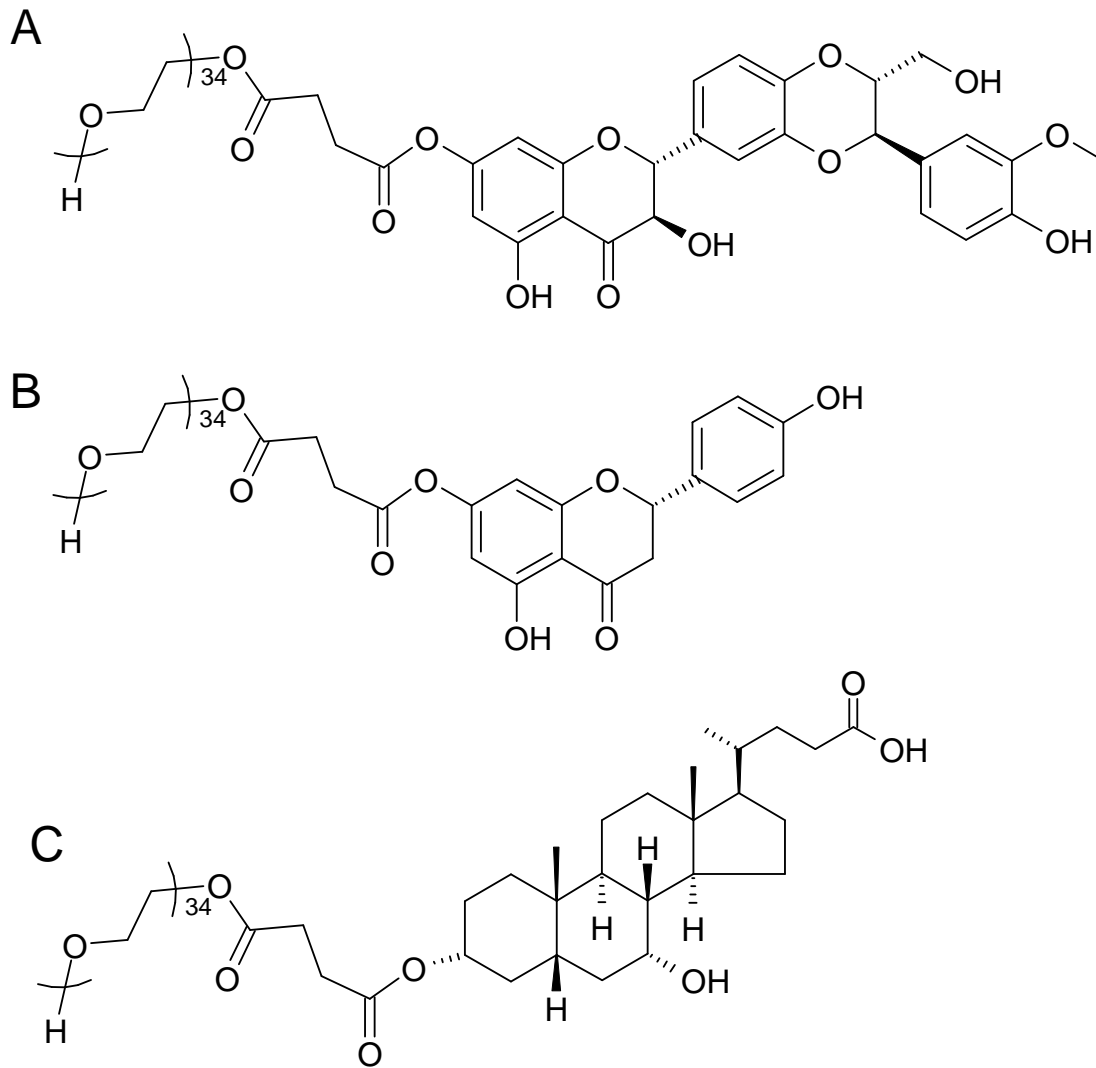


Figure 3-12 Suggested new TPGS analogues to be investigated in the next step of a TPGS SAR study; A: Silybin PEG 1500 succinate; B: Naringenin PEG 1500 succinate; C chendesoxy cholic acid PEG 1500 succinate.

3.6 Conclusion

The ability of different TPGS analogues to inhibit verapamil induced ATPase activity was found to correlate with their inhibitory potential in the Caco-2 cell transport assay. The correlation supports the notion that efflux pump energy source depletion is a major factor in the inhibitory mechanism of TPGS. ATPase inhibition seems to be a function of sterically blocking substrate binding and/or allosteric modulation of P-gp rather than a competitive inhibition or an unspecific rigidification or fluidization of the cell membrane; such effects were only observed at concentrations about 100 fold higher than those needed to achieve full efflux inhibition and did not correlate with the activity pattern in bidirectional transport studies. The theory of an allosteric modulation of P-gp activity is further supported by findings in the UIC2 assay. A reduction of antibody reactivity was observed, which may be explained by a blocking of drug translocation and dissociation.

4 Summary

Efflux transporters such as P-glycoprotein may influence pharmacokinetics of substrate drugs. The water soluble vitamin E derivative and non-ionic detergent, TPGS 1000, was demonstrated to be one of the most potent modulators of P-gp among surfactants. However, the P-gp inhibiting properties were merely discovered by chance and molecule structure was not optimized for this purpose. In order to study, and potentially improve P-gp inhibition, two groups of homologous TPGS analogues were synthesized.

TPGS inhibitory potential may be increased by a modification of the PEG chain length. Optimum efflux inhibition was achieved at a chain length of ~1500 Da, as predicted from the Weibull distribution describing the activity pattern. The lack of P-gp inhibitory activity in TPGS analogues with either very short (e.g. TPGS 400) or long (e.g. TPGS 6000) PEG chains, opens up other potential applications of the novel TPGS analogues. As non-active excipients with sufficient solubilizing potential but no transporter modulating 'side effects', they may present lower risks of drug-formulation, formulation-food, or formulation-formulation interaction and may be better suited as solubility enhancers in *in vitro* permeability studies, as they don't mask potential P-gp involvement in substrate bioavailability.

New P-gp inhibitors could also be developed by the exchange of the hydrophobic moiety of TPGS for other compounds. Thus far, cholesteryl PEG 1000 succinate represents the most potent TPGS analogues. Cholesteryl PEG 1000 surpassed both TPGS 1000 and TPGS 1500 in their P-gp modulating effect.

P-gp inhibition by TPGS was shown to be mediated via the TPGS monoester, while the diester component, a by-product of the TPGS synthesis negatively influences the P-gp modulation. In consequence, the inhibitory activity of TPGS and its analogue cholesteryl PEG 1000 succinate could be increased about 10 times by purification of the monoester. Furthermore, TPGS ether derivatives were introduced as an interesting alternative to non-etherified TPGS analogues. They allow for the synthesis of pure TPGS monoesters, thus indirectly increasing the inhibitory potential.

Sensitivity of TPGS inhibitory activity to exposure time (and to a lesser degree application side) may help explain the differing reports on TPGS ability to inhibit P-gp *in vitro*, and may have dramatic influence on its performance as an *in vivo* P-gp inhibitor and bioavailability enhancer. Delivery systems, which allow for a delayed

release of the drug in relation to TPGS, could help further improve the circumvention of P-gp mediated drug efflux.

With regards to the mechanism of P-gp inhibition by TPGS, no correlation could be detected between activity of the TPGS analogues and their physicochemical parameters, determined experimentally and *in silico*. Activity of TPGS is not linearly related to CMC, lipophilicity, molecular weight or molecule volume. A cut off seems to exist at a molecular weight of ~2100 Da, explaining the declining part of the Weibull activity curve. As the TPGS molecules become increasingly larger and more hydrophilic, their distribution into and transport across the cell membrane is reduced, hinting at target/ side of action of TPGS that is located intracellularly or in the membrane region.

An unspecific alteration of the membrane environment by TPGS, negatively influencing the conformational mobility of P-gp, could be ruled out as a possible mechanism of action: TPGS neither significantly increased nor decreased membrane fluidity at P-gp active concentrations (33 μ M). A statistically significant decrease of membrane microviscosity could only be detected at concentrations about 100 times higher than those needed to inhibit P-gp and the effect did not correlate with the Weibull activity pattern observed in the bidirectional transport studies. Furthermore the equally P-gp active cholesteryl analogue of TPGS showed opposing effects as it rigidized the membrane at concentrations of > 1.65 mM. The results of these ESR experiments match the differences observed in the inhibitory activity of TPGS analogues with modified hydrophobic moieties, where only specific modifications of the TPGS structure were found to be P-gp active while others completely lacked any inhibitory effect, an activity pattern best explained by a specific interaction of TPGS with the efflux pump.

Instead of an unspecific alteration of P-gp membrane environment the inhibitory mechanism of TPGS involves an inhibition of efflux pump ATPase, which could be demonstrated to correlate directly with the inhibitory effect of varying TPGS analogues in Caco-2 transport experiments. The efflux pump inhibition is not the result of a competitive inhibition of substrate binding as TPGS 1000 isn't a substrate of P-gp and doesn't bind to one of the transport active binding sites of the efflux pump: in the UIC2 shift assay TPGS failed to induce the characteristic conformational

change observed in the presence of a P-gp substrate. Furthermore in the ATPase assay, TPGS 1000 could not induce significant ATPase activity by itself and therefore is not transported by the efflux pump. The results of the UIC2 shift assay are inconclusive with regards to a further exploration of the essential energy depletion. At this moment it can't be distinguished if the reduction of substrate induced ATPase activity is due to a sterical blocking of substrate binding, thus only representing an indirect effect of TPGS on the ATPase function or if an allosteric modulation or intracellular complex formation with the ATPase traps P-gp in a transition state. The low resolution of the UIC2 shift in Caco-2 cells, doesn't allow to definitively interpret if the observed slight but statistically not significant shift of UIC2 binding to lower affinities represents an actual reduction of UIC2 affinity.

5 Zusammenfassung

Die Pharmakokinetik von Arzneistoffen wird durch Effluxtransporter wie P-gp beeinflusst. Das wasserlösliche Vitamin E Derivat und nicht-ionische Tensid TPGS 1000 ist einer der potentesten P-gp Modulatoren in der Gruppe der oberflächenaktiven Substanzen. Seine P-gp hemmenden Eigenschaften wurden jedoch eher durch Zufall entdeckt und seine Molekülstruktur wurde folglich auch nicht auf diesen Zweck hin optimiert. Um die P-gp Hemmung durch TPGS zu genauer zu untersuchen und wenn möglich zu verbessern, wurden zwei Gruppen von TPGS-Analoga synthetisiert.

Die Hemmwirkung von TPGS konnte durch Modifikation der PEG Kettenlänge verbessert werden. Wie aus der Weibull Verteilung, die das Aktivitätsmuster von TPGS Derivaten mit unterschiedlicher Kettenlänge beschreibt, vorhergesagt, wurde die optimale Hemmung des P-gp Effluxes dabei von Molekülen mit einer Kettenlänge von ungefähr 1500 Da erzielt. Die fehlende Hemmwirkung anderer TPGS Derivate mit sehr kurzer (z.B. TPGS 400) oder langer (z.B. TPGS 6000) PEG Kette eröffnet zusätzlich weitere Anwendungsmöglichkeiten der neuen TPGS Analoga. Die nicht-aktiven TPGS Derivate stellen Hilfsstoffe mit ausreichenden Löslichkeitsverbessernden Eigenschaften dar, jedoch ohne die Transporter modulierenden Nebenwirkungen anderer Tenside, weshalb ihnen ein geringeres Risiko für Arzneistoff-Formulierungs-, Formulierungs-Nahrungs-, oder Formulierungs-Formulierungs-Wechselwirkungen innewohnt. Des weiteren könnten sie als Lösungsverbesserer in *in vitro* Permeabilitätsstudien Einsatz finden, da sie mögliche P-gp Efflux Effekte auf die Bioverfügbarkeit von Arzneistoffen nicht überspielen oder verbergen.

Neue P-gp Hemmstoffe konnten außerdem durch Austausch der hydrophoben TPGS Komponente durch andere Strukturen synthetisiert werden: Cholesteryl PEG 1000 succinat stellt dabei den zur Zeit potentesten P-gp Hemmstoff unter allen bekannten TPGS Derivaten dar, da es sowohl TPGS 1000 als auch TPGS 1500 in ihrem Effekt auf P-gp noch übertrifft.

Es konnte weiterhin gezeigt werden, dass die eigentliche aktive Komponente des Stoffgemischs TPGS 1000 der TPGS Monoester ist, während der TPGS Diester, ein Nebenprodukt der TPGS Synthese die Hemmung sogar negativ beeinflusst. Folglich

war es möglich durch Aufreinigung des Monoesters das Hemmpotenzial sowohl von TPGS 1000 also auch von Cholesteryl PEG 1000 succinat jeweils um etwa das 10-fache zu steigern. Außerdem wurden TPGS Etherderivate eingeführt, die eine interessante Alternative zu den normalen nicht veretherten TPGS Molekülen darstellen. Durch die Etherbildung ist es möglich, ausschließlich reine TPGS Monoester zu synthetisieren und dadurch indirekt die Hemmwirkung ohne vorherigen Aufreinigungsschritt zu steigern.

Die Abhängigkeit der TPGS Hemmwirkung auf P-gp von der Vorinkubationszeit in Gegenwart des Tensids (und zu einem geringeren Maße auch von der Applikationsseite des Hemmstoffs) erklärt die teilweise widersprüchlichen Berichte über die Effektivität der P-gp Hemmung durch TPGS *in vitro*. Gleichzeitig könnte die Zeitabhängigkeit des Effekts auch Auswirkungen auf die *in vivo* Wirkung von TPGS haben. Delivery Systeme, die den Arzneistoff zeitlich versetzt zu TPGS freisetzen, könnten die Minderung des P-gp Einflusses auf die Bioverfügbarkeit weiter verstärken.

Bezüglich des Hemmmechanismus von TPGS konnte keine Korrelation zwischen den experimentell und *in silico* bestimmten physikochemischen Eigenschaften der TPGS Analoga und ihrer Aktivität entdeckt werden. Die Hemmwirkung von TPGS korreliert weder mit der CMC, der Lipophilie, dem Molekulargewicht noch dem Molekülvolumen. Es läßt sich lediglich feststellen, dass bei einem Molekulargewicht von etwa 2100 Da ein Cut off zu existieren scheint, der den abfallenden Teil der Weibull Kurve erklärt. Ab einer bestimmten Größe werden die TPGS Moleküle zu hydrophil und voluminös, um sich in die Membran zu verteilen bzw. diese zu durchqueren. Indirekt kann daraus auch auf einen wahrscheinlichen intrazellulären oder membrangebundenen Wirkort des TPGS Moleküls geschlossen werden.

Eine unspezifische Änderung der Membrenumgebung durch TPGS, die die konformelle Flexibilität von P-gp beeinflussen könnte, konnte jedoch als potentieller Hemmmechanismus ausgeschlossen werden: in einer P-gp aktiven Konzentration (33 μM) wurde die Membran durch TPGS weder verflüssigt noch rigidisiert. Eine statistisch signifikante Reduktion der Membranfluidität wurde nur in Konzentrationen festgestellt die etwa 100-fach höher liegen, als die zur P-gp Hemmung notwendigen Mengen. Der Effekt korrelierte auch nicht mit dem Weibull Aktivitätsmuster aus dem bidirektionalen Transportversuch. Das ebenfalls P-gp aktive TPGS Derivat

Cholesteryl PEG 1000 succinat, zeigte genau den gegenteiligen Effekt, indem es die Membran in Konzentrationen über 1,65 mM rigidisierte. Die Ergebnisse aus den ESR Versuchen passen damit zu den beobachteten Unterschieden bei den TPGS Derivaten mit modifiziertem hydrophoben Kern. Nur bestimmte Modifikationen erhöhten die Hemmwirkung auf P-gp, während andere keine hemmenden Effekt auf die P-gp Aktivität beinhalten, was auf eine spezifische Wechselwirkung mit der Effluxpumpe schließen läßt.

Anstatt einer unspezifischen Änderung der P-gp Membrenumgebung beinhaltet der Hemmmechanismus von TPGS eine Hemmung der P-gp ATPase, ein Effekt der mit dem Ausmaß der Hemmung im Caco-2 Transportversuch korreliert. Die Hemmung der Effluxpumpe kann dabei nicht das Resultat einer kompetitiven Hemmung der Substratbindung und indirekten Reduktion der ATPase Aktivität sein, da gezeigt werden konnte, dass TPGS kein P-gp Substrat ist und nicht an eine der transportaktiven Bindungsstellen der Effluxpumpe bindet: im UIC2 shift assay konnte nicht die normalerweise in Gegenwart von P-gp Substraten beobachtete Zunahme der UIC2 Affinität festgestellt werden. Zusätzlich induzierte TPGS allein, ohne die Zugabe von P-gp Substraten, im ATPase Assay keine nennenswerte ATPase Aktivität und wird folglich auch nicht von der Effluxpumpe transportiert. Statt dessen könnte die essentielle Energiedepletion durch eine sterische Abschirmung der Substratbindung, eine allosterische Modulation von P-gp oder eine direkte Interaktion mit den intrazellulären Nukleotidbindungsdomänen erklärt werden. Die Ergebnisse des UIC2 shift Assay erlauben leider keine eindeutige Einschränkung dieser Möglichkeiten. Es konnte zwar eine leichte Reduktion der UIC2 Affinität in Gegenwart von TPGS beobachtet werden, was darauf hinweisen könnte, dass die Effluxpumpe in einem Übergangszustand gefangen sein könnte, jedoch ist die Differenzierungsgenauigkeit im UIC2 Assay mit Caco-2 Zellen zu gering um eine statistische Signifikanz des Effekts zu beweisen.

6 Appendix: ESR spectroscopy

6.1 Theoretical background

Besides mass and electric charge, an electron is defined by its angular momentum J . J is the sum of the intrinsic angular momentum S of the electron due to the electron spin and the orbital angular momentum L arising out of the rotation of the electron around an atom's nucleus.

An electric current circulating in a planar loop produces a magnetic dipole moment, which is positioned perpendicularly to the plane of the loop. The total magnetic moment of an electron μ_J consists of the intrinsic magnetic dipole moment of the electron spin μ_S and the orbital magnetic dipole moment μ_l . For most applications, when free radicals are considered, the orbital magnetic dipole moment can be neglected, and the magnetic dipole moment is reduced to the intrinsic magnetic dipole moment μ_S .

$$|\mu_J| = |\mu_S| = -g^*|S|\mu_B$$

where μ_B is the Bohr magneton ($9.27 \times 10^{-24} \text{ J T}^{-1}$) and g is a factor of proportionality, the so called 'Lande factor'. A free electron (on its own) has a g value of 2.002319304386 (g_e , the electronic g factor).

When placed in an external magnetic field of strength B_0 , the magnetic dipole moment of the electron can align itself parallel or anti-parallel to the external field, with two distinct energy levels of:

$$E_+ = +\frac{1}{2} * g_e * \mu_B * B_0$$

$$E_- = -\frac{1}{2} * g_e * \mu_B * B_0.$$

This splitting of energy levels by an external magnetic field is called the 'Zeeman effect' (Figure 6-1). The strength of the external magnetic field B_0 determines the energy difference ΔE between both energy states.

If this energy ΔE is applied to the system in the form of electromagnetic radiation ($h \cdot \nu$, where ν is the speed of the electromagnetic wave and h is Planck's constant), resonance conditions are reached and energy will be absorbed leading to a 'flipping' of the magnetic moment.

$$\Delta E = g_e \cdot \mu_B \cdot B_0 = h \cdot \nu$$

In ESR spectroscopy, resonance conditions are generally achieved by the variation of the strength of the external magnetic field (0.1 -1 Tesla), while the wavelength of the absorbed microwave radiation is kept constant.

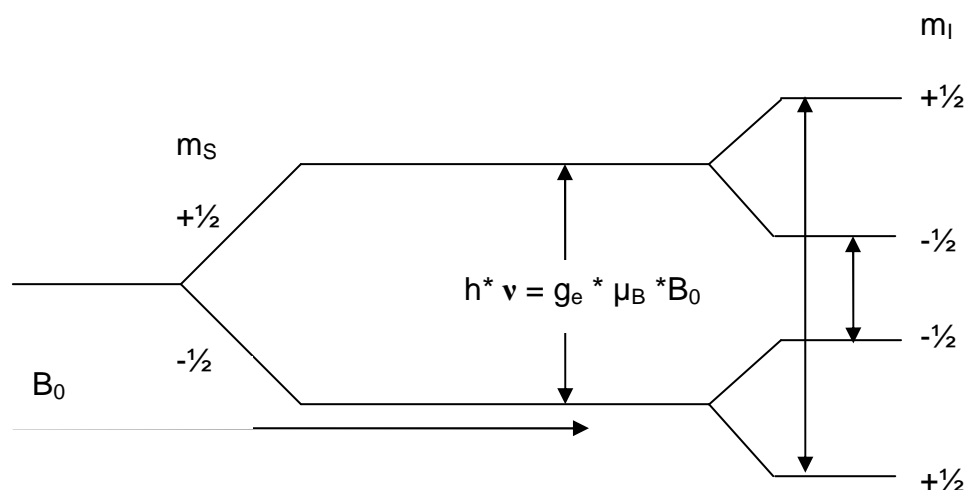


Figure 6-1 Zeeman splitting of electron energy levels in a homogeneous external magnetic field and further splitting of the electron energy levels due to hyperfine coupling with a nucleus ($m_I = 1/2$).

Electrons are normally associated with atoms, which can change the angular momentum of the electrons in different ways. Firstly, the electron may gain or lose intrinsic angular momentum through the interaction with the orbital angular momentum. This so called spin-orbit coupling influences the value of the g-factor, which then varies from the theoretical value of 2.002319304386. Spin-orbit coupling is most pronounced in transition metal compounds ($1 < g < 4$), while radicals are less affected.

Secondly, this change in angular momentum is not the same for all orientations of the atom or molecule in an external magnetic field. In other words, the g-factor changes according to the orientation of the paramagnetic atom in the magnetic field—it is anisotropic. This anisotropy depends upon the electronic structure of the atom in question, and therefore can yield information about the atomic (or molecular) orbitals containing the unpaired electron.

Thirdly, interaction may occur between the electron spin and spin of the atom's nucleus. A nucleus with a nuclear spin of $I = \frac{1}{2}$ generates a local magnetic field B_{loc} , which can again align itself parallel or anti-parallel to the external magnetic field. The corresponding electron therefore is subject to two different magnetic fields $B_{eff} = B_0 + B_{loc}$ and $B_{eff} = B_0 - B_{loc}$, leading to a further splitting in two energy levels and thereby spectral lines, the so called 'hyperfine structure' (Figure 6-1). Hyperfine splitting is observed with all nuclei, with a nuclear spin $I > 0$. In general, a paramagnetic probe with the electron spin $S = \frac{1}{2}$ and the nucleus spin I will give an ESR spectrum with $2S^* (2I + 1) = 2I + 1$ ESR transitions. Resonance conditions are reached in a resonance field B_{res} with

$$B_{res} = B_{res}^0 - a^* m_I,$$

where B_{res}^0 is the resonance field in the absence of electron- nucleus coupling, m_I is the magnetic quantum number and 'a' is the hyperfine coupling constant, which describes the distance of the lines of the hyperfine structure. Often there is more than one nucleus interacting with the electrons. Consequently the number of transition processes (and spectral lines) will increase. In the case of varying hyperfine coupling constants smaller and longer couplings may overlay, a phenomenon known as the 'super hyperfine structure'.

6.2 Spectral anisotropy

As mentioned above and indicated in Figure 6-2, both the g -factor and the hyperfine coupling constant 'a' depend on the orientation of the spin active group (in this case the p -orbital of a nitroxide group) in the outer magnetic field B_0 .

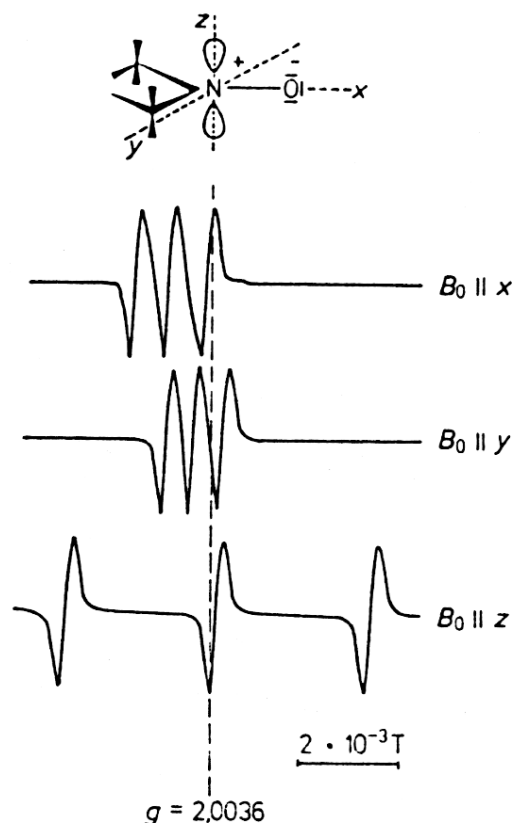


Figure 6-2 Dependency of the ESR spectra of nitroxide spin probes on the orientation; frame of reference is the orientation of outer magnetic field B_0 ; adopted from [168]

The z -axis in the pictured coordinate system corresponds to the orientation of the p -orbital that lies parallel to the longitudinal molecule axis of the spin probe. In a single crystal, aligning B_0 parallel to any of the three main axes of the system, leads to three distinctly different signals, each described by their own g -factor and hyperfine coupling constant:

$$a_{xx} = 5.9 \cdot 10^{-4} \text{ T}, a_{yy} = 5.4 \cdot 10^{-4} \text{ T} \text{ and } a_{zz} = 3.29 \cdot 10^{-3} \text{ T}$$

$$g_{xx} = 2.0088, g_{yy} = 2.00548 \text{ and } g_{zz} = 2.0021.$$

If, as in most cases, the molecule system is symmetric to one axis, two components, $a_{||} = a_{zz}$, $a_{\perp} = a_{xx}$ and $g_{||} = g_{zz}$, $g_{\perp} = g_{xx}$ respectively, are enough to describe the ESR

spectrum. For orientations in between the two main axes values in between are assumed.

As the hyperfine coupling constant and the g-factor only depend on the angle Φ between the magnetic field and the molecular axes, the orientation of the molecule can be derived from the experimentally determined parameters a_0 and g_0 according to:

$$g_0 = \sqrt{g_{\parallel}^2 * \cos^2 \Phi + g_{\perp}^2 * \sin^2 \Phi}$$

$$a_0 = \sqrt{a_{\parallel}^2 * \cos^2 \Phi + a_{\perp}^2 * \sin^2 \Phi}$$

All contemplations so far were restricted to single crystals. However in reality, more often poly-crystalline powder spectra will be encountered, in which all orientations occur statistically. The spectrum then contains all g-factors and hyperfine coupling constants, giving an overall signal as indicated in Figure 3-3

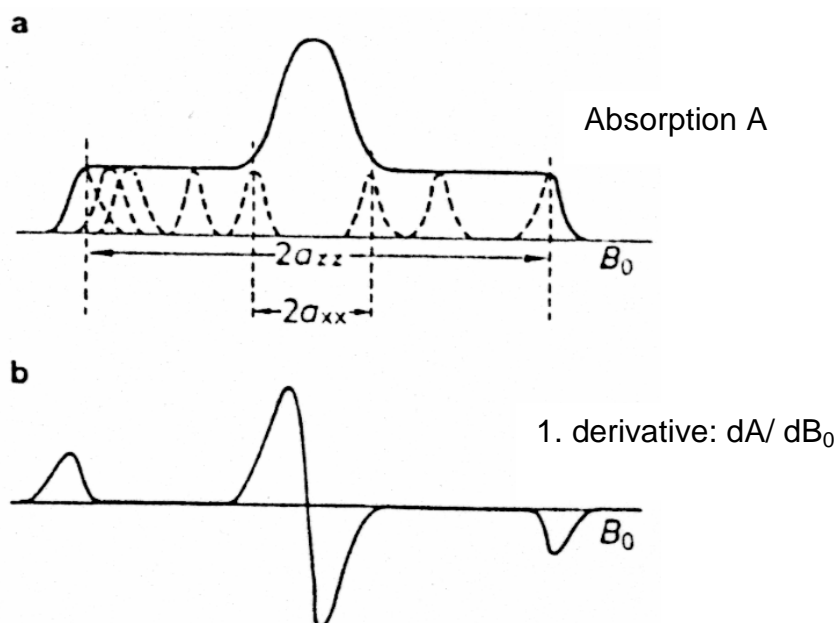


Figure 6-3 Origin of an anisotropic ESR signal of a statistically distributed spin probe; a = overall absorption; the dotted lines represent the absorption signals of the different orientations; b = first derivative of the overall signal; adopted from [168]

In a non-viscous solution, in contrast to the powder spectra, the probe molecules can rotate rapidly and freely around their axes. If the rotation correlation time is smaller than the duration of the absorption process, the anisotropy of 'a' and 'g' averages out and the spectrum becomes independent of the orientation of B_0 . The hyperfine coupling constant and the g factor assume so called isotropic mean values with

$a_0 = 1/3 (a_{zz} + a_{yy} + a_{xx})$, $g_0 = 1/3 (g_{zz} + g_{yy} + g_{xx})$ and $a_0 = 1/3 (a_{||} + 2a_{\perp})$, $g_0 = 1/3 (g_{||} + 2g_{\perp})$ in a system that is symmetric to the axes, respectively. The resulting spectrum is characterized by three sharp lines (Figure 6-4 b).

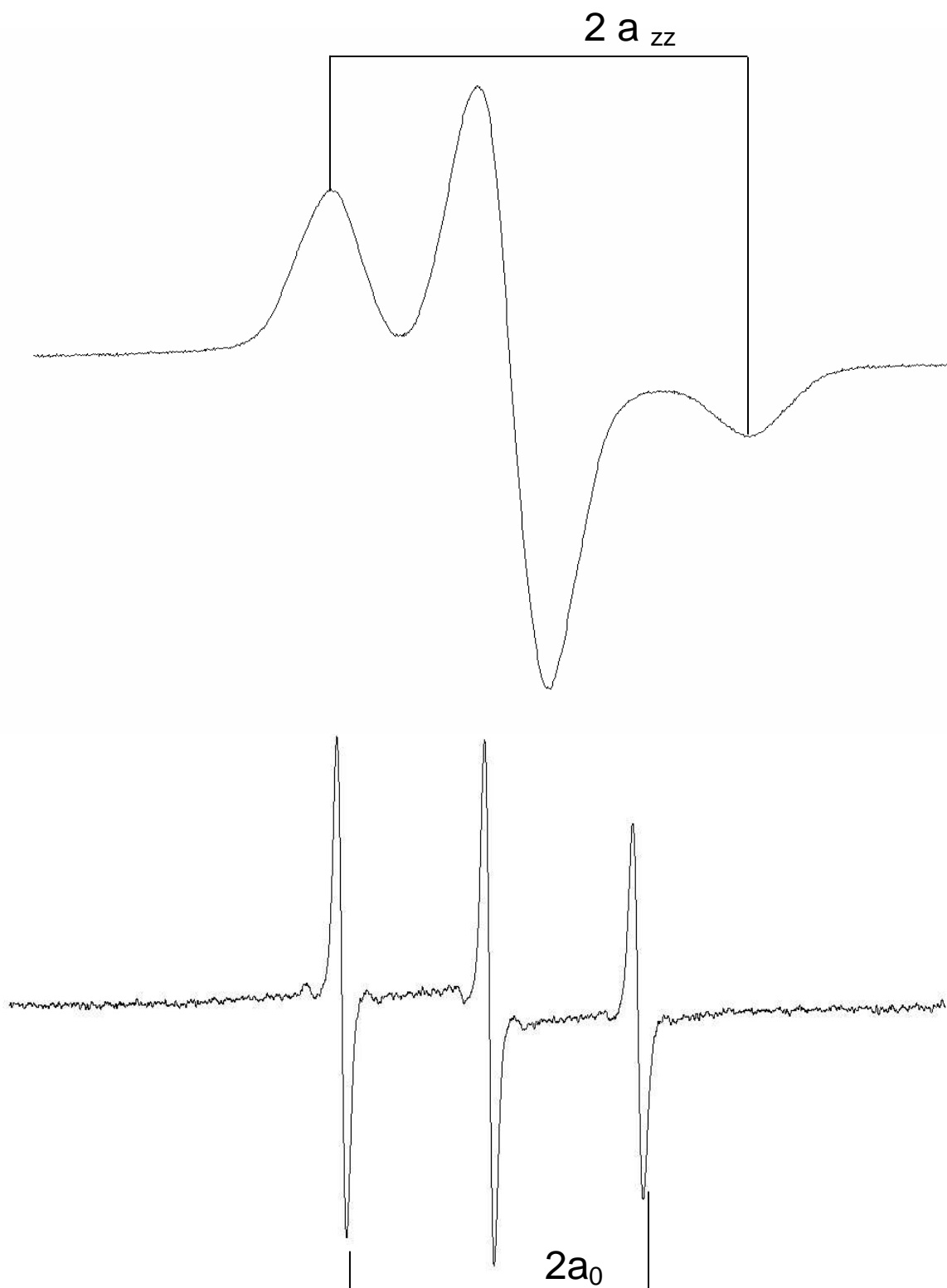


Figure 6-4: a. anisotropic spectrum of 5-doxyl stearic acid, measured at 77K in a 0.5 mM solution in water b: quasi isotropic spectrum of 5-doxyl stearic acid in a 0.5 mM solution in water at 298K, a_{zz} is the maximal hyperfine coupling constant; a_0 is the isotropic hyperfine coupling constant.

6.3 Spin probes and the order parameter S

ESR measurements can only be performed on probes containing unpaired electrons, such as paramagnetic metal ions (e.g. Fe^{3+} , Cu^{2+} , Mn^{2+}), organic molecules containing electron triplets, and free radicals. With the help of ESR spectroscopy, structural information about the environment of the unpaired electrons, such as the orientation of the spin-active group and its mobility in its environment, as well as the concentration of the spin-active group may be acquired. However, most often biomolecules don't include paramagnetic groups or unpaired electrons. Therefore indirect measurements have to be conducted, using stable organic radicals, so called spin labels. The spin labels are attached covalently or via H-bonds or hydrophobic interactions to macromolecules. Those macromolecules can either be the molecules to be investigated themselves or they can function as probes, examples being derivatives of lipidic acids such as 5-doxyl stearic acid (5-SA, figure 6-6) or T-SASL (2,2,6,6-tetramethyl piperidin-1-oxyl-4-yl-octadecanoate). Generally, nitroxide radical ($\text{N-O}\cdot$) probes are used either in the form of derivatives of oxazolidine or piperidine/ pyrrolidine.

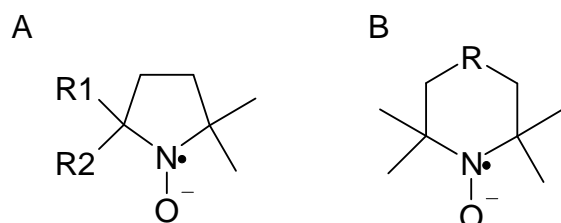


Figure 6-5 Spin active oxazolidine (A) and piperidine/ pyrrolidine (B) groups.

Methyl groups located close to the $\text{N-O}\cdot$ group reduce the reactivity of the radical, making the spin label stable in solution for weeks. In the nitroxide spin probes, the unpaired electron is located in the $2p_{\pi}$ -orbital of the nitrogen and is subject to hyperfine coupling with the nitrogen ^{14}N nucleus ($I=1$), resulting in a hyperfine splitting into three transition lines.

As noted above, ESR spectra of paramagnetic substances depend on the orientation of paramagnetic atom in the outer magnetic field. This is utilized in the construction of spin probes to obtain information about the probe environment. A lipid spin label is constructed in a way that the axes of the nitroxide group assume definite positions in the molecular coordinate system: The z-axis (the direction of the outer magnetic field

B_0) is the longitudinal axis of the molecule and defines the direction of the maximal hyperfine splitting with $a_{zz} = 3.2 \cdot 10^{-3}$ T. The p-orbital of the nitroxide nitrogen is orientated along the z-axis, while the two other components of the hyperfine coupling with $a_{yy} = a_{xx} = 5.6 \cdot 10^{-4}$ T are located perpendicularly to the longitudinal axis.

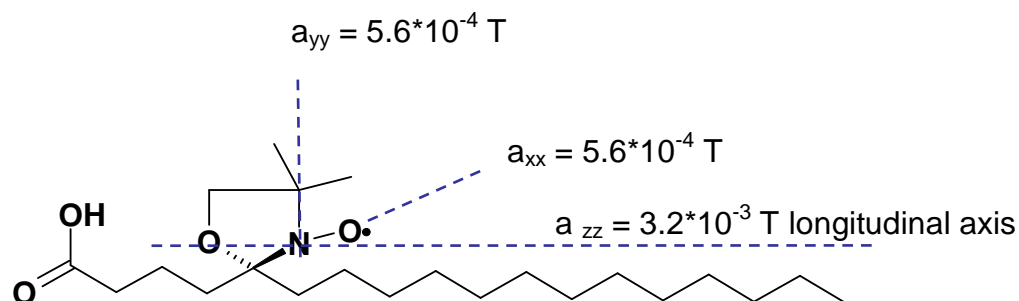


Figure 6-6 Structure of the spin label 5-doxyl stearic acid and orientation of the molecule axes.

In a membrane, the spin probe will align itself parallel to the membrane normal. If the spin label is rigidly incorporated into the membrane system or covalently bound to a macromolecule, the resulting spectrum will resemble an anisotropic powder spectrum via statistical distribution of the orientations. In reality, the spin label will not be completely immobilized. Therefore the theoretically possible maximal hyperfine splitting a_{zz} and minimal hyperfine splitting a_{xx} will not be reached. Instead, the experimentally determined parameters $a_{||}$ and a_{\perp} will assume other values ($a_{||} < a_{zz}$ and $a_{\perp} > a_{xx}$). The divergence from the theoretical values will be increase along with the mobility of the spin probe. To quantify the mobility of the spin probe the order parameter 'S' is introduced as the ratio of the actual hyperfine coupling constants to their theoretical values:

$$S = (a_{||} - a_{\perp}) / (a_{zz} - a_{xx}); 1 \leq S \leq 0$$

When $S = 0$, molecular mobility is unhindered and fluidity is maximal. When $S = 1$, molecular motion is negligible and powder like spectra are obtained. In biological membranes, a membrane order gradient may be observed. The gradient typically stretches from a highly ordered zone (0.60-0.80) in the polar-non-polar interface region to the non-polar membrane core where it may approach 0.20.

7 References

1. Artursson, P., A.L. Ungell, and J.E. Lofroth. Selective paracellular permeability in two models of intestinal absorption: cultured monolayers of human intestinal epithelial cells and rat intestinal segments. *Pharm Res* 1993; 10(8): 1123-9.
2. Lipinski, C.A., F. Lombardo, B.W. Dominy, and P.J. Feeney. Experimental and computational approaches to estimate solubility and permeability in drug discovery and development settings. *Adv Drug Deliv Rev* 2001; 46(1-3): 3-26.
3. Leslie, E.M., R.G. Deeley, and S.P. Cole. Multidrug resistance proteins: role of P-glycoprotein, MRP1, MRP2, and BCRP (ABCG2) in tissue defense. *Toxicol Appl Pharmacol* 2005; 204(3): 216-37.
4. DuBuske, L.M. The role of P-glycoprotein and organic anion-transporting polypeptides in drug interactions. *Drug Saf* 2005; 28(9): 789-801.
5. Ambudkar, S.V., C. Kimchi-Sarfaty, Z.E. Sauna, and M.M. Gottesman. P-glycoprotein: from genomics to mechanism. *Oncogene* 2003; 22(47): 7468-85.
6. Gottesman, M.M., T. Fojo, and S.E. Bates. Multidrug Resistance in Cancer: Role of ATP-dependent Transporters. *Nat Rev Cancer* 2002; 2(1): 48-58.
7. Dean, M., A. Rzhetsky, and R. Allikmets. The Human ATP-Binding Cassette (ABC) Transporter Superfamily. *Genome Res* 2001; 11(7): 1156-1166.
8. Leonard, G.D., T. Fojo, and S.E. Bates. The role of ABC transporters in clinical practice. *Oncologist* 2003; 8(5): 411-424.
9. Tian, Q., J. Zhang, E. Chan, W. Duan, and S. Zhou. Multidrug resistance proteins (MRPs) and implication in drug development. *Drug Dev Res* 2005; 64(1): 1-18.
10. Staud, F. and P. Pavek. Breast cancer resistance protein (BCRP/ABCG2). *Int J Biochem Cell Biol* 2005; 37(4): 720-725.
11. Borst, P., R. Evers, M. Kool, and J. Wijnholds. The multidrug resistance protein family. *Biochim Biophys Acta - Biomembranes* 1999; 1461(2): 347-357.
12. Juliano, R.L. and V. Ling. A surface glycoprotein modulating drug permeability in Chinese hamster ovary cell mutants. *Biochim Biophys Acta* 1976; 455(1): 152-62.
13. Roninson, I.B. Molecular mechanism of multidrug resistance in tumor cells. *Clin Physiol Biochem* 1987; 5(3-4): 140-51.
14. Burger, H., J.A. Foekens, M.P. Look, M.E. Meijer-van Gelder, J.G. Klijn, E.A. Wiemer, G. Stoter, and K. Nooter. RNA expression of breast cancer resistance protein, lung resistance-related protein, multidrug resistance-associated proteins 1 and 2, and multidrug resistance gene 1 in breast cancer: correlation with chemotherapeutic response. *Clin Cancer Res* 2003; 9(2): 827-36.
15. Materna, V., J. Pleger, U. Hoffmann, and H. Lage. RNA expression of MDR1/P-glycoprotein, DNA-topoisomerase I, and MRP2 in ovarian carcinoma patients: correlation with chemotherapeutic response. *Gynecol Oncol* 2004; 94(1): 152-60.

16. Ueda, K., M.M. Cornwell, M.M. Gottesman, I. Pastan, I.B. Roninson, V. Ling, and J.R. Riordan. The *mdr1* gene, responsible for multidrug-resistance, codes for P-glycoprotein. *Biochem Biophys Res Commun* 1986; 141(3): 956-962.
17. Rosenberg, M.F., R. Callaghan, S. Modok, C.F. Higgins, and R.C. Ford. Three-dimensional structure of P-glycoprotein: the transmembrane regions adopt an asymmetric configuration in the nucleotide-bound state. *J Biol Chem* 2005; 280(4): 2857-62.
18. Higgins, C.F., R. Callaghan, K.J. Linton, M.F. Rosenberg, and R.C. Ford. Structure of the multidrug resistance P-glycoprotein. *Semin Cancer Biol* 1997; 8(3): 135-42.
19. Rosenberg, M.F., R. Callaghan, R.C. Ford, and C.F. Higgins. Structure of the multidrug resistance P-glycoprotein to 2.5 nm resolution determined by electron microscopy and image analysis. *J Biol Chem* 1997; 272(16): 10685-94.
20. Hrycyna, C.A., L.E. Airan, U.A. Germann, S.V. Ambudkar, I. Pastan, and M.M. Gottesman. Structural flexibility of the linker region of human P-glycoprotein permits ATP hydrolysis and drug transport. *Biochemistry* 1998; 37(39): 13660-73.
21. Schinkel, A.H., S. Kemp, M. Dolle, G. Rudenko, and E. Wagenaar. N-glycosylation and deletion mutants of the human MDR1 P-glycoprotein. *J Biol Chem* 1993; 268(10): 7474-81.
22. Seigneuret, M. and A. Garnier-Suillerot. A Structural Model for the Open Conformation of the *mdr1* P-glycoprotein Based on the MsbA Crystal Structure. *J Biol Chem* 2003; 278(32): 30115-30124.
23. Raviv, Y., H.B. Pollard, E.P. Bruggemann, I. Pastan, and M.M. Gottesman. Photosensitized labeling of a functional multidrug transporter in living drug-resistant tumor cells. *J Biol Chem* 1990; 265(7): 3975-80.
24. Loo, T.W. and D.M. Clarke. Do drug substrates enter the common drug-binding pocket of P-glycoprotein through "gates"? *Biochem Biophys Res Commun* 2005; 329(2): 419-22.
25. Eytan, G.D. Mechanism of multidrug resistance in relation to passive membrane permeation. *Biomed Pharmacother* 2005; 59(3): 90-7.
26. Higgins, C.F. and K.J. Linton. The ATP switch model for ABC transporters. *Nat Struct Mol Biol* 2004; 11(10): 918-26.
27. Varma, M.V.S., Y. Ashokraj, C.S. Dey, and R. Panchagnula. P-glycoprotein inhibitors and their screening: A perspective from bioavailability enhancement. *Pharmacol Res* 2003; 48(4): 347-359.
28. Wang, R.B., C.L. Kuo, L.L. Lien, and E.J. Lien. Structure-activity relationship: analyses of p-glycoprotein substrates and inhibitors. *J Clin Pharm Ther* 2003; 28(3): 203-228.
29. Ford, J.M. and W.N. Hait. Pharmacology of drugs that alter multidrug resistance in cancer. *Pharmacol Rev* 1990; 42(3): 155-99.
30. Shapiro, A.B. and V. Ling. Positively cooperative sites for drug transport by P-glycoprotein with distinct drug specificities. *Eur J Biochem* 1997; 250(1): 130-7.
31. Shapiro, A.B., K. Fox, P. Lam, and V. Ling. Stimulation of P-glycoprotein-mediated drug transport by prazosin and progesterone. Evidence for a third drug-binding site. *Eur J Biochem* 1999; 259(3): 841-50.

32. Pascaud, C., M. Garrigos, and S. Orlowski. Multidrug resistance transporter P-glycoprotein has distinct but interacting binding sites for cytotoxic drugs and reversing agents. *Biochem J* 1998; 333 (Pt 2): 351-8.
33. Martin, C., G. Berridge, C.F. Higgins, P. Mistry, P. Charlton, and R. Callaghan. Communication between Multiple Drug Binding Sites on P-glycoprotein. *Mol Pharmacol* 2000; 58(3): 624-632.
34. Qu, Q. and F.J. Sharom. Proximity of bound Hoechst 33342 to the ATPase catalytic sites places the drug binding site of P-glycoprotein within the cytoplasmic membrane leaflet. *Biochemistry* 2002; 41(14): 4744-52.
35. Lugo, M.R. and F.J. Sharom. Interaction of LDS-751 with P-glycoprotein and mapping of the location of the R drug binding site. *Biochemistry* 2005; 44(2): 643-55.
36. Pleban, K., S. Kopp, E. Csaszar, M. Peer, T. Hrebicek, A. Rizzi, G.F. Ecker, and P. Chiba. P-Glycoprotein Substrate Binding Domains Are Located at the Transmembrane Domain/Transmembrane Domain Interfaces: A Combined Photoaffinity Labeling-Protein Homology Modeling Approach. *Mol Pharmacol* 2005; 67(2): 365-374.
37. Loo, T.W. and D.M. Clarke. Recent progress in understanding the mechanism of P-glycoprotein-mediated drug efflux. *J Membr Biol* 2005; 206(3): 173-185.
38. Krishna, R. and L.D. Mayer. Multidrug resistance (MDR) in cancer. Mechanisms, reversal using modulators of MDR and the role of MDR modulators in influencing the pharmacokinetics of anticancer drugs. *Eur J Pharm Sci* 2000; 11(4): 265-83.
39. Lugo, M.R. and F.J. Sharom. Interaction of LDS-751 and rhodamine 123 with P-glycoprotein: evidence for simultaneous binding of both drugs. *Biochemistry* 2005; 44(42): 14020-9.
40. Loo, T.W. and D.M. Clarke. Identification of Residues within the Drug-binding Domain of the Human Multidrug Resistance P-glycoprotein by Cysteine-scanning Mutagenesis and Reaction with Dibromobimane. *J Biol Chem* 2000; 275(50): 39272-39278.
41. Lin, J.H. and M. Yamazaki. Role of P-glycoprotein in pharmacokinetics: clinical implications. *Clin Pharmacokinet* 2003; 42(1): 59-98.
42. Campbell, L., A.-N.G. Abulrob, L.E. Kandalaf, S. Plummer, A.J. Hollins, A. Gibbs, and M. Gumbleton. Constitutive Expression of P-Glycoprotein in Normal Lung Alveolar Epithelium and Functionality in Primary Alveolar Epithelial Cultures. *J Pharmacol Exp Ther* 2003; 304(1): 441-452.
43. Thiebaut, F., T. Tsuruo, H. Hamada, M.M. Gottesman, I. Pastan, and M.C. Willingham. Cellular Localization of the Multidrug-Resistance Gene Product P-glycoprotein in Normal Human Tissues. *PNAS* 1987; 84(21): 7735-7738.
44. Fromm, M.F. Importance of P-glycoprotein at blood-tissue barriers. *Trends Pharmacol Sci* 2004; 25(8): 423-9.
45. Mizuno, N., T. Niwa, Y. Yotsumoto, and Y. Sugiyama. Impact of drug transporter studies on drug discovery and development. *Pharmacol Rev* 2003; 55(3): 425-61.
46. Lankas, G.R., L.D. Wise, M.E. Cartwright, T. Pippert, and D.R. Umbenhauer. Placental P-glycoprotein deficiency enhances susceptibility to chemically induced birth defects in mice. *Reprod Toxicol* 1998; 12(4): 457-463.

47. Choo, E.F., B. Leake, C. Wandel, H. Imamura, A.J.J. Wood, G.R. Wilkinson, and R.B. Kim. Pharmacological inhibition of P-glycoprotein transport enhances the distribution of HIV-1 protease inhibitors into brain and testes. *Drug Metab Dispos* 2000; 28(6): 655-660.
48. van der Valk, P., C.K. van Kalken, H. Ketelaars, H.J. Broxterman, G. Scheffer, C.M. Kuiper, T. Tsuruo, J. Lankelma, C.J. Meijer, and H.M. Pinedo. Distribution of multi-drug resistance-associated P-glycoprotein in normal and neoplastic human tissues. Analysis with 3 monoclonal antibodies recognizing different epitopes of the P-glycoprotein molecule. *Ann Oncol* 1990; 1(1): 56-64.
49. Puddu, P., S. Fais, F. Luciani, G. Gherardi, M.L. Dupuis, G. Romagnoli, C. Ramoni, M. Cianfriglia, and S. Gessani. Interferon-gamma up-regulates expression and activity of P-glycoprotein in human peripheral blood monocyte-derived macrophages. *Lab Invest* 1999; 79(10): 1299-309.
50. Seral, C., S. Carryn, P.M. Tulkens, and F. Van Bambeke. Influence of P-glycoprotein and MRP efflux pump inhibitors on the intracellular activity of azithromycin and ciprofloxacin in macrophages infected by *Listeria monocytogenes* or *Staphylococcus aureus*. *J Antimicrob Chemother* 2003; 51(5): 1167-73.
51. Hunter, J., B.H. Hirst, and N.L. Simmons. Drug absorption limited by P-glycoprotein-mediated secretory drug transport in human intestinal epithelial Caco-2 cell layers. *Pharm Res* 1993; 10(5): 743-9.
52. Milne, R., L. Larsen, K. Jargensen, J. Bastlund, G. Stretch, and A. Evans. Hepatic Disposition of Fexofenadine: Influence of the Transport Inhibitors Erythromycin and Dibromosulphophthalein. *Pharm Res* 2000; 17(12): 1511-1515.
53. Raub, T.J. P-glycoprotein recognition of substrates and circumvention through rational drug design. *Mol Pharm* 2006; 3(1): 3-25.
54. Cisternino, S., C. Rousselle, M. Debray, and J.-M. Scherrmann. In Vivo Saturation of the Transport of Vinblastine and Colchicine by P-Glycoprotein at the Rat Blood-Brain Barrier. *Pharm Res* 2003; 20(10): 1607-1611.
55. Pachot, J.I., R.P. Botham, K.D. Haegle, and K. Hwang. Experimental estimation of the role of P-Glycoprotein in the pharmacokinetic behaviour of telithromycin, a novel ketolide, in comparison with roxithromycin and other macrolides using the Caco-2 cell model. *J Pharm Sci* 2003; 6(1): 1-12.
56. Moon Kyoung Kim, L.H., Min Koo Choi, Yong-Hae Han, Dae-Duk Kim, Suk-Jae Chung, Chang-Koo Shim,. Dose dependency in the oral bioavailability of an organic cation model, tributylmethyl ammonium (TBuMA), in rats: Association with the saturation of efflux by the P-gp system on the apical membrane of the intestinal epithelium. *J Pharm Sci* 2005; 94(12): 2644-2655.
57. Varma, M.V.S., K. Sateesh, and R. Panchagnula. Functional Role of P-Glycoprotein in Limiting Intestinal Absorption of Drugs: Contribution of Passive Permeability to P-Glycoprotein Mediated Efflux Transport. *Mol Pharm* 2005; 2(1): 12-21.

58. Varma, M.V. and R. Panchagnula. Enhanced oral paclitaxel absorption with vitamin E-TPGS: effect on solubility and permeability in vitro, in situ and in vivo. *Eur J Pharm Sci* 2005; 25(4-5): 445-53.
59. Lin, J.H. How significant is the role of P-glycoprotein in drug absorption and brain uptake? *Drugs Today (Barc)* 2004; 40(1): 5-22.
60. Kuppens, I.E.L.M., T.M. Bosch, M.J. Van Maanen, H. Rosing, A. Fitzpatrick, J.H. Beijnen, and J.H.M. Schellens. Oral bioavailability of docetaxel in combination with OC144-093 (ONT-093). *Cancer Chemother Pharmacol* 2005; 55(1): 72-78.
61. Kruijtzter, C.M.F., J.H. Beijnen, H. Rosing, W.W. Ten Bokkel Huinink, M. Schot, R.C. Jewell, E.M. Paul, and J.H.M. Schellens. Increased oral bioavailability of topotecan in combination with the breast cancer resistance protein and P-glycoprotein inhibitor GF120918. *J Clin Oncol* 2002; 20(13): 2943-2950.
62. Sokol, R.J., K.E. Johnson, F.M. Karrer, M.R. Narkewicz, D. Smith, and I. Kam. Improvement of cyclosporin absorption in children after liver transplantation by means of water-soluble vitamin E. *Lancet* 1991; 338(8761): 212-4.
63. Pusztai, L., P. Wagner, N. Ibrahim, E. Rivera, R. Theriault, D. Booser, F.W. Symmans, F. Wong, G. Blumenschein, D.R. Fleming, R. Rouzier, G. Boniface, and G.N. Hortobagyi. Phase II study of tariquidar, a selective P-glycoprotein inhibitor, in patients with chemotherapy-resistant, advanced breast carcinoma. *Cancer* 2005; 104(4): 682-691.
64. Fracasso, P.M., L.J. Goldstein, D.P. De Alwis, J.S. Rader, M.A. Arquette, S.A. Goodner, L.P. Wright, C.L. Fears, R.J. Gazak, V.A.M. Andre, M.F. Burgess, C.A. Slapak, and J.H.M. Schellens. Phase I study of docetaxel in combination with the P-glycoprotein inhibitor, zosuquidar, in resistant malignancies. *Clin Cancer Res* 2004; 10(21): 7220-7228.
65. Chi, K.N., S.K. Chia, R. Dixon, M.J. Newman, V.J. Wacher, B. Sikic, and K.A. Gelmon. A phase I pharmacokinetic study of the P-glycoprotein inhibitor, ONT-093, in combination with paclitaxel in patients with advanced cancer. *Invest New Drugs* 2005; 23(4): 311-315.
66. Minderman, H., K.L. O'Loughlin, L. Pendyala, and M.R. Baer. VX-710 (biricodar) increases drug retention and enhances chemosensitivity in resistant cells overexpressing P-glycoprotein, multidrug resistance protein, and breast cancer resistance protein. *Clin Cancer Res* 2004; 10(5): 1826-34.
67. Wandel, C., R.B. Kim, S. Kajiji, P. Guengerich, G.R. Wilkinson, and A.J. Wood. P-glycoprotein and cytochrome P-450 3A inhibition: dissociation of inhibitory potencies. *Cancer Res* 1999; 59(16): 3944-8.
68. Choi, J.S., H.K. Choi, and S.C. Shin. Enhanced bioavailability of paclitaxel after oral coadministration with flavone in rats. *Int J Pharm* 2004; 275(1-2): 165-70.
69. Zhang, S. and M.E. Morris. Effect of the flavonoids biochanin A and silymarin on the P-glycoprotein-mediated transport of digoxin and vinblastine in human intestinal Caco-2 cells. *Pharm Res* 2003; 20(8): 1184-91.
70. Schuldes, H., J.H. Dolderer, G. Zimmer, J. Knobloch, R. Bickeboller, D. Jonas, and B.G. Woodcock. Reversal of multidrug resistance and increase in plasma membrane fluidity in CHO cells with R-verapamil and bile salts. *Eur J Cancer* 2001; 37(5): 660-7.

71. Lo, Y.L. Phospholipids as multidrug resistance modulators of the transport of epirubicin in human intestinal epithelial Caco-2 cell layers and everted gut sacs of rats. *Biochem Pharmacol* 2000; 60(9): 1381-90.
72. Rege, B.D., J.P. Kao, and J.E. Polli. Effects of nonionic surfactants on membrane transporters in Caco-2 cell monolayers. *Eur J Pharm Sci* 2002; 16(4-5): 237-46.
73. Hugger, E.D., B.L. Novak, P.S. Burton, K.L. Audus, and R.T. Borchardt. A comparison of commonly used polyethoxylated pharmaceutical excipients on their ability to inhibit P-glycoprotein activity in vitro. *J Pharm Sci* 2002; 91(9): 1991-2002.
74. Shono, Y., H. Nishihara, Y. Matsuda, S. Furukawa, N. Okada, T. Fujita, and A. Yamamoto. Modulation of intestinal P-glycoprotein function by cremophor EL and other surfactants by an in vitro diffusion chamber method using the isolated rat intestinal membranes. *J Pharm Sci* 2004; 93(4): 877-85.
75. Johnson, B.M., W.N. Charman, and C.J. Porter. An in vitro examination of the impact of polyethylene glycol 400, Pluronic P85, and vitamin E d-alpha-tocopheryl polyethylene glycol 1000 succinate on P-glycoprotein efflux and enterocyte-based metabolism in excised rat intestine. *AAPS PharmSci* 2002; 4(4): E40.
76. Lo, Y.L. Relationships between the hydrophilic-lipophilic balance values of pharmaceutical excipients and their multidrug resistance modulating effect in Caco-2 cells and rat intestines. *J Control Release* 2003; 90(1): 37-48.
77. Yu, L., A. Bridgers, J. Polli, A. Vickers, S. Long, A. Roy, R. Winnike, and M. Coffin. Vitamin E-TPGS increases absorption flux of an HIV protease inhibitor by enhancing its solubility and permeability. *Pharm Res* 1999; 16(12): 1812-7.
78. Ganem-Quintanar, A., Y.N. Kalia, F. Falson-Rieg, and P. Buri. Mechanisms of oral permeation enhancement. *Int J Pharm* 1997; 156(2): 127-142.
79. Imanidis, G., K.C. Hartner, and N.A. Mazer. Intestinal permeation and metabolism of a model peptide (leuprolide) and mechanisms of permeation enhancement by non-ionic surfactants. *Int J Pharm* 1995; 120(1): 41-50.
80. Mine, Y. and J.W. Zhang. Surfactants Enhance the Tight-Junction Permeability of Food Allergens in Human Intestinal Epithelial Caco-2 Cells. *Int Arch Allergy Immunol* 2003; 130(2): 135-142.
81. Cornaire, G., J. Woodley, P. Hermann, A. Cloarec, C. Arellano, and G. Houin. Impact of excipients on the absorption of P-glycoprotein substrates in vitro and in vivo. *Int J Pharm* 2004; 278(1): 119-31.
82. Bittner, B., A. Guenzi, P. Fullhardt, G. Zuercher, R.C. Gonzalez, and R.J. Mountfield. Improvement of the bioavailability of colchicine in rats by co-administration of D-alpha-tocopherol polyethylene glycol 1000 succinate and a polyethoxylated derivative of 12-hydroxystearic acid. *Arzneimittelforschung* 2002; 52(9): 684-8.
83. Batrakova, E.V., S. Li, V.Y. Alakhov, D.W. Miller, and A.V. Kabanov. Optimal Structure Requirements for Pluronic Block Copolymers in Modifying P-glycoprotein Drug Efflux Transporter Activity in Bovine Brain Microvessel Endothelial Cells. *J Pharmacol Exp Ther* 2003; 304(2): 845-854.

84. Bogman, K., F. Erne-Brand, J. Alsenz, and J. Drewe. The role of surfactants in the reversal of active transport mediated by multidrug resistance proteins. *J Pharm Sci* 2003; 92(6): 1250-61.
85. Cool, R.H., M.K. Veenstra, W. Van Klompenburg, R.I.R. Heyne, M. Müller, E.G.E. De Vries, H.W. Van Veen, and W.N. Konings. S-Decyl-glutathione nonspecifically stimulates the ATPase activity of the nucleotide-binding domains of the human multidrug resistance-associated protein, MRP1 (ABCC1). *Eur J Biochem* 2002; 269(14): 3470-3478.
86. Miller, D.W., E.V. Batrakova, and A.V. Kabanov. Inhibition of multidrug resistance-associated protein (MRP) functional activity with pluronic block copolymers. *Pharm Res* 1999; 16(3): 396-401.
87. Rothnie, A., D. Theron, L. Soceneantu, C. Martin, M. Traikia, G. Berridge, C.F. Higgins, P.F. Devaux, and R. Callaghan. The importance of cholesterol in maintenance of P-glycoprotein activity and its membrane perturbing influence. *Eur Biophys J* 2001; 30(6): 430-442.
88. Kamau, S.W., S.D. Kramer, M. Gunthert, and H. Wunderli-Allenspach. Effect of the modulation of the membrane lipid composition on the localization and function of P-glycoprotein in MDR1-MDCK cells. *In Vitro Cell Dev Biol Anim* 2005; 41(7): 207-16.
89. Gayet, L., G. Dayan, S. Barakat, S. Labialle, M. Michaud, S. Cogne, A. Mazane, A.W. Coleman, D. Rigal, and L.G. Baggetto. Control of P-glycoprotein activity by membrane cholesterol amounts and their relation to multidrug resistance in human CEM leukemia cells. *Biochemistry* 2005; 44(11): 4499-509.
90. Orłowski, S., S. Martin, and A. Escargueil. P-glycoprotein and 'lipid rafts': some ambiguous mutual relationships (floating on them, building them or meeting them by chance?). *Cell Mol Life Sci* 2006; 63(9): 1038-1059.
91. Woodcock, D.M., M.E. Linsenmeyer, G. Chojnowski, A.B. Kriegler, V. Nink, L.K. Webster, and W.H. Sawyer. Reversal of multidrug resistance by surfactants. *Br J Cancer* 1992; 66(1): 62-8.
92. Dudeja, P.K., K.M. Anderson, J.S. Harris, L. Buckingham, and J.S. Coon. Reversal of multidrug resistance phenotype by surfactants: relationship to membrane lipid fluidity. *Arch Biochem Biophys* 1995; 319(1): 309-15.
93. Batrakova, E.V., S. Li, S.V. Vinogradov, V.Y. Alakhov, D.W. Miller, and A.V. Kabanov. Mechanism of pluronic effect on P-glycoprotein efflux system in blood-brain barrier: Contributions of energy depletion and membrane fluidization. *J Pharmacol Exp Ther* 2001; 299(2): 483-493.
94. Kabanov, A.V., E.V. Batrakova, S. Li, and Y. Alakhov V. Selective energy depletion and sensitization of multiple drug-resistant cancer cells by pluronic block copolymer. *Macromol Symp* 2001; 172: 103-112.
95. Traber, M.G., T.D. Schiano, A.C. Steephen, H.J. Kayden, and M. Shike. Efficacy of water-soluble vitamin E in the treatment of vitamin E malabsorption in short-bowel syndrome. *Am J Clin Nutr* 1994; 59(6): 1270-4.
96. Sokol, R.J., N. Butler-Simon, C. Conner, J.E. Heubi, F.R. Sinatra, F.J. Suchy, M.B. Heyman, J. Perrault, R.J. Rothbaum, and J. Levy. Multicenter trial of d-alpha-tocopheryl polyethylene glycol 1000 succinate for treatment of vitamin E deficiency in children with chronic cholestasis. *Gastroenterology* 1993; 104(6): 1727-35.

97. Sokol, R.J., N.A. Butler-Simon, D. Bettis, D.J. Smith, and A. Silverman. Tocopheryl polyethylene glycol 1000 succinate therapy for vitamin E deficiency during chronic childhood cholestasis: neurologic outcome. *J Pediatr* 1987; 111(6 Pt 1): 830-6.
98. Traber, M.G., C.A. Thellman, M.J. Rindler, and H.J. Kayden. Uptake of intact TPGS (d-alpha-tocopheryl polyethylene glycol 1000 succinate) a water-miscible form of vitamin E by human cells in vitro. *Am J Clin Nutr* 1988; 48(3): 605-11.
99. Ismailos, G., C. Reppas, and P. Macheras. Enhancement of cyclosporin A solubility by d-alpha-tocopheryl-polyethylene-glycol-1000 succinate (TPGS). *Eur J Pharm Biopharm* 1994; 1(5): 269-271.
100. Sheu, M.T., S.Y. Chen, L.C. Chen, and H.O. Ho. Influence of micelle solubilization by tocopheryl polyethylene glycol succinate (TPGS) on solubility enhancement and percutaneous penetration of estradiol. *J Control Release* 2003; 88(3): 355-68.
101. Dintaman, J.M. and J.A. Silverman. Inhibition of P-glycoprotein by D-alpha-tocopheryl polyethylene glycol 1000 succinate (TPGS). *Pharm Res* 1999; 16(10): 1550-6.
102. Chan, L.M., S. Lowes, and B.H. Hirst. The ABCs of drug transport in intestine and liver: efflux proteins limiting drug absorption and bioavailability. *Eur J Pharm Sci* 2004; 21(1): 25-51.
103. Win, K.Y. and S.S. Feng. In vitro and in vivo studies on vitamin E TPGS-emulsified poly(D,L-lactic-co-glycolic acid) nanoparticles for paclitaxel formulation. *Biomaterials* 2006; 27(10): 2285-91.
104. Bogman, K., Y. Zysset, L. Degen, G. Hopfgartner, H. Gutmann, J. Alsenz, and J. Drewe. P-glycoprotein and surfactants: effect on intestinal talinolol absorption. *Clin Pharmacol Ther* 2005; 77(1): 24-32.
105. Hyafil, F., C. Vergely, P. Du Vignaud, and T. Grand-Perret. In vitro and in vivo reversal of multidrug resistance by GF120918, an acridonecarboxamide derivative. *Cancer Res* 1993; 53(19): 4595-4602.
106. Dantzig, A.H., K.L. Law, J. Cao, and J.J. Starling. Reversal of multidrug resistance by the P-glycoprotein modulator, LY335979, from the bench to the clinic. *Curr Med Chem* 2001; 8(1): 39-50.
107. Wachter, V.J., S. Wong, and H.T. Wong. Peppermint oil enhances cyclosporine oral bioavailability in rats: comparison with D-alpha-tocopheryl poly(ethylene glycol 1000) succinate (TPGS) and ketoconazole. *J Pharm Sci* 2002; 91(1): 77-90.
108. Neuzil, J., T. Weber, A. Schroder, M. Lu, G. Ostermann, N. Gellert, G.C. Mayne, B. Olejnicka, A. Negre-Salvayre, M. Sticha, R.J. Coffey, and C. Weber. Induction of cancer cell apoptosis by alpha-tocopheryl succinate: molecular pathways and structural requirements. *FASEB J* 2001; 15(2): 403-415.
109. Yu, W., L. Qiao Yin, F.M. Hantash, B.G. Sanders, and K. Kline. Activation of extracellular signal-regulated kinase and c-Jun-NH2-terminal kinase but not p38 mitogen-activated protein kinases is required for RRR-[alpha]-tocopheryl succinate-induced apoptosis of human breast cancer cells. *Cancer Res* 2001; 61(17): 6569-6576.

110. Zhang, Y., J. Ni, E.M. Messing, E. Chang, C.-R. Yang, and S. Yeh. Vitamin E succinate inhibits the function of androgen receptor and the expression of prostate-specific antigen in prostate cancer cells. *PNAS* 2002; 99(11): 7408-7413.
111. Youk, H.J., E. Lee, M.K. Choi, Y.J. Lee, J.H. Chung, S.H. Kim, C.H. Lee, and S.J. Lim. Enhanced anticancer efficacy of alpha-tocopheryl succinate by conjugation with polyethylene glycol. *J Control Release* 2005; 107(1): 43-52.
112. Wang, J., C.W. Ng, K.Y. Win, P. Shoemakers, T.K. Lee, S.S. Feng, and C.H. Wang. Release of paclitaxel from polylactide-co-glycolide (PLGA) microparticles and discs under irradiation. *J Microencapsul* 2003; 20(3): 317-27.
113. Mu, L. and P.H. Seow. Application of TPGS in polymeric nanoparticulate drug delivery system. *Colloids Surf B Biointerfaces* 2006; 47(1): 90-7.
114. Win, K.Y. and S.S. Feng. Effects of particle size and surface coating on cellular uptake of polymeric nanoparticles for oral delivery of anticancer drugs. *Biomaterials* 2005; 26(15): 2713-22.
115. Zhang, Z. and S.S. Feng. Nanoparticles of poly(lactide)/vitamin E TPGS copolymer for cancer chemotherapy: synthesis, formulation, characterization and in vitro drug release. *Biomaterials* 2006; 27(2): 262-70.
116. Zhang, Z. and S.S. Feng. Self-assembled nanoparticles of poly(lactide)-Vitamin E TPGS copolymers for oral chemotherapy. *Int J Pharm* 2006; 324(2): 191-198.
117. Mu, L. and S.S. Feng. A novel controlled release formulation for the anticancer drug paclitaxel (Taxol): PLGA nanoparticles containing vitamin E TPGS. *J Control Release* 2003; 86(1): 33-48.
118. Somavarapu, S., S. Pandit, G. Gradassi, M. Bandera, E. Ravichandran, and O.H. Alpar. Effect of vitamin E TPGS on immune response to nasally delivered diphtheria toxoid loaded poly(caprolactone) microparticles. *Int J Pharm* 2005; 298(2): 344-7.
119. Mu, L., T.A. Elbayoumi, and V.P. Torchilin. Mixed micelles made of poly(ethylene glycol)-phosphatidylethanolamine conjugate and d-alpha-tocopheryl polyethylene glycol 1000 succinate as pharmaceutical nanocarriers for camptothecin. *Int J Pharm* 2005; 306(1-2): 142-9.
120. Seeballuck, F., M.B. Ashford, and C.M. O'Driscoll. The effects of pluronics block copolymers and Cremophor EL on intestinal lipoprotein processing and the potential link with P-glycoprotein in Caco-2 cells. *Pharm Res* 2003; 20(7): 1085-92.
121. Hugger, E.D., K.L. Audus, and R.T. Borchardt. Effects of poly(ethylene glycol) on efflux transporter activity in Caco-2 cell monolayers. *J Pharm Sci* 2002; 91(9): 1980-90.
122. Hugger, E.D., C.J. Cole, T.J. Raub, P.S. Burton, and R.T. Borchardt. Automated analysis of polyethylene glycol-induced inhibition of P-glycoprotein activity in vitro. *J Pharm Sci* 2003; 92(1): 21-6.
123. Artursson, P., K. Palm, and K. Luthman. Caco-2 monolayers in experimental and theoretical predictions of drug transport. *Adv Drug Deliv Rev* 2001; 46(1-3): 27-43.

124. Artursson, P. and J. Karlsson. Correlation between oral drug absorption in humans and apparent drug permeability coefficients in human intestinal epithelial (Caco-2) cells. *Biochem Biophys Res Commun* 1991; 175(3): 880-885.
125. Taipalensuu, J., H. Tornblom, G. Lindberg, C. Einarsson, F. Sjoqvist, H. Melhus, P. Garberg, B. Sjoström, B. Lundgren, and P. Artursson. Correlation of Gene Expression of Ten Drug Efflux Proteins of the ATP-Binding Cassette Transporter Family in Normal Human Jejunum and in Human Intestinal Epithelial Caco-2 Cell Monolayers. *J Pharmacol Exp Ther* 2001; 299(1): 164-170.
126. Zimmer, C. (2006) *Calcein AM uptake assay for the screening of TPGS 1000 derivatives as potential P-glycoprotein inhibitors*, Master's thesis; 80 pages. Department of Biopharmaceutics and Pharmaceutical Technology, Saarland University; Saarbrücken
127. Wang, Y., D. Hao, W.D. Stein, and L. Yang. A kinetic study of Rhodamine123 pumping by P-glycoprotein. *Biochim Biophys Acta* 2006; 1758(10): 1671-6.
128. Gao, J., O. Murase, R.L. Schowen, J. Aubé, and R.T. Borchardt. A Functional Assay for Quantitation of the Apparent Affinities of Ligands of P-Glycoprotein in Caco-2 Cells. *Pharm Res* 2001; V18(2): 171-176.
129. Lee, C.G.L., M.M. Gottesman, C.O. Cardarelli, M. Ramachandra, K.-T. Jeang, S.V. Ambudkar, I. Pastan, and S. Dey. HIV-1 Protease Inhibitors Are Substrates for the MDR1 Multidrug Transporter. *Biochemistry* 1998; 37(11): 3594-3601.
130. Troutman, M.D. and D.R. Thakker. Rhodamine 123 requires carrier-mediated influx for its activity as a P-glycoprotein substrate in Caco-2 cells. *Pharm Res* 2003; 20(8): 1192-9.
131. Troutman, M.D. and D.R. Thakker. Efflux ratio cannot assess P-glycoprotein-mediated attenuation of absorptive transport: asymmetric effect of P-glycoprotein on absorptive and secretory transport across Caco-2 cell monolayers. *Pharm Res* 2003; 20(8): 1200-9.
132. Troutman, M. and D. Thakker. Efflux ratio cannot assess P-glycoprotein-mediated attenuation of absorptive transport: asymmetric effect of P-glycoprotein on absorptive and secretory transport across Caco-2 cell monolayers. *pharm Res* 2003; 20(8): 1200-1209.
133. Wang, S.W., J. Monagle, C. McNulty, D. Putnam, and H. Chen. Determination of P-glycoprotein inhibition by excipients and their combinations using an integrated high-throughput process. *J Pharm Sci* 2004; 93(11): 2755-67.
134. Boudreaux, J.P., D.H. Hayes, S. Mizrahi, P. Maggiore, J. Blazek, and D. Dick. Use of water-soluble liquid vitamin E to enhance cyclosporine absorption in children after liver transplant. *Transplant Proc* 1993; 25(2): 1875.
135. Sokol, R.J., J.E. Heubi, N. Butler-Simon, H.J. McClung, J.R. Lilly, and A. Silverman. Treatment of vitamin E deficiency during chronic childhood cholestasis with oral d-alpha-tocopheryl polyethylene glycol-1000 succinate. *Gastroenterology* 1987; 93(5): 975-85.
136. Brouwers, J., J. Tack, F. Lammert, and P. Augustijns. Intraluminal drug and formulation behavior and integration in in vitro permeability estimation: a case study with amprenavir. *J Pharm Sci* 2006; 95(2): 372-83.
137. Batrakova, E.V., S. Li, Y. Li, V.Y. Alakhov, and A.V. Kabanov. Effect of pluronic P85 on ATPase activity of drug efflux transporters. *Pharm Res* 2004; 21(12): 2226-2233.

138. Orłowski, S., M.A. Selosse, C. Boudon, C. Micoud, L.M. Mir, J. Belehradek, Jr., and M. Garrigos. Effects of detergents on P-glycoprotein atpase activity: differences in perturbations of basal and verapamil-dependent activities. *Cancer Biochem Biophys* 1998; 16(1-2): 85-110.
139. Batrakova, E.V., S. Li, W.F. Elmquist, D.W. Miller, V.Y. Alakhov, and A.V. Kabanov. Mechanism of sensitization of MDR cancer cells by Pluronic block copolymers: Selective energy depletion. *Br J Cancer* 2001; 85(12): 1987-1997.
140. Collnot, E.M., C. Baldes, M.F. Wempe, J. Hyatt, L. Navarro, K.J. Edgar, U.F. Schaefer, and C.M. Lehr. Influence of vitamin E TPGS poly(ethylene glycol) chain length on apical efflux transporters in Caco-2 cell monolayers. *J Control Release* 2006; 111(1-2): 35-40.
141. Gaffney, B. and D. Lin, *Spin-label measurement of membrane-bound enzymes*, in *The Enzymes of Biological Membranes*, Martonosi, Editor. 1973, John Wiley & Sons: New York. p. 71-90.
142. Marsh, D., *Electron spin resonance*, in *Membrane Spectroscopy. Molecular Biology, Biochemistry and Biophysics*, E. Grell, Editor. 1981, Springer: New York. p. 51-142.
143. Garrigues, A., J. Nugier, S. Orłowski, and E. Ezan. A high-throughput screening microplate test for the interaction of drugs with P-glycoprotein. *Anal Biochem* 2002; 305(1): 106-14.
144. Mechetner, E. and I. Roninson. Efficient Inhibition of P-Glycoprotein-Mediated Multidrug Resistance with a Monoclonal Antibody. *PNAS* 1992; 89(13): 5824-5828.
145. Mechetner, E.B., B. Schott, B.S. Morse, W.D. Stein, T. Druley, K.A. Davis, T. Tsuruo, and I.B. Roninson. P-glycoprotein function involves conformational transitions detectable by differential immunoreactivity. *PNAS* 1997; 94(24): 12908-12913.
146. Urbatsch, I.L., B. Sankaran, J. Weber, and A.E. Senior. P-glycoprotein Is Stably Inhibited by Vanadate-induced Trapping of Nucleotide at a Single Catalytic Site. *J Biol Chem* 1995; 270(33): 19383-19390.
147. Druley, T.E., W.D. Stein, and I.B. Roninson. Analysis of MDR1 P-Glycoprotein Conformational Changes in Permeabilized Cells Using Differential Immunoreactivity. *Biochemistry* 2001; 40(14): 4312-4322.
148. Zhou, Y., M.M. Gottesman, and I. Pastan. The extracellular loop between TM5 and TM6 of P-glycoprotein is required for reactivity with monoclonal antibody UIC2. *Arch Biochem Biophys* 1999; 367(1): 74-80.
149. Glover, R.E., R.R. Smith, M.V. Jones, S.K. Jackson, and C.C. Rowlands. An EPR investigation of surfactant action on bacterial membranes. *FEMS Microbiol Lett* 1999; 177(1): 57-62.
150. Drori, S., G.D. Eytan, and Y.G. Assaraf. Potentiation of Anticancer-Drug Cytotoxicity by Multidrug-Resistance Chemosensitizers Involves Alterations in Membrane Fluidity Leading to Increased Membrane Permeability. *Eur J Biochem* 1995; 228(3): 1020-1029.
151. Goni, F.M., M.-A. Urbaneja, J.L.R. Arrondo, A. Alonso, A.A. Durrani, and D. Chapman. The interaction of phosphatidylcholine bilayers with Triton X-100. *Eur J Biochem* 1986; 160(3): 659-665.

152. Callaghan, R., A. Stafford, and R.M. Epand. Increased accumulation of drugs in a multidrug resistant cell line by alteration of membrane biophysical properties. *Biochim Biophys Acta-Molecular Cell Research* 1993; 1175(3): 277-282.
153. Carmena, M.J., C. Hueso, L.G. Guijarro, and J.C. Prieto. Cholesterol modulation of membrane fluidity and VIP receptor/effector system in rat prostatic epithelial cells. *Regul Pept* 1991; 33(3): 287-297.
154. Yeagle, P.L. Lipid regulation of cell membrane structure and function. *FASEB J* 1989; 3(7): 1833-1842.
155. Galson, S. and J. Campisi. Local anesthetics decrease membrane fluidity of sea urchin eggs. *Fed Proc* 1979; 38(3 I).
156. Sweet, W.D. and F. Schroeder. Charged anaesthetics alter LM-fibroblast plasma-membrane enzymes by selective fluidization of inner or outer membrane leaflets. *Biochem J* 1986; 239(2): 301-310.
157. Constantinescu, A., L. Bajenaru, P.T. Frangopol, and D.G. Margineanu. Does procaine really fluidize the erythrocyte membrane? *Biochemistry* 1986; 25(20): 97-102.
158. Yun, I., E.-S. Cho, H.-O. Jang, U.-K. Kim, C.-H. Choi, I.-K. Chung, I.-S. Kim, and W.G. Wood. Amphiphilic effects of local anesthetics on rotational mobility in neuronal and model membranes. *Biochim Biophys Acta - Biomembranes* 2002; 1564(1): 123-132.
159. Drori, S., G.D. Eytan, and Y.G. Assaraf. Potentiation of anticancer-drug cytotoxicity by multidrug-resistance chemosensitizers involves alterations in membrane fluidity leading to increased membrane permeability. *Eur J Biochem* 1995; 228(3): 1020-9.
160. Dolderer, J.H., G. Zimmer, B.G. Woodcock, H. Bockhorn, R. Bickeboller, and H. Schuldes. Resistance modulation in CHO cells by R-verapamil and bile salts is associated with physical and chemical changes in the cell membrane. *Int J Clin Pharmacol Ther* 2000; 38(4): 196-203.
161. Pagano, R.E., K. Ozato, and J.M. Ruyschaert. Intracellular distribution of lipophilic fluorescent probes in mammalian cells. *Biochim Biophys Acta* 1977; 465(3): 661-6.
162. Loo, T.W., M.C. Bartlett, and D.M. Clarke. Simultaneous Binding of Two Different Drugs in the Binding Pocket of the Human Multidrug Resistance P-glycoprotein. *J Biol Chem* 2003; 278(41): 39706-39710.
163. Batrakova, E., S. Lee, S. Li, A. Venne, V. Alakhov, and A. Kabanov. Fundamental Relationships Between the Composition of Pluronic Block Copolymers and Their Hypersensitization Effect in MDR Cancer Cells. *Pharm Res* 1999; 16(9): 1373-1379.
164. Dey, S., M. Ramachandra, I. Pastan, M.M. Gottesman, and S.V. Ambudkar. Evidence for two nonidentical drug-interaction sites in the human P-glycoprotein. *Proc Natl Acad Sci U S A* 1997; 94(20): 10594-9.
165. Maki, N., P. Hafkemeyer, and S. Dey. Allosteric modulation of human P-glycoprotein. Inhibition of transport by preventing substrate translocation and dissociation. *J Biol Chem* 2003; 278(20): 18132-9.
166. Martin, C., G. Berridge, C.F. Higgins, and R. Callaghan. The multi-drug resistance reversal agent SR33557 and modulation of vinca alkaloid binding to P-glycoprotein by an allosteric interaction. *Br J Pharmacol* 1997; 122(4): 765-71.

167. Loo, T.W. and D.M. Clarke. Drug-stimulated ATPase activity of human P-glycoprotein requires movement between transmembrane segments 6 and 12. *J Biol Chem* 1997; 272(34): 20986-9.
168. Galla, H., *Spektroskopische Methoden in der Biochemie*. 1988, Stuttgart, New York: Georg Thieme Verlag.

8 Abbreviations

BCRP	breast cancer resistance protein
BSA	bovine serum albumin
ClogP	octanol/ water partition coefficient
CMA	Connolly Molecular Area
CsA	cyclosporine A
DIG	digoxin
EC50	concentration at which half maximal inhibitory effects are observed
ER	efflux ratio
ESR	electron spin resonance
F_{mean}	mean fluorescence intensity
FU	fluorescence units
IC50	concentration at which half maximal cytotoxic effects are observed
LDH	lactate dehydrogenase
MDR	multidrug resistance
MRP	multidrug resistance associated protein
P_{app}	apparent permeability coefficient
P-gp	P-glycoprotein
RHO	rhodamine 123
S	order parameter
SEV	Connolly Solvent-Excluded Volume
TPGS	D-alpha-tocopheryl poly(ethylene glycol 1000) succinate

9 Curriculum vitae

Personal Information

name	Eva-Maria Collnot
address	Hofweg 71-73, 66125 Dudweiler
born	19.06.1978, Ottweiler
nationality	German

School

09/1985-07/1989	Grundschule Neumünster, Ottweiler
09/1989-07/1998	Gymnasium Ottweiler

Undergraduate studies

10/1998-10/2002	Pharmacy, Saarland University, Saarbrücken
-----------------	--

Master thesis

05/2003-10/2003	Department of Biopharmaceutics and Pharmaceutical technology, Saarland University, Saarbrücken „Charakterisierung der humanen Bronchialepithelzelllinie CFBE41o- als Modell für Untersuchungen zur Zystischen Fibrose“
-----------------	---

PhD thesis

11/2003- 01/200d7	Department of Biopharmaceutics and Pharmaceutical technology, Saarland University, Saarbrücken
-------------------	--

10 List of publications

Scientific publications

Collnot E-M, Baldes C, Wempe M, Hyatt J, Navarro L, Edgar KJ, Schaefer UF, Lehr C-M, Influence of vitamin E TPGS poly(ethylene glycol) chain length on apical efflux transporters in Caco-2 cell monolayers, *Journal of Controlled Release*, 111 (1-2): 35 – 40, 2006

Collnot E-M, Baldes C, Wright C, Little JL, Schaefer UF, Lehr C-M, Wachter VJ, Edgar KJ, Wempe M, Vitamin E TPGS modulation of P-gp efflux in Caco-2 cells: Significance of compound purity, pre-incubation time and application side, *European Journal of Pharmaceutical Sciences*, submitted

Collnot E-M, Baldes C, Wempe M, Kappl R, Huettermann J, Hyatt J, Edgar KJ, Schaefer UF, Lehr C-M, Mechanism of inhibition of P-glycoprotein mediated efflux by Vitamin E TPGS: Influence on ATPase activity and membrane fluidity, *Molecular Pharmaceutics*, in press

Beck RCR, Pohlmann A, Hoffmeister C, Galas MR, Collnot EM, Schaefer UF, Guternes S, Lehr CM, Dexamethasone-loaded nanoparticle coated microparticles: correlation between *in vitro* drug release and drug transport across Caco-2 monolayers; *European Journal of Pharmaceutics and Biopharmaceutics*, accepted

Ehrhardt C, Collnot E-M, Baldes C, Becker U, Laue M, Kim KJ, Lehr CM, Towards an *in vitro* model of cystic fibrosis small airway epithelium: characterisation of the human bronchial epithelial cell line CFBE410-, *Cell and Tissue Research*, 323 (3): 405 - 415, 2006

Oral presentations

Collnot E-M, Baldes C, Wempe MF, Kappl R, Huettermann J, Edgar KJ, Schaefer UF, Lehr CM, Inhibition of P-glycoprotein mediated efflux by Vitamin E TPGS: effects on ATPase activity and membrane fluidity, 33rd Annual Meeting & Exposition of the Controlled Release Society, July 22-26, Vienna, 2006; awarded with the 2006 Capsugel Innovative Aspects of Oral Drug Delivery & Absorption Award

Posters/ abstracts

Collnot E-M, Baldes C, Wempe M, Hyatt J, Navarro L, Wachter V, Edgar KJ, Schaefer UF, Lehr C-M, Improving potency of oral absorption enhancers: new analogues of vitamin E TPGS, 32nd Annual Meeting & Exposition of the Controlled Release Society, June 18-22, Miami Beach, Florida, 2005

Collnot E-M, Bies C, Hyatt J, Navarro I, Edgar K, Schaefer U, Ehrhardt C, Lehr CM, Inhibition of O-glycoprotein by TPGS: Influence of the PEG-chain length, AAPS Annual Meeting November 7-11, Baltimore, 2004

Patent applications

US, WO002006039268A2: Pharmaceutical Formulations Containing Vitamin E TPGS Molecules That Solubilize Lipophilic Drugs Without Significant Efflux Inhibition, And Use Of Such Formulations. (2006); Hyatt, JA, Zima GC, Edgar KJ, Navarro LT, Lehr C-M, Collnot E-M, Singleton AH, Baldes C, Schafer UF, and Wempe MF

Submitted, decision pending: Methods And Pharmaceutical Formulations For Increasing Bioavailability (2006); Wempe MF, Lehr C-M, Collnot E-M, Baldes C, and Schaefer UF

11 Danksagung

An dieser Stelle möchte ich mich bei Herrn Prof. Dr. Claus-Michael Lehr, für die Bereitstellung des Themas und die gute, engagierte Betreuung in den letzten drei Jahren bedanken. Des weiteren danke ich Herrn Prof. Helms für die Anfertigung des Zweitgutachtens, sowie den anderen Mitgliedern der Prüfungskommission.

Mein Dank gilt außerdem meiner Betreuerin Frau Dr. Christiane Baldes, die mir, wie bereits während meiner Diplomarbeit, immer mit Rat und Tat zur Seite stand. Nicht vergessen darf ich außerdem Dr. Ulrich Schäfer, der trotz seiner ohnehin schon sehr hohen Arbeitsbelastung im Institut, immer noch Zeit gefunden hat, sich auch meiner Probleme anzunehmen.

Besonders danken will ich außerdem Michael Wempe, Lisa Navarro, Kevin Edgar und ihren Kollegen bei Eastman. Ohne das Engagement von Eastman wäre diese Doktorarbeit nie zu Stande gekommen. Im offenen Dialog mit Eastman, wurden immer wieder konstruktive Vorschläge gemacht. Gleichzeitig hatte ich aber ausreichend Spielraum, um meine eigenen Ideen zu entwickeln und zu untersuchen. (Special thanks go to Michael Wempe, Lisa Navarro, Kevin Edgar and all the other guys at Eastman. This PhD project would not have been possible without their dedication and commitment. The open dialog with Eastman led to many constructive suggestions; at the same time I was given the opportunity to develop and investigate my own ideas).

Wahrscheinlich hätte ich ohne die Hilfe von Dr. Reinhard Kappl vom Institut für Biophysik in Homburg nie die Geheimnisse der ESR ergründet. Natürlich danke ich auch dem Institutsleiter Prof. Jürgen Hüttermann, der mir erlaubt hat die ESR Spektrometer in Homburg für meine Messungen zu nutzen.

Mein Dank gilt auch den Technikerinnen Susanne Kossek, Katja Klein und Heike Stumpf, die sich für mich um einen Großteil der Routinezellkultur gekümmert haben und mir das Leben dadurch nicht unwesentlich erleichterten.

Meinen Eltern danke ich für die moralische und finanzielle Unterstützung während meines Studiums und meiner Promotion. Sie haben bei meiner Entscheidung nicht in die öffentliche Apotheke zu gehen voll hinter mir gestanden, auch wenn ich Ihnen dadurch noch 3 Jahre länger auf der Tasche gelegen habe.

Abschließend, möchte ich hier noch alle meine Leidensgenossen (Mitdoktoranden) am Institut erwähnen, die im Rahmen der Selbsthilfegruppe „AK Lehr“ Trost und Ratschläge gespendet und auch sonst immer für eine gute Stimmung gesorgt haben.